12-2012

Implementing Conductive Concrete with Photovoltaic Energy to Develop Anti-Icing Airfield Runways

Adam Benjamin Osweiler
University of Arkansas, Fayetteville

IMPLEMENTING CONDUCTIVE CONCRETE WITH PHOTOVOLTAIC ENERGY TO DEVELOP ANTI-ICING AIRFIELD RUNWAYS

IMPLEMENTING CONDUCTIVE CONCRETE WITH PHOTOVOLTAIC ENERGY TO DEVELOP ANTI-ICING AIRFIELD RUNWAYS

A thesis submitted in partial fulfillment
of the requirements for the degree of
Master of Science in Civil Engineering

By

Adam B. Osweiler
University of Arkansas
Bachelor of Science in Civil Engineering, 2010

December 2012
University of Arkansas

ABSTRACT

Snow and ice accumulation on airport runways force airports to cancel or significantly delay flights. Winter weather can also drastically affect airport safety during times of aircraft takeoff and landing. During these times, countless dollars are used to remove snow and return airports to their functional conditions. In this thesis, a conductive concrete solar energy system will be examined in order to prevent snow and ice accumulation. The objective of this research is to implement a conductive concrete overlay system on airport runways in conjunction with photovoltaic energy so that no frost precipitation accumulates on the runway surface.

Keywords: cold weather; anti-icing; electrically conductive concrete; fiber-reinforced concrete; photovoltaics

This thesis is approved for recommendation
to the Graduate Council.

Thesis Director:

_____
Dr. Ernie Heymsfield

Thesis Committee:

_____
Dr. Paneer Selvam

_____
Dr. Micah Hale

THESIS DUPLICATION RELEASE

I hereby authorize the University of Arkansas Libraries to duplicate this thesis when needed for research and/or scholarship.

Agreed _____
Adam B. Osweiler

Refused _____
Adam B. Osweiler

ACKNOWLEDGEMENTS

The author of this article would like to acknowledge all the people and companies that were involved in the process of this research. First, the author would like to thank his parents, Kevin and Anita Osweiler, for all of their encouragement and support throughout his collegiate career at the University of Arkansas. Secondly, the author would like to thank Joseph Breen, Ryan King, and the Federal Aviation Administration for their assistance and financial support. Dr. Ernie Heymsfield is very much appreciated for his advising and guidance throughout the career of his graduate student. The author would also like to thank Dr. Heymsfield for the opportunity to work with him on such an exciting project. Dr. Paneer Selvam and Dr. Micah Hale are given special thanks for their assistance and knowledge provided toward the completion of this project.

For their technical support and assistance over the duration of the project, Mark Kuss and David Peachee are greatly appreciated. The following people are acknowledged for their aid in providing materials used for research: Albert Tamashausky of Asbury Graphite Mills, Inc. for supplying graphite powder, Alexander Yancy of Propex Brands for providing the steel fibers, and Jason Drake of Grace Construction Products for supplying high range water reducer. Lastly, special thanks go to Bradley Brown for assisting in the formwork construction and concrete batching.

TABLE OF CONTENTS

LIST OF FIGURES

LIST OF TABLES

CHAPTER 1: INTRODUCTION

Problem Statement

Current techniques to combat ice and snow buildup include: salts, deicing chemicals, and heat pipes. Airport personnel use methods involving snow blowers, plows, and sweepers for the physical removal of snow. For the removal and breakdown of icy situations, deicing salts and chloride/acetate solutions are used. While these methods and systems are being used worldwide, the disadvantages of using such methods often outweigh their advantages. Although deicing chemicals and salts are relatively inexpensive, a disadvantage of their usage is that they deteriorate concrete and corrode steel reinforcement (Lee *et al*, 2000).

Heat pipes, on the other hand, cause very little damage to concrete pavement, but their high construction costs and their tendency to deteriorate often deter many agencies from installing them. The idea of using conductive concrete to melt snow and ice on contact is a relatively new concept. Implementing conductive concrete with an electric energy source provides a means to raise concrete slab temperature. If the slab temperature is raised to above freezing, the process will prevent ice and snow accumulation. Consequently, implementing a system that includes conductive concrete and electric energy provides airports with a potential solution for snow removal. If successful, this solution will allow airport personnel to decrease the safety risks that accompany winter weather. In this study, a photovoltaic energy system is used to generate the electric energy supplied to the conductive concrete system. While the deicing system would be functional for airport runways, aprons, and taxiways, the practical uses of the deicing system may pertain mostly to shorter sections dividing runways where maintenance equipment mobility is limited.

Background Information

Throughout history, concrete has been used mainly for its high compressive strength in slabs, piers, foundations, and columns. Even in the past ten years, advancements in mix design, mix proportioning, and chemical additives have allowed concrete to become less expensive, stronger, lighter, and more resistant to damage caused by environmental and chemical effects. Concrete's intrinsic mechanical properties qualify it as an ideal airfield runway pavement.

Salt and acetate chemical mixtures are typically used for melting and preventing ice and snow accumulation. While these mixtures are very effective in deicing pavements, they can cause damage in the form of spalling, scaling, pattern cracking and deterioration line cracking. Conversely, energized conductive concrete provides an alternative solution that negates the need for chemical treatment. Snow and ice removal on airport runway pavements cost airport agencies millions of dollars each year due to deicing chemicals and their related labor costs. As we move to a more environmentally friendly design procedure, the United States Environmental Protection Agency (US EPA) will begin to require stricter rules and regulations for deicing chemicals used. More importantly, snow and ice accumulation at airports dramatically increases the risk for a variety of tragic accidents to occur. Additionally, delayed and cancelled flights due to snow and ice removal significantly hinder airlines.

Photovoltaics (PV) is the process by which light source is converted into usable electricity (Mooney *et al*, 1997). While a photovoltaic energy system has high initial costs, the subsequent energy costs are minimal. When coupled with an energy storage bank of deep cell batteries, a PV system is capable of providing electric energy constantly.

The most recent implementation of a conductive concrete system is in Roca, Nebraska (Tuan, 2004), where the University of Nebraska in Lincoln constructed a bridge deck overlay. Tuan and his team used a proprietary concrete mix design and energy from the electric grid to power his system. In this thesis, a conductive concrete mix will be developed. In addition, solar energy will be coupled with the electrically conductive concrete to assist in developing a safe airfield runway and taxiway in cold, wet weather conditions.

Primary Objectives

To satisfy the requirements for a successful self-sustainable anti-icing system, the following objectives will be investigated:

- Optimizing the concrete mix design to achieve high electrical conductivity
- Developing a self-reliant system
- Ensure uniform heat distribution throughout the pavement surface

Approach

Research was conducted on a 20' x 24' test slab. It includes a 10" base mat slab of unreinforced 4,000 psi conventional concrete. The base mat supports a 4" thick concrete overlay. The overlay consists of 10 conductive concrete panels and two conventional concrete panels each 4' x 10'. The conductive concrete panels are designed and constructed for high electrical conductivity, relatively high compressive strength, and high flexural strength. The experimental test system is located at the University of Arkansas Engineering Research Center in an open area exposed to full sunlight to maximize solar panel energy production.

The 4" overlay is divided into ten 4' x 10'conductive concrete panels and two conventional concrete panels. The conductive concrete mix design consists of electrically conductive particles

including graphite powder and steel fibers. Two 4' x 10' panels are used as a control and located at the slab end. Consequently, the control panels serve as a basis to compare temperature results with the conductive concrete overlay panels.

The conductive concrete system using photovoltaic energy consists of solar panels, a battery storage bank, and the conductive concrete overlay, Figure 1.1. A regulator is included in the system to direct energy to the battery storage bank and then into the concrete overlay.

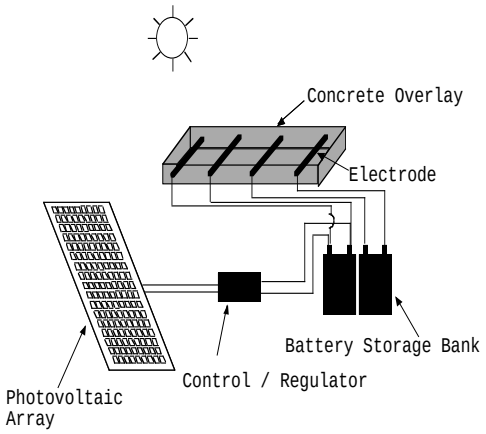

Figure 1.1: Conductive Concrete System Using Photovoltaic Energy

Electrodes within the conductive concrete slab are sized and positioned to create a uniform temperature field throughout the panels. Since direct sunlight is not always readily available, batteries are incorporated into the energy system to store energy and provide energy during times when sunlight is unavailable. Size and the number of batteries required were determined based on the test mat energy demand. Energy usage and internal slab temperature are monitored continually using thermocouples that are embedded within the slab.

CHAPTER 2: LITERATURE REVIEW

This literature review includes:

- general information about concrete temperature effects
- anti-icing and deicing procedures
- electrically conductive concrete
- photovoltaic energy.

The purpose of this review is to identify previously used methods of preventing snow and ice accumulation on pavements while identifying the modes at which concrete fails in both cold weather and high temperatures.

How Temperature Affects Concrete

According to ACI Journal 306R (ACI Committee 306, 1992), the surrounding environment is defined as being cold when two conditions exist: [1] the air temperature for any 12 hours of a 24-hour period is equal to or less than 10^{o}C (50^{o}F) and [2] the average of the maximum and minimum air temperatures documented on three consecutive days is equal to or less than 5^{o}C (40^{o}F). Concrete fails due to freezing action: internally and/or externally (Peterson *et al*, 2007). An example of external failure is scaling, or surface cracking. Conversely, internal failure may develop when concrete is exposed to numerous freeze-thaw cycles. An example of internal failure would be spalling. Internal damage, in the form of small microscopic cracks within the structure, deteriorates the slab structural integrity by weakening the concrete mechanical properties and is consequently more difficult to protect against and detect in the field.

As water undergoes freezing within the concrete matrix air cavities, it expands about 9 percent in volume from its liquid state to its solid state (Powers, 1975). Lack of air cavity volume restricts water's ability to expand and is the primary reason concrete deteriorates in cold weather climates. Due to the variability in concrete's air cavity size, the time it takes for water to freeze within a concrete mix varies. Frost action occurs when internal stresses are developed from freezing the concrete structure, and water molecules within the concrete expand. Since concrete is subjected to countless freeze-thaw cycles, preventing frost action is critical. Frost action results in the following: spalling, deterioration line cracking, scaling, and pattern cracking.

a) Spalling (Browning *et al*., 2007, Lee *et al*., 2000) – Spalling results from water entering concrete and forcing surface concrete to peel or pop off, Figure 2.1. If deicing salts are used to protect against ice, salt mixes with surface water and permeates through spalling concrete to cause deterioration. Additionally, salt water permeating to rebar causes it to corrode and swell. This swelling results in additional spalling. Extreme cases of spalling can cause steel rebar exposure.

Figure 2.1: Effects of spalling, exposure of steel rebar (Buell, 2009)

b) Deterioration-Line (D-Line) Cracking (Browning *et al*., 2007, Lee *et al*., 2000) - D-line cracking results from water entering the pavement joints that run parallel to the concrete surface joints. Figure 2.2 shows that over time, these cracks begin to occur further away from the joints.

Figure 2.2: D-Line cracking at joints of slab (Omaha, 2012)

c) Scaling (Browning *et al*., 2007, Lee *et al*., 2000) – Concrete scaling occurs when the cement paste deteriorates at the surface and exposes the coarse aggregate, Figure 2.3. Scaling usually occurs as a result of chemical reactions between the cement paste and deicing chemicals. Small particles or flakes are gradually lost due to the formation of brucite or magnesium silicate hydrate.

Figure 2.3: Scaling of aggregate (Concrete Ideas, 2011)

d) Pattern Cracking (Browning *et al*., 2007, Lee *et al*., 2000) Pattern cracking results from volume changes caused by embedded water that expands and contracts due to freeze-thaw cycles, Figure 2.4.

Figure 2.4: Pattern cracking of concrete pavement (LGAM, 2011)

Concrete damage during freeze-thaw cycles occurs from a pumping action created by the expansion and contraction of water. After multiple freeze-thaw cycles, the concrete structure becomes fully saturated with no additional void space for future water passage. After the

concrete system attains a fully saturated state, additional water freezing causes microscopic cracks to provide pathways for the newly formed ice crystals to expand (Petersen *et al*, 2007). Conversely, in 1975 Powers concluded that concrete is not a closed vessel and that all concrete contains enough air voids to account for the increase in water volume when frozen (Powers, 1975). The stress that occurs from frost action is not from freezing, but from the expanded water being absorbed during the cooling process. Powers hypothesized that these stresses are created from water flow away from the regions of freezing where the resistance of the water flow at a given rate is proportional to the flow path length. Once this additional hydraulic pressure exceeds the enclosing material strength, material cracking develops.

Effects of High Temperatures on Concrete

Concrete structures and materials are known for their exceptional resistivity to temperatures up to 400° C (750° F) and little deterioration is found when concrete is exposed up to these high temperatures. Resistance to high temperatures in concrete is dependent on many material and environmental factors (Khoury, 2000). According to Khoury, the main material factors are: physicochemical changes in the cement paste, physicochemical changes in the aggregate and thermal incompatibility between the aggregate and cement paste. Environmental factors also influence concrete deterioration. These environmental factors include: (1) temperature level, (2) heating rate, (3) applied load, (4) and the concrete structure's external sealing, which influences moisture loss from the surface.

There are three elevated critical temperatures for concrete (Khoury, 2000):

- 250° - 400° C (480° - 750° F): Critical surface temperature for spalling
- ≈ 300° C (≈ 570° F): Critical temperature for the initiation of strength loses

- 550° C - 600° C (1,000° - 1,110° F): Temperature that there is a generic loss of load bearing capacity

As temperatures increase, mechanical properties such as strength, modulus of elasticity, and volume deformation degrade (Bingöl *et al*, 2009). This results in deterioration of concrete quality. Of the damaging mechanisms that are present in concrete at high temperatures, the formation of mesocracks due to thermal expansion is the most destructive (Xuan *et al*, 2009). Mesocracks often form between the interface of limestone aggregate and cement paste, the weakest region in the concrete structure. Mesocracks are a result of thermal induced stress around the limestone aggregate. At a room temperature of 20° C(70° F) to 100° C (212° F), these tangential mesocracks between the aggregate and cement paste are the dominating cracking pattern. It has been recorded that between room temperature and approximately 170° C (340° F), peak tensile stress around the limestone aggregate occurs at 110° C (230° F), with a maximum tensile stress of about 10.0 MPa (1,450 psi) (Xuan *et al*, 2009).

Starting at 110° C (230° F), dehydration of water molecules chemically bonded to calcium-silicate-hydrate (CSH) becomes apparent (Bingöl *et al*, 2009). Thus, a reduction in CSH hydration causes a decrease in concrete strength. During their research, Bingöl *et al* (2009) found that concrete loses 9 percent of its original compressive strength when it is exposed to 100° C (212° F) and then allowed to air cool to room temperature. Arioz also noted that at the same temperature range, 10 percent of the split tensile strength is lost (Arioz 2009). At temperatures of 530° C (990° F), one of the most important compounds of cement paste, $Ca(OH)_2$, begins to breakdown. This results in concrete shrinkage.

Concrete water content decreases at higher temperature, which negatively impacts concrete structural integrity and reduces concrete material weight (Willam *et al,* 2005). Weight reduction infers air void growth. An increase in air voids greatly increases the electric current path length; therefore reducing conductivity.

Figure 2.5: Effects of fire and rapid heating rates on conventional concrete (Hale, 2010).

For the purposes of this research discussed in this thesis, temperature will not exceed 100° C (212° F). 45° C (113° F) was the maximum concrete temperature that occurred during this research. Accordingly, the effects of high heat considering electrically conductive concrete are inconsequential.

Surface Cracking in Concrete

Thermal cracking occurs when the internal temperature of the concrete structure differs from the surrounding ambient temperature (NRMCA, 2009). Cracks form when cooler concrete portions contract more than warmer sections. These warmer concrete portions restrain the cooler portions from contracting, thus inducing a thermal crack. If the concrete section is restrained

from contracting, tensile stresses developed may exceed the in-place concrete tensile strength (NRMCA, 2009).

Recognizing thermal cracking is easily identifiable. Thermal cracks occur within a few days of casting and formwork removal along the pavement surface. The cracks can result in the form of lines running perpendicular to joints and also in a checkerboard pattern occurring throughout the length of the concrete pavement. Cracking creates barriers to the electric current flow path in the conductive concrete overlay, which results in a reduction in the conductive concrete's conductivity.

Plastic shrinkage cracks occur on the surface of fresh concrete after it is allowed to set and during its plastic stage (NRMCA, 1998). The cracks occur perpendicular and parallel along the horizontal surface of the concrete. While these cracks rarely impair the concrete compressive strength, they can be detrimental to the conductivity of the concrete panel.

Plastic shrinkage cracks are caused by a rapid loss of surface water due to high temperatures or prolonged exposure to the sun. When the rate at which water evaporates from the surface exceeds the rate at which water bleeds to the concrete surface, plastic shrinkage cracks are formed. A tensile force is formed below the surface, and thus a crack is formed. Several conditions exist that cause concrete to form plastic shrinkage cracking; they are:

1. Wind velocities that exceed 5 miles per hour
2. High ambient or environmental temperatures when compared to the concrete temperature
3. Low relative humidity

Anti-Icing and Deicing Procedures

There is an increasing need for an effective solution to minimize ice and snow impact on transportation systems. In the past, deicing chemicals, including salts, have been used on pavement surfaces. Although this technique to rid ice is effective, deicing chemicals can cause reinforcing steel corrosion within concrete pavements (Browning *et al*, 2007; Lee *et al*, 2000). Steel reinforcement within a concrete pavement begins to corrode when exposed to a combination of water and deicing chemicals, that includes chloride and/or acetate. Deicing chemicals cause physical and chemical transformations in the cement paste and aggregates. Steel reinforcement corrosion is costly to restore. Additionally, when used in large amounts, deicing chemicals and salts can be detrimental to the surrounding environment.

There are several different chemical deicing solutions that are currently being used. These solutions can be separated into two categories; deicing solutions containing chloride salts and solutions containing acetate salts (Browning *et al*, 2007). In 2000, Lee *et al*. (2000) studied salt effects on concrete during freeze/thaw and wet/dry conditions. When subject to deicing salts such as sodium chloride and calcium chloride at low concentrations, concrete showed relatively minimal deterioration and cracking when compared to acetate of the same quantities. Although the concrete displayed greater deterioration at high chloride concentrations, this was quite low in comparison to deicing chemicals containing acetate. Damage caused by chemicals containing acetate appeared to result from the development of crystalline structures within the concrete. Other chemicals considered in the Lee *et al.* (2000) study were magnesium chloride and calcium magnesium acetate. Even at low concentrations, magnesium chloride and calcium magnesium acetate resulted in significant concrete damage. While these chemicals are beneficial for deicing, they can significantly deteriorate the concrete structure over a long time period. Deterioration

due to magnesium chloride and calcium magnesium is generally due to the formation of brucite (Browning *et al*, 2007; Lee *et al*, 2000) and is formed when cement paste or concrete is exposed to concentrations of magnesium. Brucite is the mineral form of magnesium hydroxide and is an expansive gel-like material. Once brucite is produced within the concrete structure, cracks are created.

Techniques to prevent ice accumulation without using deicing chemicals are currently under research. Research is currently being conducted on heat pipe exchangers, heat pumps, and geothermal heat pipes. Heat pipe exchangers are being used in China as a way to prevent ice and snow accumulation (Wei *et al*, 2011). These pipes use a fluid that evaporates when heated and condenses into liquid form when cooled. A heat pump enables this process to be repeatable through raising the temperature of the cooled fluid. When the heated fluid rises to the top of the heat exchange pipe embedded within a concrete pavement, heat energy is transferred from the heat exchange pipe to the pavement. Once this heat transfer occurs, the evaporated liquid condenses to tiny droplets that fall to the bottom of the pipe due to gravity. Ammonia is commonly used since it does not freeze in the considered temperature range. The primary disadvantages to this process are the high construction and maintenance costs. Together, the drilling process and pipe assembly account for the majority of the cost.

Another technique for deicing roads was developed in the late 1950s in the United Kingdom (Tuan, 2004). This procedure included the use of electric heating cables that were embedded into the pavement at the road pavement-foundation interface. This method for deicing proved very effective by transferring heat from the embedded cables to the slab to melt the ice or snow evenly throughout the concrete slab. A high density of cables was required throughout the

concrete in order to produce an even heat distribution. The major disadvantage to using electric cables is due to their very high installation costs.

Most recently, the Federal Aviation Administration is currently funding a project at Binghamton University in New York to implement a radiant geothermal heating system. The Binghamton University geothermal heating system uses water that is pumped underground to absorb the earth's natural geothermal energy. This energy is then pumped through a piping system to distribute the energy evenly throughout the runway pavement (Binghamton, 2010).

Electrically Conductive Concrete

Promoting electric flow through concrete is a relatively new idea. Major research has been done in the past 15 years to implement the use of steel and graphite in concrete to increase its electrical conductivity (Xie *et al*, 1995; Yehia *et al*, 1999, 2000, 2004). There are two types of electrical conduction that occur in a moist specimen: electronic and electrolytic. Electronic conduction is the movement of electrons in conductive materials such as carbon and steel particles. Conversely, electrolytic conduction is the movement of electrons in the specimen's pore solution. Conductive concrete is unique from other concrete mixes in that it contains electrically conductive particles to reduce the material's electrical resistivity. Conductive concrete's advantageous characteristic is its ability to transfer heat in a concrete mass uniformly. A conductive concrete energy system converts electricity entering the concrete mass into a uniform heat field. Consequently, the conductive concrete system provides a means to melt ice or snow by converting a material used for its strength properties into an above freezing temperature slab. In metals, such as graphite and steel, freely moving valence electrons transfer not only electric current but also heat energy as well. An energized conductive concrete system is composed of an electric energy source and conductive concrete with embedded electrodes

positioned to introduce energy to the concrete to create an electrical circuit throughout the concrete mass.

Conventional concrete has minimal electrical conductivity. The reciprocal of electrical conductivity is electrical resistivity. Typical normal weight concrete has an electric resistivity range of 6.54-11 kΩ*m (Xie *et al*, 1995). This range is very high in comparison to a known electrical conductor such as copper, which has an electrical resistivity of 1.68×10^{-8} kΩ*m. Consequently, conventional concrete is a good insulator but a bad conductor. Two ways are used to increase concrete conductivity: [1] the addition of conductive aggregates, such as iron ore or slag or [2] introducing conductive particles, such as steel fibers, carbon or graphite powders. A patent for conductive concrete exists (Xie *et al*, 1995), and the specific mix proportions are proprietary.

Tuan (2004, 2008) tested several hundred concrete batches to optimize the concrete mixture proportions within a conductive concrete mix. His research found that adding steel fibers at 20 percent by concrete volume, lowered the concrete's electrical resistivity to 2.2×10^3 Ω*m. This decrease in resistivity is due to the interaction of the steel fibers to create an electrical flow path through the concrete mass between the embedded electrodes. Further research considered implementing carbon and graphite powders to provide an improved electrical travel path (Xie *et al*, 1995, 1996). Many different graphite grain sizes and multiple graphite grain size distributions were considered. Tuan found that a mix design including 25 percent by volume of variable sized carbon particles and 1.5 percent by volume of steel fibers produced a concrete mixture with adequate structural strength and low resistivity. This mix design yielded an electrical resistivity range between 0.101-0.435 Ω*m, 0.00151 percent of conventional concrete's electrical resistivity.

Electrical resistivity is measured by applying a known current, I, to two embedded electrodes in the material under analysis. The resistance, R, can then be determined from the drop in voltage, V, using Ohm's Law:

$$R = \frac{V}{I} \qquad (1)$$

The material's resistivity, ρ, is a material property. It is equal to:

$$\rho = \frac{RA}{L} \qquad (2)$$

where ρ is the material's average electric resistivity, L is the electrode spacing, and A is the cross-sectional area of the testing material parallel to the electrodes that the current flows through.

There are two different concrete mixtures typically used to create conductive concrete. The first design mixture procedure involves adding steel fibers and graphite particles to a conventional concrete mixture. This design has a high electrical resistivity at about 0.100 Ω*m, however, the mechanical properties are comparable to normal weight concrete (Yehia *et al*, 1999, 2000, 2004). The second design incorporates conductive aggregate. While the addition of conductive aggregate lowers the relative compressive strength of the concrete, the electrical resistivity of the mix ranges between 0.010-0.030 Ω*m.

The transfer of electricity through concrete is greatly dependent on the contact area between adjacent conductive particles. Consequently, the purpose of adding conductive particles is to reduce low conductivity concrete mass between particles. Movement of electrons in concrete freely occurs when particles are in continuous contact with each other. This phenomenon is called "electrical percolation" in concrete (Xie *et al*, 1996). To enhance electron movement, different steel fiber lengths are incorporated to enhance mechanical properties as well

as to improve conductivity. Short fiber lengths and carbon powder optimize current travel between adjacent conductive masses.

Photovoltaic Energy: A Renewable Energy Source

Photovoltaics (PV) is the process of obtaining renewable energy by converting solar radiation into direct current (DC) electricity (Mooney, 1997). Light sensitive diodes, called solar cells, are configured in an array to comprise a complete solar panel. When solar radiation enters a solar cell, the photons provided by the radiation energize the electrons within the solar cell to a higher state of energy. The energized electrons produce DC electricity, which can either be used for immediate usage or stored in a battery for later usage. A two to four inch square individual solar cell can produce a half of a volt DC voltage.

The factors that control energy production from a solar cell are the intensity of the light source, and the solar cell surface area. Due to sun availability during a 24-hour time period, batteries are integrated into PV systems to store energy for later usage when sunlight is unavailable. By implementing renewable PV energy with conductive concrete, it is envisioned that an airfield pavement system can be developed that is self-sufficient in preventing snow and ice accumulation on airport runways.

CHAPTER 3: ELECTRICALLY CONDUCTIVE CONCRETE MIX DESIGN

Electrically Conductive Concrete Overview

The idea of using concrete as a semiconductor, rather than an insulator, is relatively new. Research is being conducted worldwide using electrically conductive concrete for a wide variety of uses including: grounding and shielding, storage battery pavement, and data storage and transmission (Miller and Ramme, 2011).

Typical concrete includes some form of the following: coarse and fine aggregates, cementitious material, and water. Other materials such as fly ash, high range water reducers, air-entraining agents, and lightweight aggregates are alternative components introduced to normal concrete mix designs to alter its characteristic properties. When electrically conductive particles replace coarse and fine aggregates, concrete's ability to improve electric flow dramatically increases. Consequently, adding electrically conductive particles to concrete transforms concrete from an insulator to a semiconductor.

Conductive Concrete Heating

The process incorporated to heat conductive concrete is called Joule heating. Joule heating is the process by which heat is released when an electric current passes through a conductor (Freedman, 2007). Joule heating is caused by the electrons interacting with the atomic ions of the conductor. Kinetic energy is released during this interaction by the electric current when it comes into contact with ions of a conductor, which in this case is concrete. Consequently, the release of kinetic energy creates heat and causes a temperature increase in the concrete. Joule's first law is as follows:

$$q = I^2 \cdot R \cdot t \qquad (3)$$

where q is the heat generated by a constant current I flowing through a conductor of electrical resistance R, for a time t.

This heat energy is distributed evenly through the concrete mass by heat conduction (Corson, 1962).

The three-dimensional governing equation for an electric field is given as

$$\frac{\partial}{\partial \mathrm{x}}\left(\kappa \frac{\partial \mathrm{V}}{\partial \mathrm{x}}\right)+\frac{\partial}{\partial \mathrm{y}}\left(\kappa \frac{\partial \mathrm{V}}{\partial \mathrm{y}}\right)+\frac{\partial}{\partial \mathrm{z}}\left(\kappa \frac{\partial \mathrm{V}}{\partial \mathrm{z}}\right)=0 \qquad (4)$$

where V is the electric potential, and κ is the electrical conductivity of the conductive concrete. In Equation (4), conductivity and resistivity are reciprocals of one another.

The three-dimensional heat conduction equation for internal heat generation is given as

$$\frac{\partial \mathrm{T}}{\partial \mathrm{t}}=\alpha\left(\frac{\partial^2 T}{\partial x^2}+\frac{\partial^2 T}{\partial y^2}+\frac{\partial^2 T}{\partial z^2}\right)+\mathrm{q} \qquad (5)$$

$$\alpha=\frac{k}{\rho c_p} \qquad (6)$$

where T is the temperature and is a function of time. α is the thermal diffusivity where k, ρ, and c_p are the thermal conductivity, mass density, and specific heat capacity, respectively. The heat generation rate is q.

Joule heating in conductive concrete is a function of electric current and heat generation. The three-dimensional equation for heat generation due to an electrical current is expressed as:

$$q=\kappa(\mathrm{T})\left(\left(\frac{\partial \mathrm{V}}{\partial \mathrm{x}}\right)^2+\left(\frac{\partial \mathrm{V}}{\partial \mathrm{y}}\right)^2+\left(\frac{\partial \mathrm{V}}{\partial \mathrm{z}}\right)^2\right) \qquad (7)$$

There are three governing equations that must be satisfied, however the three equations are coupled, or linked together. Equations 4, 5, and 7 are coupled since electrical conductivity is a function of temperature. Boundary conditions for the coupled equation must satisfy energy balance along the surface of the solid. With no imposed external thermal flux, and neglecting radiation thermal flux, the following boundary conditions are imposed:

$$-k\left(n_x\frac{\partial T}{\partial x}+\ n_y\frac{\partial T}{\partial y}+\ n_z\frac{\partial T}{\partial z}\right)=\ h_b(T-T_a) \qquad (8)$$

where n_x, n_y, and n_z are unit normals to the surface, h_b is the convective heat transfer coefficient, T is the temperature at the boundary point, and T_a is the ambient temperature at the surface point.

The solution process for Joule heating involves a numerical solution using iterative calculation procedures. The electrical conductivity, k, is a material property and a function of temperature. The iterative process begins by determining a conductivity field from an assumed temperature, T. The electrical potential field, V, is then calculated from equation (4) and used in equation (7) to approximate the heat generation rate per unit volume, q. The temperature field, T, is then recalculated in equation (8). Lastly, this calculated temperature, T, is compared to the assumed value of T at the beginning of the process. This process is continued until the assumed and calculated values demonstrate convergence. Coding software using numerical algorithms for thermoelectricity are included in ANSYS and are publically available.

Concrete Materials

The materials used for trial batching are summarized in Table 3.1. These materials are consistent throughout each trial batch.

Table 3.1: Basic Concrete Materials Used for Testing	
Material	**Classification**
Cement	Type I
Fly Ash	Class C
Coarse Aggregate	Maximum Aggregate Size ½" Crushed Limestone
Fine Aggregate	River sand with fineness modulus of 2.50
High Range Water Reducer	Adva Cast 575 Superplasticizer
w/c	0.35-0.42

Limestone and river sand aggregates, Class C fly ash, and Adva Cast 575 superplasticizer were used for all test batching because of their availability at the Engineering Research Center in Fayetteville, Arkansas. Water to cement ratios (w/c) were chosen based upon previous research done by Xie et al. (Xie, 1995) and Tuan et al. (Tuan, 2004) and modified accordingly.

During his research, Tuan et al. (Tuan, 2004) used a variety of conductive materials in attempts to decrease the electrical resistivity of concrete. Initially, steel shavings were used as the primary source for electrical conductivity. These shavings are a waste product and consequently need to be properly washed and cleaned before they are usable. The steel shavings were very inconsistent in size and shape and therefore eliminated from future mix designs. It is at this point in Tuan's research, that he began using graphite powder as the conductive element in the concrete mix design.

Graphite Powder

Graphite is an allotrope of the chemical element carbon (Carbons, 2011). Allotropy is the property of a chemical element to occur naturally in two or more different forms. Graphite is the most stable carbon form and is considered as the highest grade of coal. Graphite is found naturally and classified as a semimetal, a strong electrical conductor.

There are three main types of graphite: crystalline flake graphite, amorphous graphite, and vein graphite. Of the three types, the crystalline flake graphite is the most common. The crystalline flake graphite, shown in Figure 3.1, along with steel fibers, are the materials used in this research to create concrete's electrical conductivity. All graphite powder for the research work in this thesis was provided by Asbury Carbons. The trial sizes for the graphite powder ranged from 44-850 microns. Figure 3.2 shows a sieve analysis for each graphite powder grade considered during this research for trial batching.

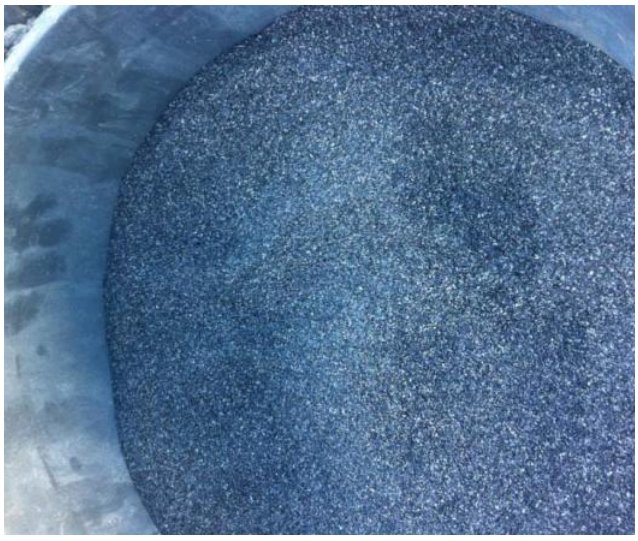

Figure 3.1: A4071 Graphite Powder from Asbury Carbons (Osweiler, 2012)

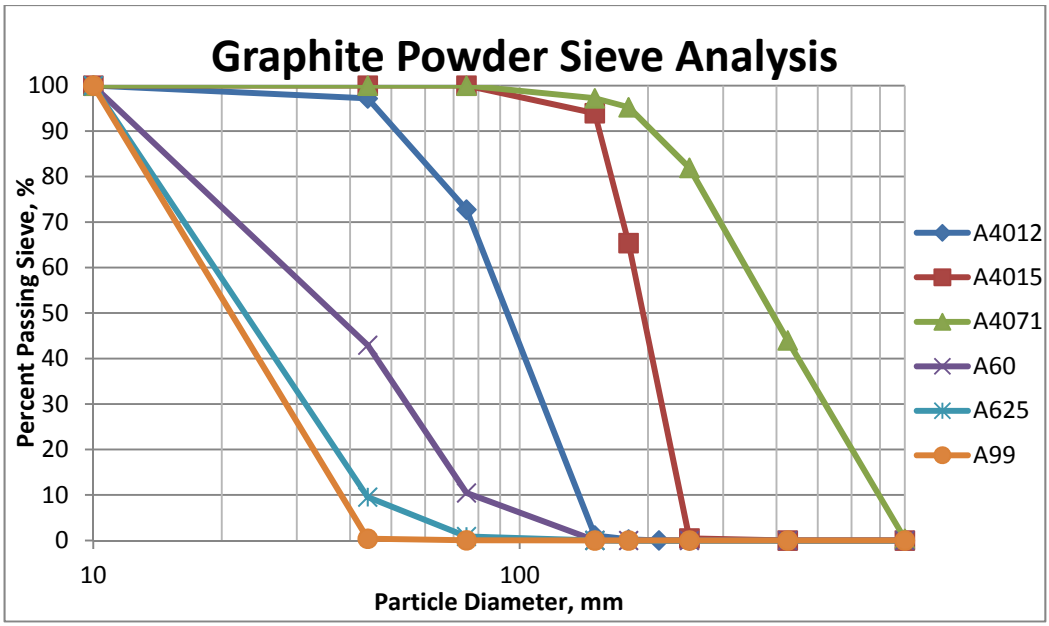

Figure 3.2: Graphite Powder Sieve Analysis

Steel Fibers

Steel fibers in concrete have been used to increase flexural strength, crack and impact resistance, and also as a secondary form of tensile reinforcement. Steel fibers were used to improve the conductivity of the concrete material. Low carbon, cold drawn steel wire fibers, as shown in Figure 3.3, were used in the conductive concrete mix design. Table 3.2 shows the specific properties of the steel fibers acquired from the company Propex.

Table 3.2: Steel Fiber Properties	
Fiber Length:	1.5 in
Equivalent Thickness:	0.045 in
Tensile Strength:	Minimum 140 - 180 Ksi (966 - 1242 MPa)
Fire Classification:	UL Report File No. R14701 (N).
Aspect Ratio:	34 and 44
Conformance:	ASTM A 820/A 820M, Type V.

Figure 3.3: Steel fibers used in the conductive concrete test samples (Osweiler, 2012)

Blast Furnace Slag Aggregate

By definition, blast furnace slag aggregates (BFSA) are the non-metallic by-product of steel manufacturing (Slag, 2010). BFSA is developed in a molten condition simultaneously with iron during the steel manufacturing process. BFSA exhibit mechanical properties that are

comparable to natural stone aggregates used in concrete batching. Compressive and flexural strength, durability, and resistance to abrasion are similar, if not better, to that of natural aggregates.

Since BFSA is a by-product of steel manufacturing, it was thought that a residual amount of metallic particles may be embedded in the cavities of the aggregate. Figure 3.4 shows a close up view of coarse BFSA. Although small, any additional metallic particles within the aggregate would improve the concrete conductivity if it were used as a substitute for limestone aggregate. It was this reason BFSA was considered for two of the eleven conductive concrete trial batches in this research. However, test results during this study, which are included in Table 5.1, showed that BFSA did not improve the overall conductivity of the concrete.

Figure 3.4: Coarse blast furnace slag aggregate (Levy, 2012)

High Range Water Reducer

When replacing fine aggregate with graphite powder during the study, there was a need to increase the w/c to ensure acceptable material workability. Since the w/c was fixed at 0.4 to develop adequate compressive strength, a high range water reducer was used as an admixture.

The initial conductive concrete mix design used six fluid ounces of HRWR per 100 lbs of concrete. While this dosage of HRWR gave a 3.5" slump, higher dosages were considered to acquire an upper bound dosage without compromising the concrete compressive strength and without developing aggregate segregation and water bleeding.

Conductive Concrete Design Procedure

The major difference between conductive concrete and normal concrete is the inclusion of graphite powder and steel fibers. The steel fibers were added to each individual test batch in accordance to ASTM C 1116C/ 1116M and ASTM C 1436 as specified by the material's supplier. Graphite absorbs water depending on its particle size; finer particles absorb more water per unit weight due to increased surface area. For the mix design procedure, graphite powder was assumed to have the same moisture content as the fine aggregate it replaced.

At project initiation, the gradation, size, and required graphite powder volume was unknown and needed to be evaluated to obtain an optimal mix design. In Mix Trial 1, equal percentages of each A60, A99, A625 graphite powder were used. This very fine graphite powder mix resulted in a high water demand, poor workability, and very low compressive strength. This initial mix was tried with the intent to optimize conductivity with no regard for strength. As seen in Figure 3.5, the preliminary conductive concrete design resulted in a very dry mix with low

workability. Figure 3.6 shows the results of a compressive test for the preliminary conductive concrete design. Figure 3.7 illustrates compressive test results from Test Mat 2.

Figure 3.5: Preliminary conductive concrete workability (Osweiler, 2012)

Figure 3.6: Preliminary conductive concrete compressive test results (Osweiler, 2012)

Figure 3.7: Compressive test results for Trial Mix 2 (Osweiler, 2012)

CHAPTER 4: ENERGY SYSTEM

Deep Cell Batteries

All batteries used in the system battery storage bank are deep cell batteries. A deep cell battery is designed to be capable of undergoing significant discharge cycles. While normal storage batteries are used when a short burst of high energy is needed, a deep-cell battery is used when a high constant current is needed for long time durations. Figure 4.1 shows the layout of four individual batteries used during this research.

Figure 4.1: Deep cell batteries (Osweiler, 2012)

Deep-cell batteries are made to be regularly drained down to 50% - 80% of their total capacity. For purposes of this research, 11-12V deep-cell batteries are used to store and release electricity to the conductive concrete system. These batteries are continually charged from the solar panels during sunlight and energy is discharged at a constant rate to the conductive concrete when needed to sustain an above freezing temperature in the concrete overlay.

Solar Panels

For this research work, 32 solar panels were used in conjunction with 11-12V deep-cell batteries to provide power to the concrete pavement. The following describes the average outputs for each solar panel.

Peak output for watts:	200 W
Peak output for voltage:	24 V
Peak output for amperage:	8.5 A

Two individual solar panels are wired in parallel and then four sets of solar panels are wired in series to provide energy to one battery storage unit comprised of four 12V deep-cell batteries (48V). The solar panels are supported and positioned at a constant 45-degree angle. The formwork was built to support two panels per support. This angle setting resulted in instances during the day when a shadow from one panel was cast on another panel in a parallel row. For calculation purposes, the solar panels were not used at full capacity, but at 80 percent of the total output. The energy provided by the entire photovoltaic system is sufficient enough to charge the battery storage bank in a single day. Figure 4.2 and Figure 4.3 displays the supports used to hold the solar panels in place at a 45 degree angle. Figure 4.4 demonstrates the arrangement of solar panels within the testing site.

Figure 4.2: Side view of solar panel supports (Osweiler, 2012)

Figure 4.3: Front view of solar panel supports (Osweiler, 2012)

Figure 4.4: Solar panels (Osweiler, 2012)

Solar Charge Regulator

A solar charge regulator was used in the conductive concrete system to prevent overcharging the deep cell batteries used for energy storage. A solar charge regulator controls the electric current applied to the system. The regulator controls energy flow in three ways:

1. Energy from the PV panels is directly supplied to the test mat
2. Energy from the PV panels is routed to the battery storage bank

3. Energy stored in the battery bank is fed into the test mat

DAQ System

A National Instruments data acquisition system (DAQ) was used during the heat experiments to record temperatures throughout the concrete overlay panels. A 32 channel DAQ card was installed and programmed to take temperature readings simultaneously at a one sample per ten second rate during experimentation. These readings were recorded to a computer that was programmed with analysis software created by Mark Kuss of the University of Arkansas research team. Figure 4.5 depicts the DAQ arrangement used to collect data throughout this research. A solar panel was used to support the energy demand of the DAQ system.

Figure 4.5: DAQ system arrangement (Osweiler, 2012)

Thermocouples

Type T (copper and copper/nickel alloy) thermocouples were used for temperature measurements and are capable of measuring within a -200^{o}C to 350^{o}C temperature range. Thermocouples were placed in the control mat at a 2'-4.5" spacing along the control slab centerline in Figure 4.6. The thermocouples were placed at a ½"depth from the surface. Test mat 1 includes a total of 9 thermocouples with 3 thermocouples at 2'-4.5" spacing down the centerline of each electrode pair. Test mat 1 also has a thermocouple embedded at a 3.5"depth and a thermocouple embedded at an 11" depth in the center of the slab. Test mat 2 has 6 thermocouples, with 3 thermocouples spaced equally down the centerline of each electrode pair at a ½" depth as seen in Figure 4.7. Test mats 3-10 have 2 thermocouples each located at mid length locations along the center points of each electrode spacing.

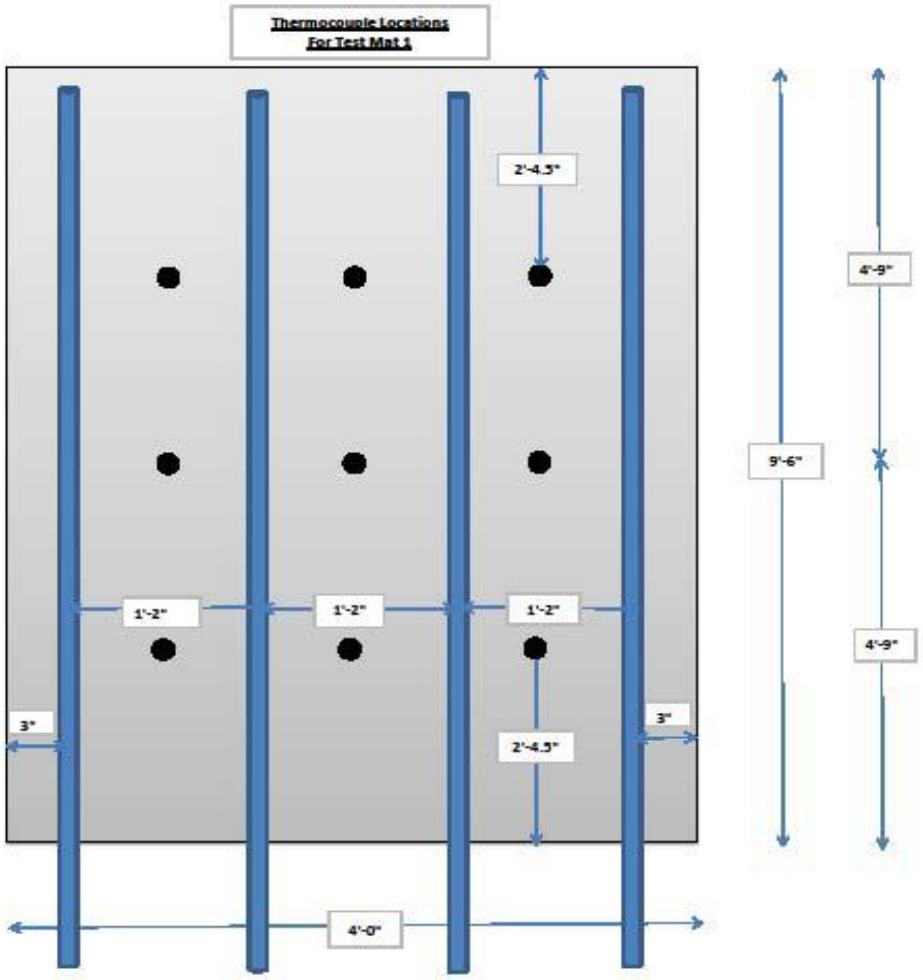

Figure 4.6: Thermocouple Location for test mat 1

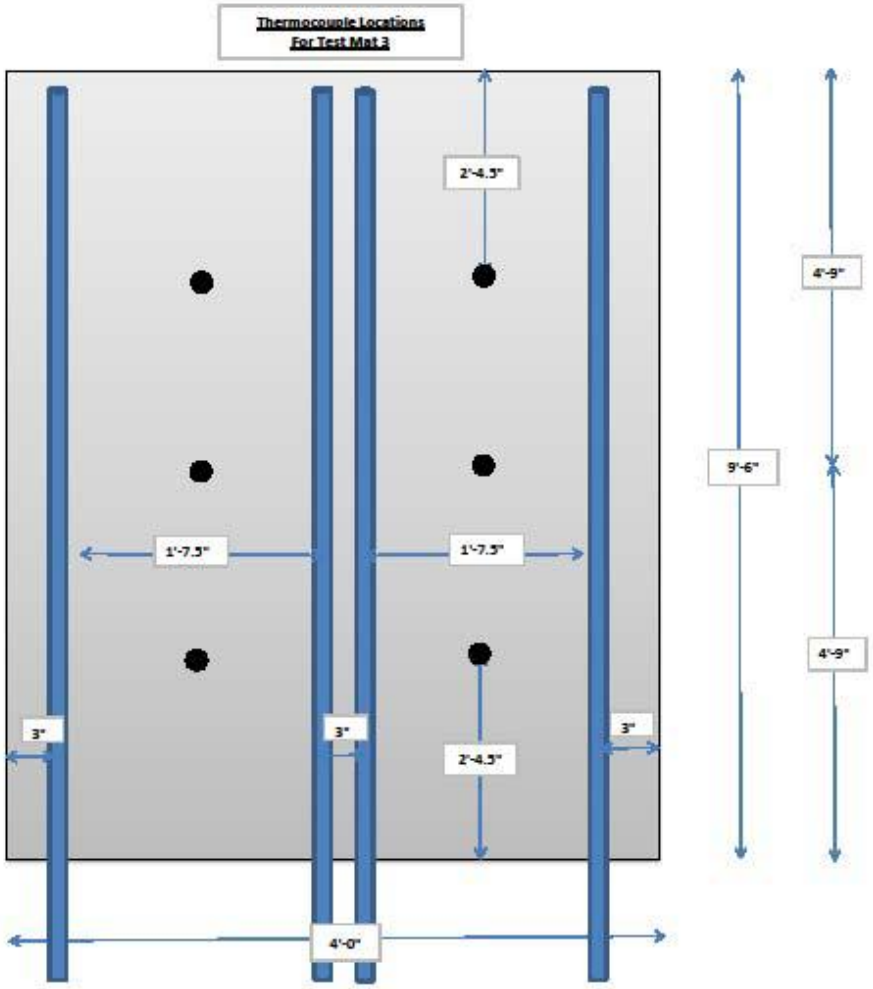

Figure 4.7: Thermocouple Location for test mat 2

Infrared Thermometer

A PCE-IR 425 Infrared thermometer was used to read surface overlay panel temperatures. The infrared thermometer has a temperature range of -60°C to 1000°C with a reading accuracy of ±2°C. The infrared thermometer readings supplemented the thermocouple readings during heating tests.

CHAPTER 5: METHODOLOGY

Optimization of Concrete Mix Design

Mix optimization was based on strength, conductivity, finishability, and workability. To increase concrete strength, lower w/c ratios are used. To increase conductivity, a high amount of fine sized graphite particles are used. The problem occurs when high strengths and high conductivity are desirable. Reducing w/c increases strength, however workability and finishability decrease due to the water demand of the small graphite particles. This water demand occurs when smaller graphite particles, with higher surface areas, are used. Conversely, using a high amount of fine particles increases conductivity, however requires a high w/c which in turn decreases the concrete strength. Table 5.1 shows each mix design along with the amount and size of graphite used, compressive strength, and electrical resistivity results.

Table 5.1: Mix design percentages, mechanical and electrical properties					
Trial	Graphite Powder	Graphite by volume, %	Steel Fiber by volume, %	Compressive Strength ($f'_{c)}$, ksi	Electrical Resistivity (ρ), ohm-in
1	A60/A99/A625	25.0	1.5	2.75	-
2	A4012	25.0	1.5	3.10	-
3	A4015	20.0	1.5	4.15	-
4	A4071	20.0	1.5	5.60	-
5	A4071	20.0	2.5	5.10	-
6	A4071	20.0	3.5	N/A	-
7	A4071	17.2	5.0	N/A	-
8	A4071	17.2	2.7	5.85	253
9	A4071	7.2	2.7	4.80	1778
10	A4071	17.2	2.7	5.70	711
11	A4071	17.2	2.7	6.15	156

The first material to be optimized was the graphite powder. Given that conductivity relies on the electric path between the electrodes, finer graphite particles were initially tried to maximize conductivity. Finer particles increase conductivity because they shorten the electric current's path. After preliminary testing, it was concluded that more coarsely graded graphite

particles were warranted because of the concrete compressive strength that was also desired. Consequently, a testing method was developed by increasing the graphite particle size incrementally until an optimal size was found. Six different graphite powder mixes were used until desired conductive concrete properties were observed. As seen in Table 5.1, the graphite powder labeled A4071 was the mix used throughout conductive concrete research.

After determining the optimal graphite powder size, the next material to be optimized was the steel fiber content. Concrete was tested with steel fibers in amounts of 1.5, 2.5, 3.5, and 5 percent by concrete volume as seen in trial mixes 4, 5, 6, and 7, respectively. It was concluded that in terms of workability and finishability, steel fibers at 2.7 percent by concrete volume were required. This percentage of steel fibers was chosen upon due to the consistent workability and finishability of the conductive concrete when compared to conventional concrete.

Considering blast furnace slag aggregate (BFSA) as a limestone aggregate replacement was the last material to be investigated in the conductive concrete optimization process. In previous work by Tuan et al. (Tuan, 2004), it was reported that BFSA could completely replace all coarse and fine aggregate and therefore allow a smaller amount of graphite powder to be used to achieve a more conductive mix design. This idea was tested because BFSA was considered to have remaining fragments of steel from refining processes. Trial mixes 9 and 10 in Table 5.1 show results of all coarse and fine aggregate replacement with BFSA. It was concluded that while the compressive strength of the BFSA concrete is comparable to normal aggregate concrete, the conductivity did not improve significantly. Consequently, BFSA was not considered in the remaining mixes for this conductive concrete research as it did not improve the concrete conductivity. Figure 5.1 shows a microscopic picture of the conductive concrete mix

after being allowed to cure for 28 days. Figure 5.2 shows an image of the contents within the conductive concrete material after 28 days of curing.

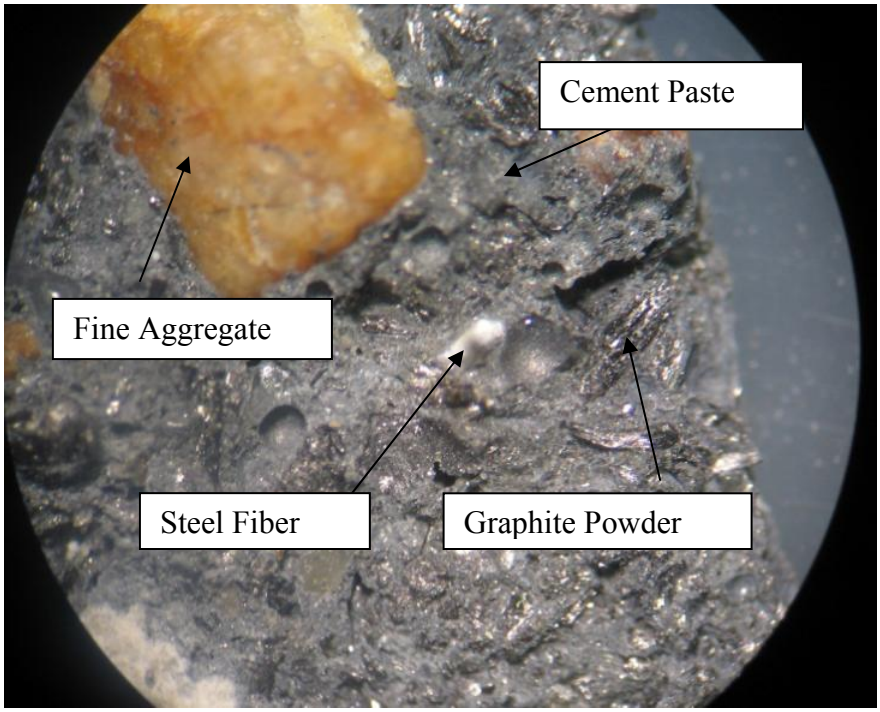

Figure 5.1: Microscopic image of electrically conductive concrete (Osweiler, 2012)

Figure 5.2: Image of materials within conductive concrete mix design (Osweiler, 2012)

Conductive Concrete Mix Procedure

The same concrete mixing procedure was used for all batch trials. During the concrete batching for the large scale test mats, 17% graphite by volume and 2.7% steel fibers by volume were used for every test slab. The concrete was mixed at the Engineering Research Facility at the University of Arkansas in Fayetteville, Arkansas. The concrete mix was then delivered to the large scale test mat, and poured for the 4" conductive concrete overlay on top of the existing 10" conventional concrete base mat as seen in Figure 5.3.

Figure 5.3: 24’ x 20’ 10” thick concrete base mat (Osweiler, 2012)

For the conductive concrete batch, graphite powder and steel fibers were added to a normal concrete mix in the following procedure:

1. The inside of the concrete mixer was sprayed with water and drained to allow materials to mix well and not accumulate on the walls of the mixer;
2. Coarse and fine aggregate were added to the concrete mixer;
3. Steel fibers were added to the aggregate mix;
4. Graphite powder was then added to the dry mix;
5. Half of the total required water was added to saturate the dry materials;
6. Cement was added to the mix;
7. Silica fume was then added to the concrete;
8. The high range water reducer (HRWR) was added to unmixed water to ensure proper distribution;

9. The HRWR/water mix was then added to the concrete and allowed to mix for a minimum of 20 minutes before being poured into the overlay forms.

For the large scale test mats, a total of 17 cu. ft. of concrete was batched for each individual mat. Shear piers were installed to achieve a bond between the base slab and the conductive concrete overlay. The shear piers were included to ensure a connection with both layers on concrete. The shear piers allowed the conductive concrete overlay to resist movement due to expansion and contraction parallel to the base slab. Three plastic 4" diameter cylinders were embedded within the base mat at a depth of 12". The elevation view in Figure 5.4 displays a four inch layer of Class 7 stone as the base course for the mat. This stone was used to create a defined layer between the concrete and existing soil. The concrete is divided into two layers: 10" of unreinforced concrete as the lower layer, and 4" of conductive concrete as the surface overlay. Figure 5.5 shows the workability and finishability of the conductive concrete.

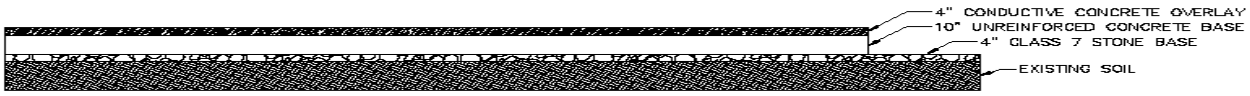

Figure 5.4: Elevation view of test mat

Figure 5.5: Finishability of electrically conductive concrete (Osweiler, 2012)

CHAPTER 6: RESULTS

Effects of Hydration on Conductivity

Concrete hydration is the process by which water comes in contact with cementitious material to form a cement paste bond between the aggregates. Cement particles within concrete hydrate while water is available. Concrete reaches 90 percent of its maximum compressive strength at approximately 28 days. Consequently, most of the moisture in the concrete has either reacted with cementitious material or evaporated at 28 days of age. While moisture within the concrete is constantly decreasing over the course of 28 days, concrete conductivity also decreases since after water's reaction with cementitious material, air voids are created.

Concrete's curing process slows down dramatically after 28 days of curing. Even though a reasonably accurate strength test can be conducted between seven and ten days, it is best for concrete to be tested at 28 days for a more accurate examination. Conductivity decreases fairly quickly for a period of ten days, and then decreases at a slower rate. As compared to concrete's strength property, concrete conductivity can also be reasonably established at ten days. Figure 6.1 demonstrates the effect of hydration on resistivity over time for the first ten days of the conductive concrete's curing process. The data points shown in Figure 6.1 are taken from the average concrete conductivity of three different trial batches.

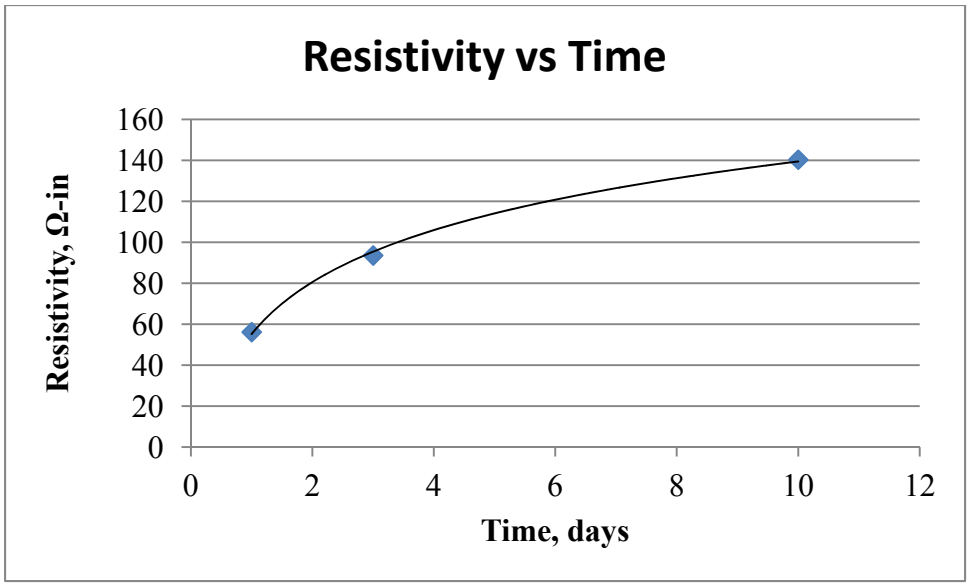

Figure 6.1: Resistivity effects from concrete hydration

Power Density

Power density, by definition, is the amount of energy transfer, or power, per unit of volume. The calculations for power density used in this research will be based upon the conductive properties found in Trial Mix 11 and a 4" thick overlay panel. The power density was calculated to optimize electrode spacing and supply voltage with respect to cost and derived power density. Figure 6.2 displays the power density of a 4' x 10' conductive concrete overlay panel using 156 Ω-in material resistivity.

Figure 6.2 is shown in multiples of 12 because during research, 12-volt batteries were used for the energy storage system. For each overlay panel, electrodes are centered 4" from the edges. Inner electrodes were then evenly spaced on the panel center line with a 3" spacing between them. These inner electrodes were given the same negatively charged polarity to control current path throughout the panel. For each individual case of electrodes, the corresponding amperages are shown in Figure 6.2.

During the research of Tuan (Tuan, 2004), the average peak power density calculated was 42 W/ft^2 for deicing during snowstorms. Conversely, for purposes of research throughout this research, energy to the conductive concrete overlay was supplied continuously to keep the concrete temperature above freezing temperatures. Electrical resistivity is dependent on material temperature. For example, an increase in temperature will result in a decrease in electrical resistivity. For purposes of this research, power density testing occurred at room temperature, 72°F. For an appropriate comparison to subfreezing temperature, Figure 6.3 illustrates the conductive concrete power density with an electrical resistivity of 468 Ω-in.

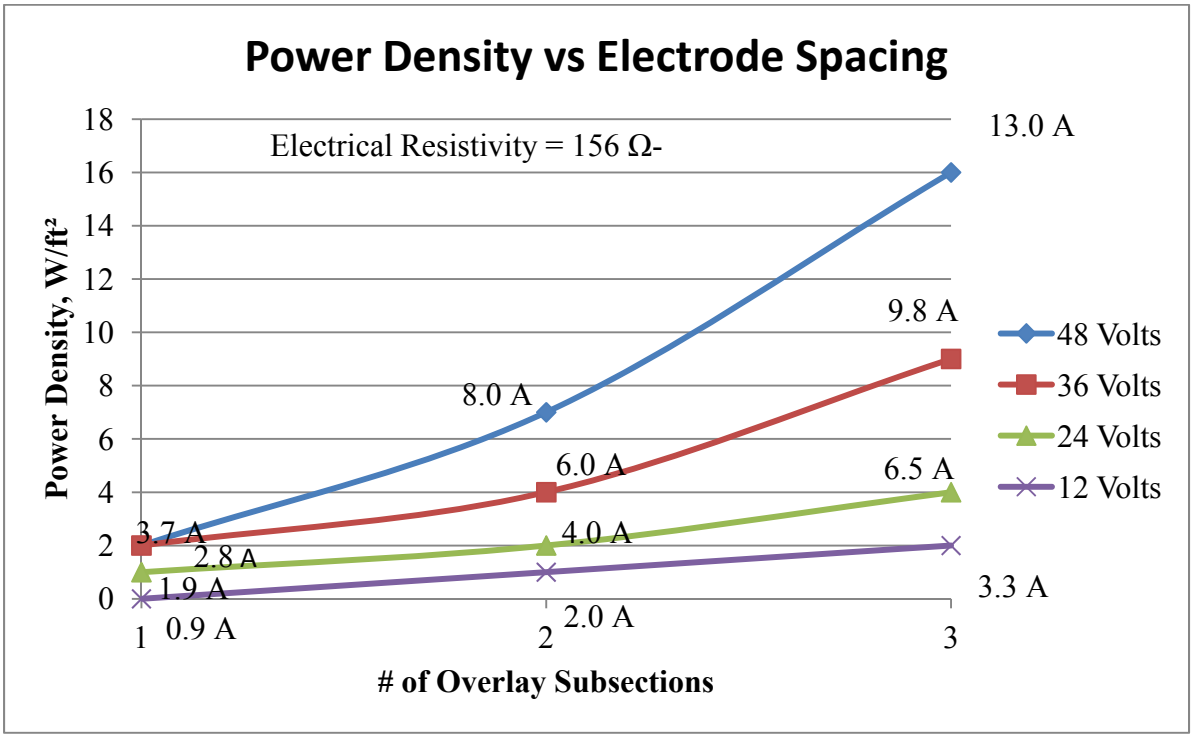

Figure 6.2: 4”x10” conductive concrete overlay panel power density, 156 Ω-in

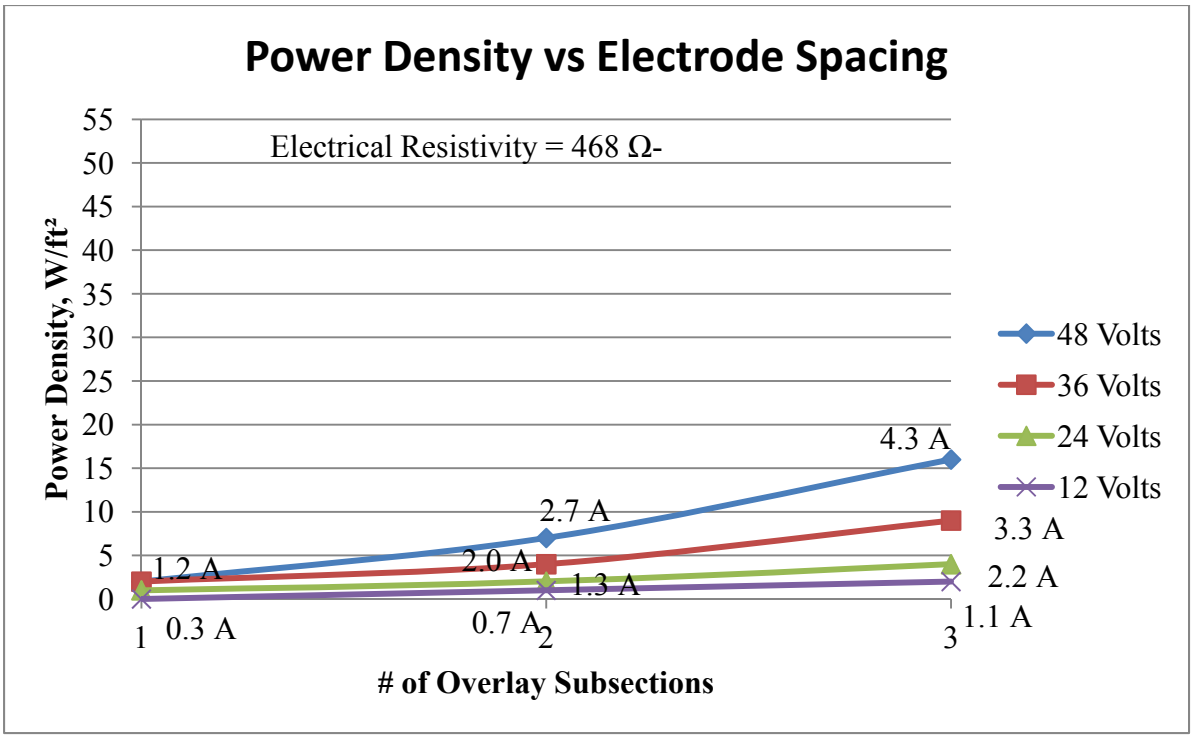

Figure 6.3: 4"x10" conductive concrete overlay panel power density, 468 Ω-in

Small Scale Heat Test

For each trial batch, three 18" x 13" x 2.5" mats were constructed and tested for conductivity and heating behavior. Figure 6.4 shows a test mat specimen under small scale heat testing conditions. Number 8 rebar were initially used as electrodes and spaced 10" apart on center. This was later revised to Number 10 rebar after electrode optimization had been tested. For the overlay panels, energy transfer between the electrode and concrete material was optimized using 1" diameter all thread zinc plated stainless steel bars. All thread bars were used to increase the electrode contact surface area.

Figure 6.4: Small scale mat under testing conditions (Osweiler, 2012)

Each test used DC current that was introduced to the mat at varying voltages. The tests were conducted in an average ambient room temperature of 72^{o} F. The voltages used were 24, 48, and 80 volts. The current going through the conductive concrete ranged from 0.2 – 3.5 amps. A thermocouple attached to the test surface and centrally positioned was used to record temperature. Figure 6.5 shows the difference in surface temperature with respect to time for trial mix 8. Since resistivity is related to temperature, it was concluded that when 80V were used as the current, the increase in temperature allowed for an even lower decrease in resistivity. This research will show that during large scale heat tests, resistivity of conductive concrete will decrease at higher temperatures as compared to lower temperatures of the same conductive concrete slab.

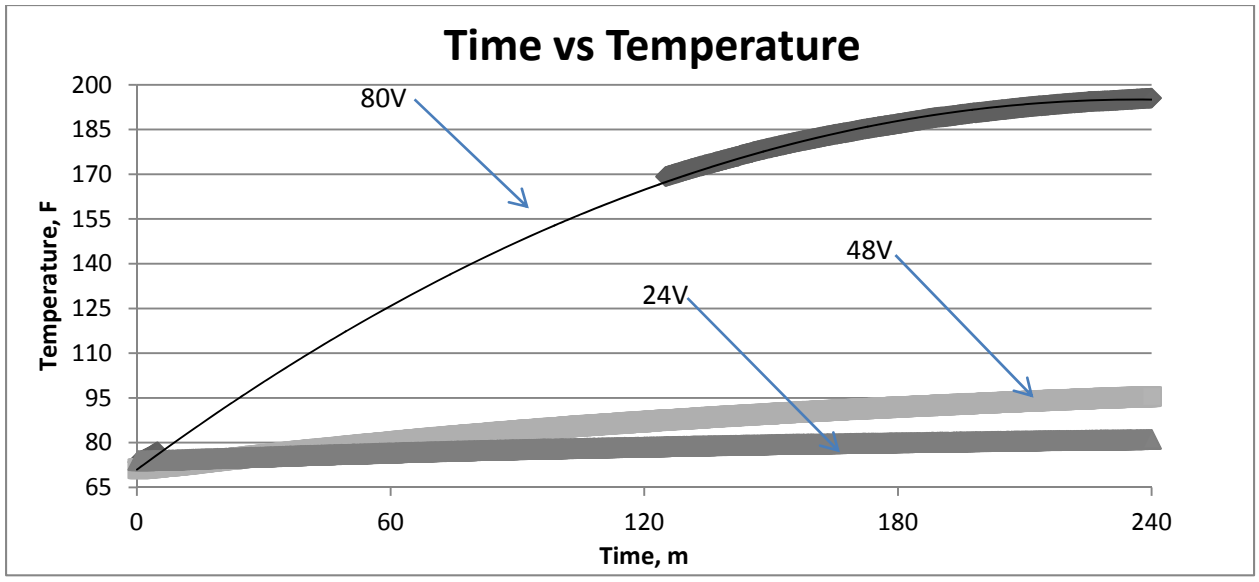

Figure 6.5: Time versus temperature graph for trial mix 8

Large Scale Heat Test

Due to the slight variability in conductive concrete test mats, each individual mat is explained in detail. Several heat tests were conducted during the construction phase of the entire concrete slab. These tests include the use of a thermal thermometer rather than the thermocouples that were embedded within the concrete surface. All initial and post experiment variables were taken and recorded in Table 6.1 for each test. The following Figure 6.6 illustrates the overall layout of the testing facilities used during the research process.

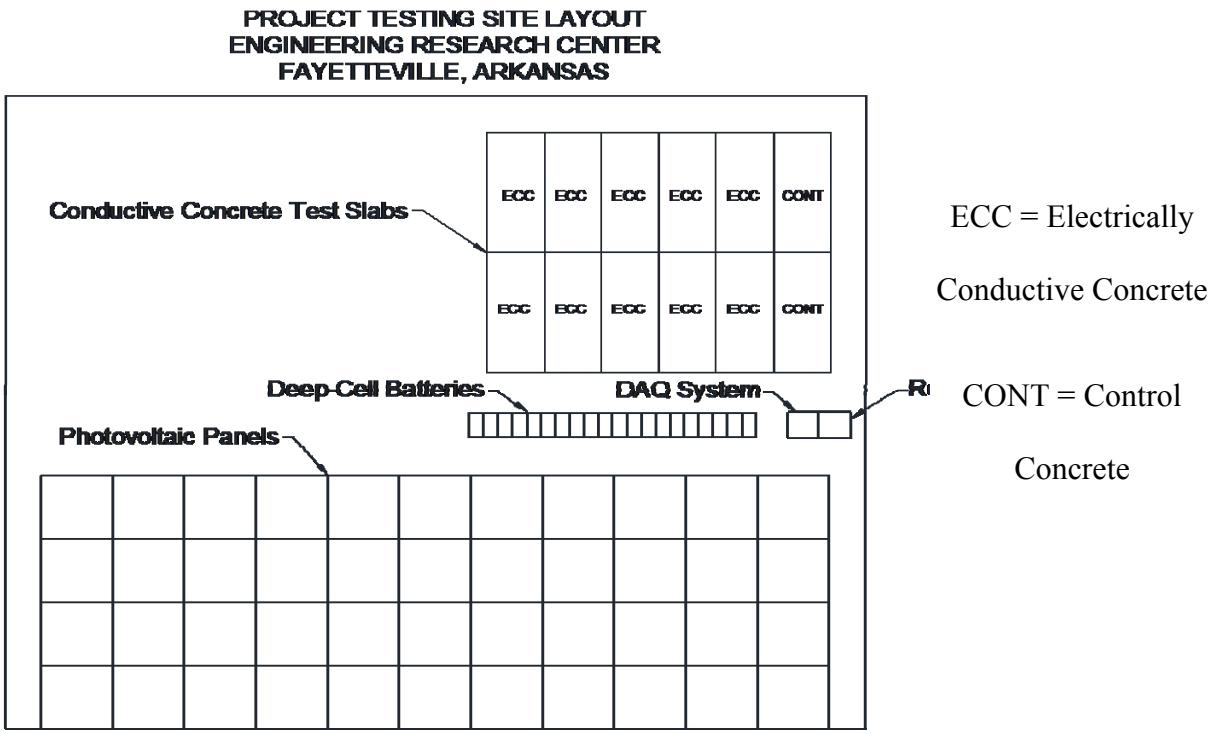

Figure 6.6: Site layout for photovoltaic system

Table 6.1: Large Scale Heat Test Results (6 Hour Duration)

Date	Test Mat	Ambient °C	Voltage V	ECC Temperature, °C	Control Temperature, °C	Heat Differential, °C
28-Jul-11	1	26.3	32.7	34.5	27.1	7.4
29-Jul-11	1	24	29.1	40.3	28.6	11.7
9-Aug-11	1	22.7	47.4	35.3	24.2	11.1
16-Aug-11	1	23	47.6	34.6	24.9	9.7
2-Sep-11	2	24.8	24	29.9	26.1	3.8
7-Oct-11	3	14.4	48.8	25.8	14.1	11.7
20-Oct-11	4	-2.2	49.8	8.7	1.6	7.1
28-Nov-11	5	0	49.3	6.1	-1.9	8
29-Nov-11	5	-1.7	48.6	3.2	-4.4	7.6

Test Mat No. 1

Batching and experimentation for the large scale test mats began in early July, 2011. Trial batch 11, Table 5.1, was used to pour the first 4' x 9.5' x 4" conductive concrete overlay test panel. This concrete mix was batched in three individual lifts and taken to the test site to be uniformly distributed. During this batching process, the first concrete set did not have any steel fibers while the second and third lift had higher than 2.7 percentages to attain an average 2.7 percent for the entire mix. This approach for the first overlay panel was used to observe whether or not the steel fibers would severely decrease concrete workability on a large scale mix.

The mix workability and finishability were comparable to that of normal concrete as seen in Figure 5.5. Each of the three lifts was placed in horizontal layers overlaying the previous lift. A concrete vibrator was used to ensure uniformity and full contact between the concrete and the electrodes. While the vibrator was successful in achieving a strong bond between concrete and electrodes, the uniformity of the concrete suffered. Since the concrete was not placed in a single pour, the mat section closest to the concrete pour spout received a higher steel fiber concentration. This problem was corrected in subsequent pours when a larger concrete mixer was available for use and only a single concrete batch was required to place each overlay panel. After completing the concrete pouring, a tarp was laid over the mat to minimize thermal shrinkage cracking and minimize heat loss during colder weather pours.

The electrode configuration for Test Mat No. 1 is shown in Figure 4.6. The equal electrode spacing was used to examine optimal electrode spacing with respect to power consumption and heating capabilities. A number of heating tests were performed to determine heat uniformity, heat capacity, heating rate, and power consumption. Figure 6.7 shows the

inadequate contact between concrete and electrodes. This lack of contact surface between the electrodes and concrete resulted in a poor concrete conductivity performance.

Figure 6.7: Contact between concrete and electrode for test mat 1 (Osweiler, 2012)

The typical heat test ran on the large scale test mats took place at night so that the sun would not influence temperature results in the experiment. Test mat readings were taken at 1'x1' grid panel points so that a total of 27 temperatures were measured. Each test began at 12:30 a.m. and finished at 6:30 a.m. Temperature readings were taken for both the conductive concrete mat as well as the control mat, constructed of normal concrete, at both test start and test end. Results from a uniformity heat test held July 28, 2011 on Test Mat No. 1 are shown in Table 6.1.

During the testing procedure, the following information was recorded:

1. Temperature readings at each grid point location on the conductive concrete overlay surface
2. Temperature readings from the control concrete slab

3. Ambient temperature
4. Battery voltage
5. Battery amperage

From this information, heat uniformity, power and amperage usages, and maximum heat temperatures could all be calculated. Heat tests were performed on each mat individually and results for these tests are found in the following sections. Figure 6.8 demonstrates an example heat test.

Initial Conditions and Surface Temperatures of Conductive and Control Testing Panels

September 2, 2011 @ 12:30 am
All temperature in °C

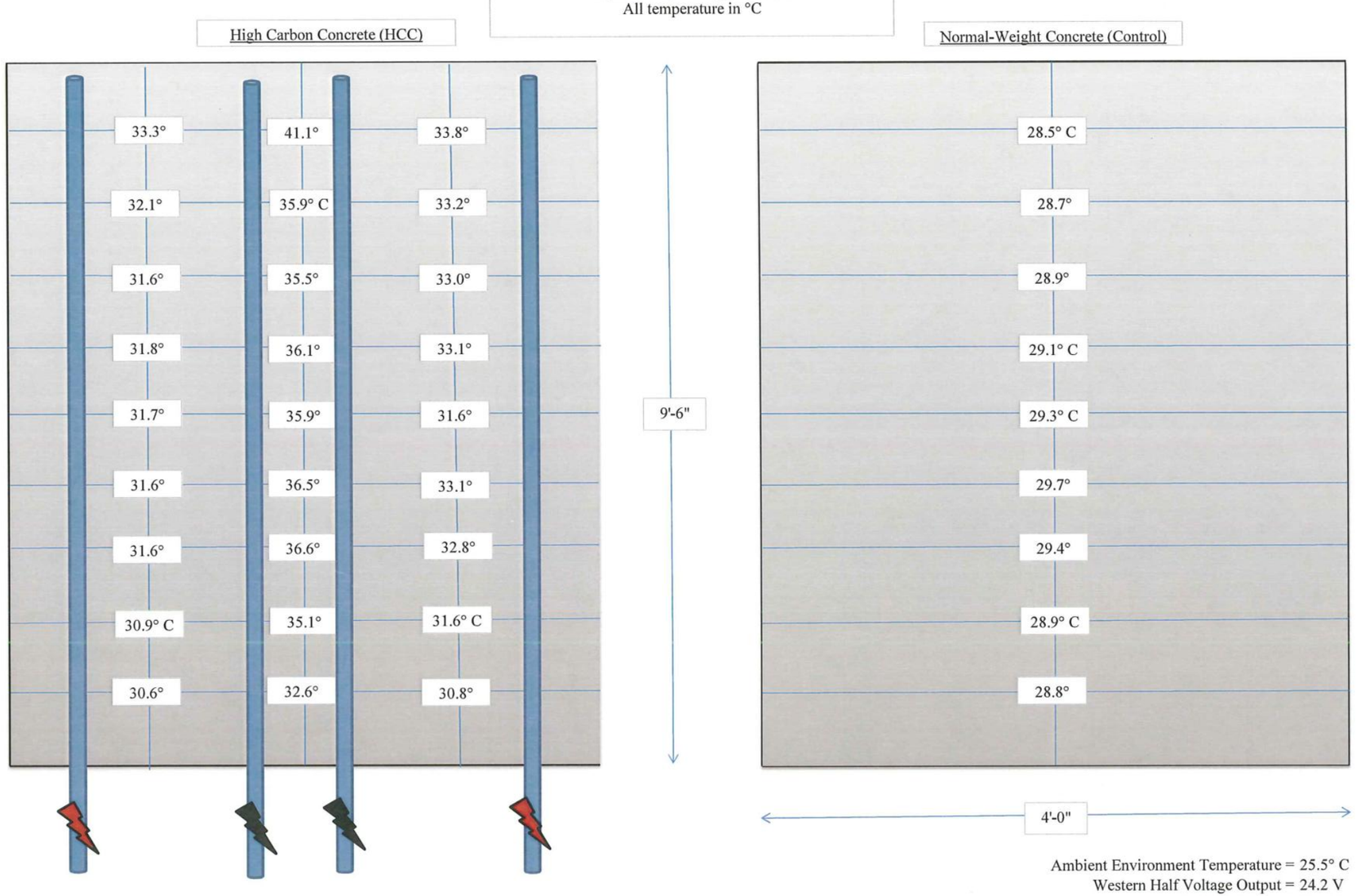

Panel is partitioned as a grid with 1'x1' sections.
Lightning signifies location of electrodes being used by current flow.

Ambient Environment Temperature = 25.5° C
Western Half Voltage Output = 24.2 V
Eastern Half Voltage Output = 25.8 V

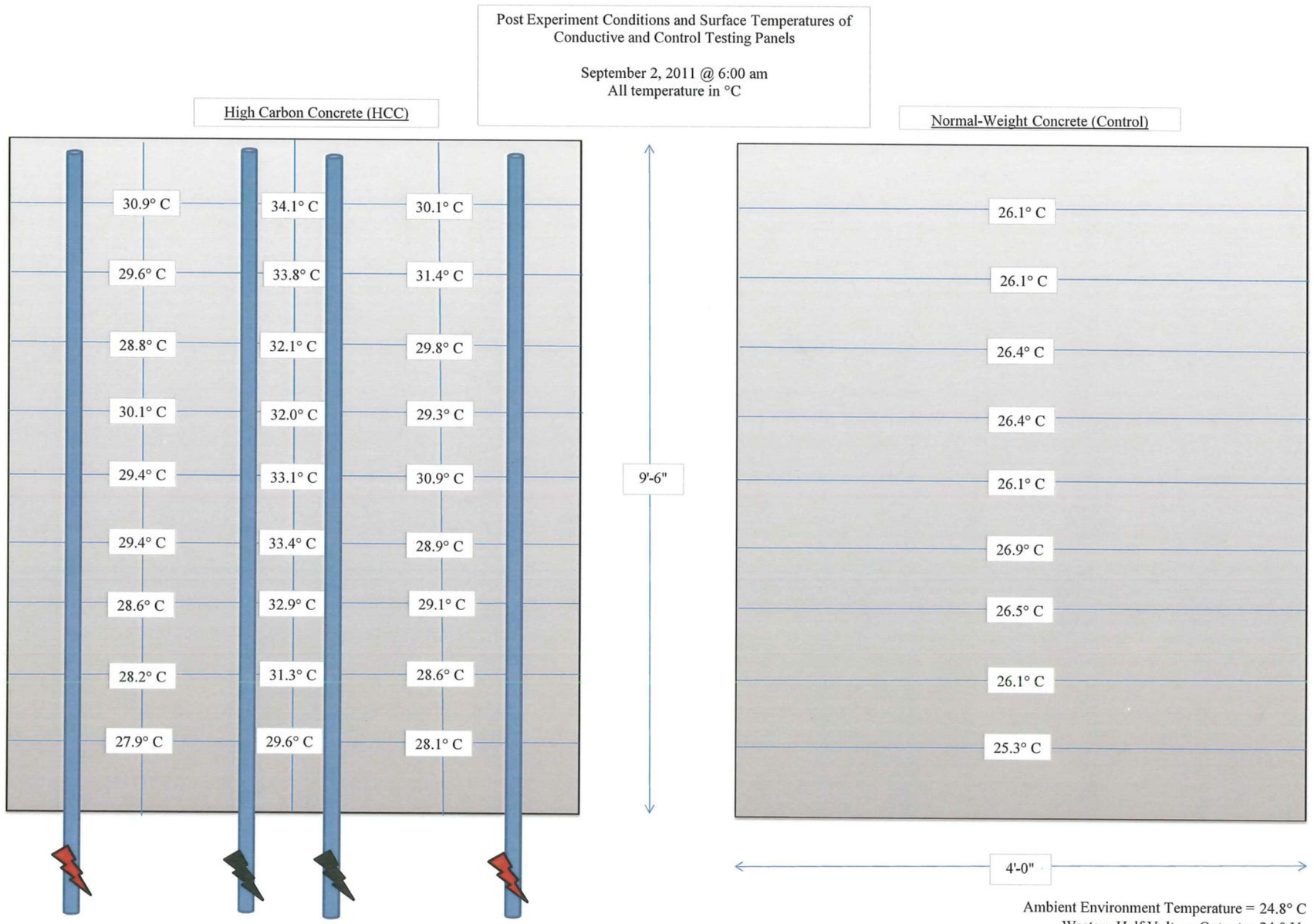

Figure 6.8: Example large scale heat uniformity test results.

Test Mat No. 2

Test mat 2 was batched and poured on August 25, 2011. The concrete mix design for test mat 2 was identical to that of test mat 1. Differences between mat 1 and mat 2 occur with the electrode spacing. Test mat 2 has an electrode configuration where the two outside electrodes are located at 3" from the test panel edge and the inside electrodes are located 1.5" from the test panel center line. Figure 4.7 shows the test mat 2 electrode configuration. Conductivity through a material is directly related to electrode spacing, thus the spacing used in test mat 2 slightly increases the current travel distance compared to test mat 1. This configuration was used in order to obtain a more uniform heat distribution throughout the concrete panel by allowing the current to flow through two sides of the concrete slab rather than the entire width.

The concrete mix for mat 2 had a larger slump than that of mat 1. Due to the increase in slump, a vibrator was not used on test mat 2.

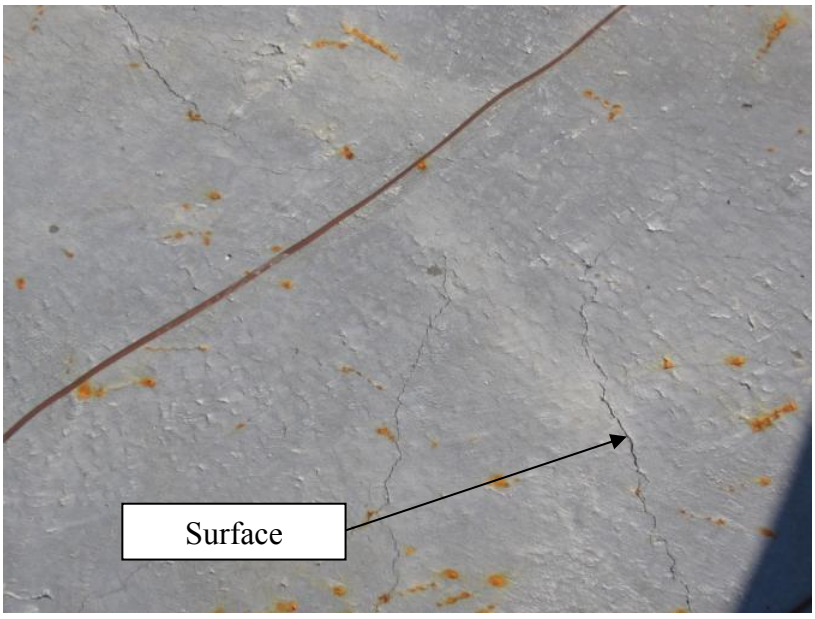

Figure 6.9: Thermal cracking of test mat 2 surface (Osweiler, 2012)

A tarp was not placed over test mat 2 after the concrete was poured. Consequently, after several days of curing, thermal cracks appeared. Figure 6.9 illustrates that the thermal cracks found in mat 2 occurred throughout this overlay panel. The concrete conductivity significantly decreased because of these cracks. Since air has a resistivity between 1.3×10^{16} to 3.3×10^{16} Ω-m at 20°C, the shrinkage cracks created barriers for the electric current flow.

Due to the thermal cracking that resulted in test mat 2, a core sample was taken to determine the depth of cracking. Figure 6.10 and 6.11 demonstrate the width and depth of cracking caused by thermal expansion experienced within the concrete.

Figure 6.10: Test mat 2 core sample surface thermal cracking (Osweiler, 2012)

Figure 6.11: Test mat 2 core sample thermal cracking depth (Osweiler, 2012)

Test Mat No. 3

Test mat 3 was batched and poured on September 29, 2011 with an electrode spacing the same as mat 2. To remedy conditions that led to a conductivity decrease in mat 2, a concrete vibrator was used during concrete placement and a tarp was placed to cover the mat after finishing. After finishing mats 1 and 2, a larger slump was desired to improve the contact surface between the electrodes and concrete. Therefore, an increase of workability was taken into consideration for Test Mat No. 3.

To keep compressive strength and conductivity constant, HRWR was increased to improve workability. HRWR was increased from 6 ounces to 9 ounces per 100 lbs of concrete. The HRWR increase resulted in a definite slump increase and improved workability; however, high HRWR dosages increase the potential for aggregate segregation. It was noticed that some of the water started to bleed to the surface once the concrete was poured. Also, when

compressive tests were conducted, slight segregation of rock and conductive material were observed. While these factors did not decrease conductivity, the compressive strength decreased from about 6,000 psi to around 4,000 psi. Figure 6.12 shows the slump of test mat 3 with the increased HRWR. This decrease in compressive strength was due to the top portion of concrete failing before the entire sample failed.

Initial data was recorded for test mat 3 on October 6, 2011. An average current of 52 V was introduced to the slab at 12:30 a.m. and was allowed to stay active until 6:30 a.m. After 6 hours of testing, test mat 3 demonstrated an average resistivity of 136.7 ohm-in. The decrease in resistivity is due to aggregate segregation within the concrete. With such a high dosage of HRWR, the aggregate and cement paste segregated so that an inch of cement paste was observed at the surface of the overlay slab with minimal aggregate content. Since the thermocouples were embedded within the top section of concrete, the resistivity observed was from current flowing through the cement paste portion. Due to the absence of coarse aggregate and increase of graphite particles, the electric current was allowed to flow more freely.

Figure 6.12: Slump of 4" for test mat 3 (Osweiler, 2012)

Test Mat No. 4

Test mat 4 was poured on October 13, 2011. This slab is identical to test mat 3, except for the HRWR dosage. The HRWR dosage was decreased from 9 ounces to 7.5 ounces per 100 lb of concrete to reduce the amount of cement paste and aggregate separation. As compared to the compressive strengths of test mats 1 and 2, the compressive strength was slightly lower at 4,700 psi.

During compression tests, the cylinders were monitored for their aggregate contents comparing the top, middle, and bottom of each cylinder. Figure 6.13 shows an example of a cylinder from test mat 4. The figure shows that the cylinder top contains a higher ratio of cement paste to coarse aggregate. While not as much segregation was noticed in test mat 4 as in test mat 3, segregation still occurred from a high dosage of HRWR.

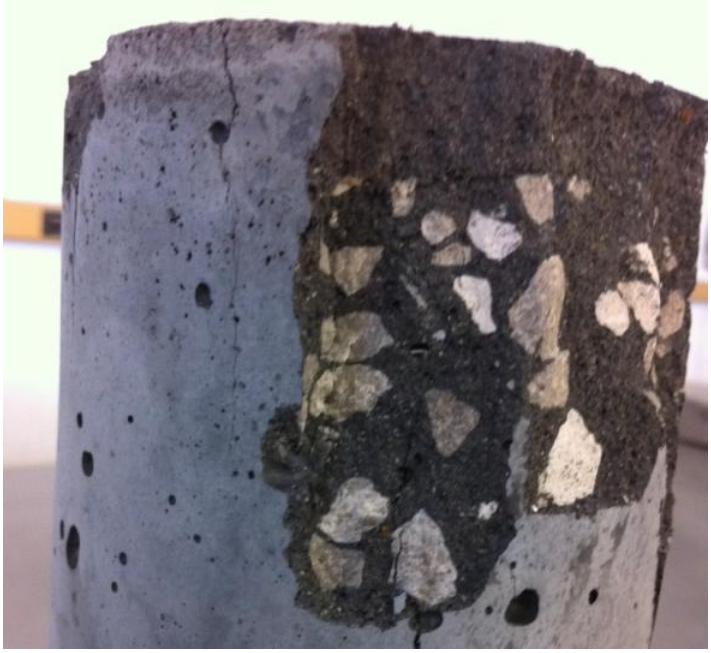

Figure 6.13: Segregation of aggregate and cement paste (Osweiler, 2012)

Test Mat No. 5

Test mat 5 batching and pouring occurred on November 4, 2011. The current conductive concrete mix design was unchanged. The amount of HRWR used was 7 oz per 100 lbs of concrete. The workability and finishability was equal to or better than conventional concrete. There was little to no aggregate segregation displayed in test mat 5. The average compressive strength of test mat 5 was 5,100 psi. The electrical resistivity for test mats 5 was 164 ohm-in at the time it was poured. A continuous electrode configuration was used between test mats 5 and 6 to observe the concrete's conductivity on a larger scale with larger test slabs. The steel electrodes were connected by couplers to allow both test mat 5 and 6 to be energized simultaneously; however this results in a higher resistance due to the increase in length, L, from 120" to 240"

Test Mat No. 6 & 7

Test mats 6 and 7 were poured on November 11, 2011. These two mats were batched concurrently because of the size of the concrete mixer used. Mechanical properties were taken for both mats and averaged. HRWR was consistent with test mat 5. The average compressive strength of test mat 6 and 7 was 4,900 psi and the average resistivity was 337.6 when connected to test mat 5. Since test mats 6 and 7 were batched together, mechanical properties were similar.

Test Mat No. 8 & 9

Batching and pouring of test mat 8 and 9 occurred on November 18, 2011. These two mats were also poured concurrently. Mechanical properties were taken for both mats and averaged. HRWR dosage was consistent with test mats 5, 6, and 7. Test mat 8 was connected to test mat 3 via couplers and extended electrodes. However, test mat 9 electrodes were disconnected with the electrodes of test mat 2. Average compressive strengths and resistivity were 5,000 psi and 306 ohm-in for test mat 8. Average compressive strength and resistivity for test mat 9 were 5,000 psi and 200 ohm-in. These results were consistent with the previous batches of conductive concrete in test mats 5, 6, and 7.

Test Mat No. 10

Batching and pouring of test mat 10 occurred on December 1, 2011. Test mat 10 included increasing the steel fibers percentage from 2.7 percent by volume to 4.5 percent by volume. The steel fiber increase was considered because of the good workability in the previous test slabs. Compressive strength and resistivity for test mat 10 were 5,100 psi and 215 ohm –in., respectively. Test mat 10 showed similar properties to test mats 5-9.

Ice Test No. 1

On July 18, 2011, the first of two ice tests were performed. Data points are collected by recording surface temperatures before, after, and during the test. Nine thermocouples were embedded into the test mat 1 concrete surface. Additionally, two other measurements were taken with thermocouples embedded in the concrete slab center at depths of 3.5" and 11.5". Figure 6.14 displays the results from the first ice test. At 120 minutes, a 3.5" layer of ice was placed on the test panel surface. Once the ice was placed on the slab surface, electricity was introduced into the concrete system. After about 200 minutes, the ice had completely melted and the electrically conductive concrete's (ECC) temperature began to increase to the ambient temperature.

In comparison to the control slab, the ECC slab did melt the ice faster, albeit not significantly faster. Where the two slabs did differ, however, is that once all the ice had melted on the ECC slab, surface water on the ECC slab began to evaporate. This was due to current flowing throughout the slab and increasing its internal temperature while the control slab relied strictly on ambient temperature. Once the ice had all melted, it was a matter of minutes before the ECC slab had reached a temperature equal to and higher than the ambient temperature.

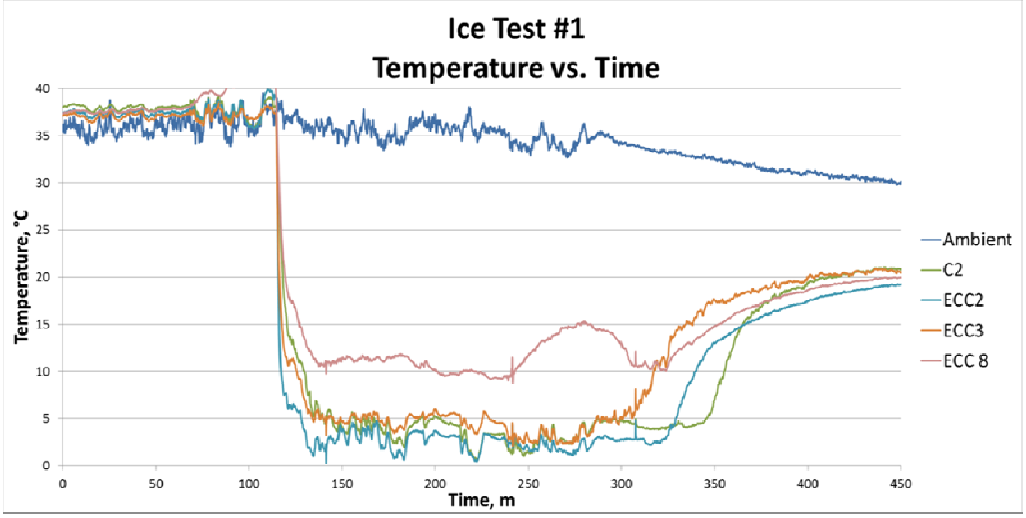

Figure 6.14: Temperature results from Ice Test #1

Thin Layer Ice Test

A similar ice test was done shortly after the 3" ice test on July 27, 2011 with a very thin layer of ice. This test was conducted to obtain a visual reference showing how quickly a conductive concrete slab can melt ice. The conductive concrete panel was supplied with electricity six hours prior to testing. This allowed the concrete to increase in temperature, when compared to ambient temperatures, before applying a layer of ice on the surface. Figure 6.15 illustrates the difference between the control concrete and conductive concrete test slabs 15 minutes after ice application. The conductive concrete panel was allowed to increase its temperature prior to the thin layer ice testing to simulate a more realistic case scenario than the first ice test, where energy was initiated at the time the ice was applied.

During the thin layer ice test, electricity was introduced within the right two-thirds of the ECC slab. At the beginning of the test, the ECC slab was 20° F warmer than the ambient temperature and 15°F warmer than the control slab. In Figure 6.15, the left panel is the control

panel using conventional concrete while the panel on the right is the conductive concrete slab. The ECC slab melted the ice quicker than the control test slab.

When compared to the first ice test, this thin ice layer test is more representative to the proposed application procedure. Because the system will be allowed to remain constantly active, it will be heated prior to an ice or snow storm to allow for a faster melting time of the ice or snow accumulation. When supplied with a consistent energy source, such as solar energy, the photovoltaic and conductive concrete system will be allowed to remain constantly active during winter conditions.

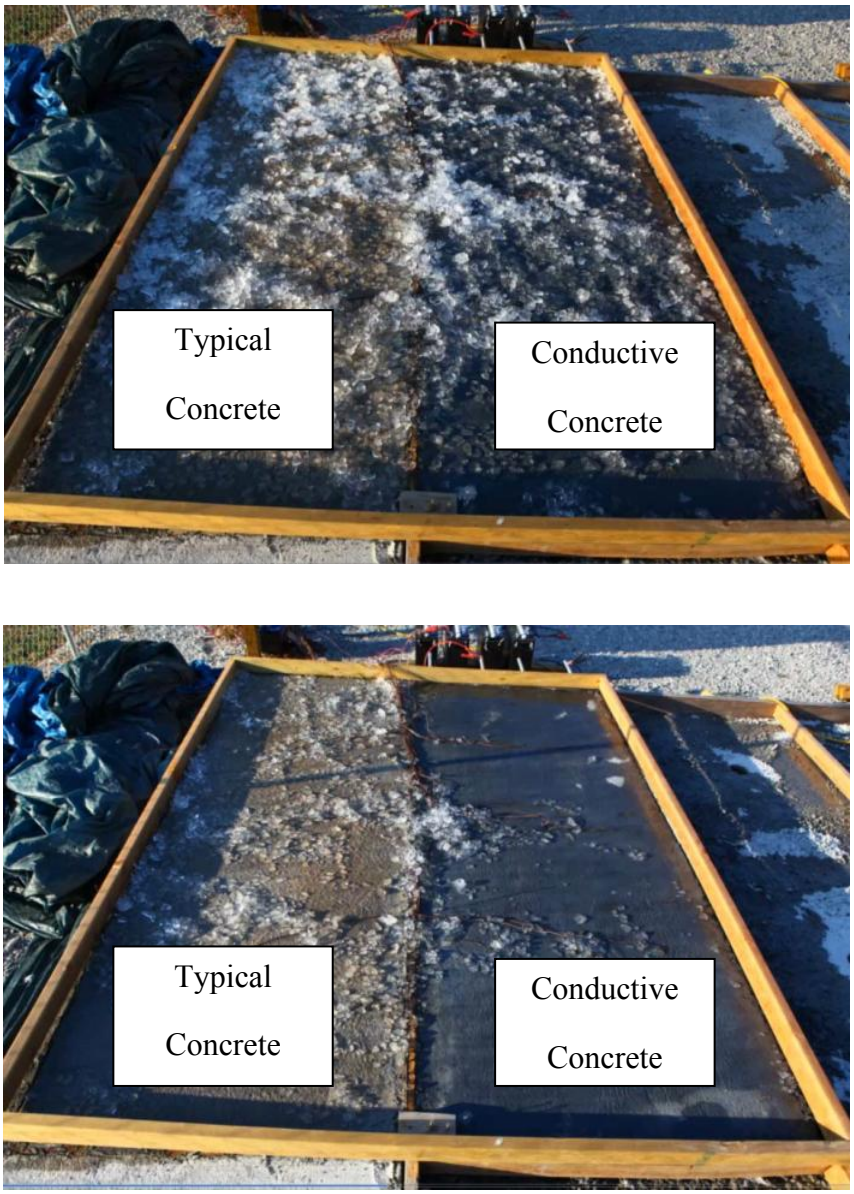

Figure 6.15: Results of Ice Test #2 after 15 minutes (Osweiler, 2012)

Experimental Surface Heat Test Results

Overlay Panel No. 1

In order to observe the benefits of a conductive concrete overlay properly, several surface heat tests were conducted. The comparison for these tests is between the respective conductive concrete overlay panel and the control concrete panel. The first test was conducted on Test Mat

No. 1. These tests were conducted at 12:00 a.m. due to the high daytime temperatures during test procedures. Before testing was underway, four 12-Volt batteries were allowed to be fully charged and connected in series. Refer to the Reference Material portion of this thesis for heat test results and configuration.

Initial surface temperatures were recorded using an infrared thermometer. Recordings were taken at 1'x1' intervals along the entire length and width of the test mat. The overlay panel was then introduced to a 48-V electric current for six hours. At the beginning of the test, both the control panel and conductive concrete panel show temperatures slightly higher than ambient temperature. At the end of six hours, the same locations were recorded on both the control panel and conductive concrete panel. The results show non-uniformity throughout the conductive concrete panel. There were considerably higher temperatures recorded toward the south end of the panel, where the electricity was supplied.

Another test was conducted on Test Mat 1, only this test had the electrodes energized at opposite ends of the mat. The easternmost electrode was energized on the south end and the westernmost electrode was energized on the north end. This method was used to explain why the conductive concrete increased in temperature more towards the energized electrodes.

A third test was conducted on Test Mat 1 to investigate the introduction of electricity and if the location was a cause for the higher temperatures displayed at the ends of the conductive concrete panel. During this test, the electrodes were energized on the north end of the panel. At the conclusion of the test, it was concluded that the location of electricity introduction was not relevant. The non-uniformity was caused by a non-uniform mix of steel fibers and poor electrode to concrete contact.

Overlay Panel No. 2

A heat test was conducted on Test Mat 2 on September 2, 2011. Test mats 2-10 use a different electrode configuration as compared to Test Mat 1. Test mat 2 electrode configuration uses two equally spaced sections of the test mat, separated at the centerline. This allowed for all electrodes to be energized with 24 volts each, simultaneously. A temperature decrease in the conductive concrete as compared to the control panel was observed, however, a less than ideal differential heat distribution was found. This relatively low temperature difference was later attributed to shrinkage cracking within the concrete developed during the concrete curing process.

Overlay Panel No. 3

Surface heat temperature tests were conducted on Test Mat 3 on October 6, 2011. Test Mat 3 uses an identical electrode configuration to Test Mat 2 where the panel is divided down the center in two separate sections. 24 volts were introduced to each section and allowed to stay energized for six hours, as were all tests. A temperature increase when compared to ambient temperatures and the control panel temperatures are observed. These recordings suggest a more homogeneous mix than the previous two conductive concrete panels.

Overlay Panel No. 4

Similar to Test Mat 3, electrodes for Test Mat 4 are divided down the centerline to allow two identical sections throughout the panel. Four 12-volt batteries were connected in series to energize only one section of Test Mat 4. Temperatures during this test were recorded at subfreezing. Over the course of the test, both the ambient and control panel temperatures

decreased with respect to the conductive concrete panel. The conductive concrete panel was observed to have a difference of 4°F when compared to the ambient temperature, and a difference of 5.6°F when compared to the control panel. The less than ideal temperature changes correspond to a lower ambient temperature. It was earlier stated that resistivity increases with decreases in temperature. Final recorded temperatures were consistent throughout the panel, which indicate a homogenous mix.

Conductive Concrete Cost Analysis

Current deicing costs using chemical treatment include:

1. Deicing chemicals
2. Trained personnel to operate snow removal equipment
3. New pavement overlays when deicing chemicals deteriorate existing pavement

While the startup costs for a conductive concrete system powered by photovoltaic energy is high, the maintenance cost will be significantly lower when compared to conventional deicing techniques. The following table gives an outline of material costs for a conductive concrete system.

Table 6.2: Material Cost for Conductive Concrete				
Material	Cost per unit	Amount of material needed per unit	Total Cost per 4"x4'x10' Overlay Panel	Total Cost/ft^2 (4" thick panel)
Carbon Powder, lb	$0.72	650 lb/yd^3	$219.49	$5.48
Steel Fibers, lb	$0.40	50 lb/yd^3	$9.38	$0.23
Normal-weight concrete, yd^3	$120	1 yd ^{3}	$56.28	$1.41
Conductive Concrete				$7.13
Steel Electrodes, ft	$5	48 ft/panel	$240.00	$6.00
Photovoltaic Panels, panel	$400	2	$800.00	$20.00
Deep-Cycle Batteries, battery	$250	2	$500.00	$12.50
		Total Cost =	**$1840.35**	**$45.63**

The total initial cost of a conductive concrete system is very high when compared to initial costs of laying normal concrete as a runway overlay. However, the primary advantage to a conductive concrete system is through minimizing operating costs. Since ice and snow will not accumulate on the concrete surface in a conductive concrete system, costs associated with deicing chemicals, airport personnel, snow plows, and deteriorated concrete repair will be removed. For airlines, preventing ice and snow accumulation is attractive in avoiding flight arrival and departure delays.

CHAPTER 7: CONCLUSIONS AND RECOMMENDATIONS

Conclusions

Mix Design

1. The upper bound for steel fibers is 4.5 percent by volume of concrete. This upper bound is possible when HRWR at 7 ounces per 100 lbs of concrete is used. If higher amounts of steel are used, poor workability and finishability results.
2. Graphite powder at an amount of 17.5 percent by volume of concrete should be used. Graphite powder with an average particle size of 650 microns was used. If higher graphite powder content or if smaller graphite particles are used, HRWR or the w/c should be increased, however increasing the w/c will result in decreasing the compressive strength. Increasing HRWR may result in aggregate and cement paste segregation
3. A w/c of 0.4 was found to work best in regard to workability and finishability. This w/c allowed for concrete compressive strengths between 5-6 ksi.
4. Use 1,000 lbs of cementitious material per cubic yard of concrete. For cementitious material, use 80 percent Type I cement and 20 percent fly ash. Fly ash was substituted to assist with late age compressive strength.

Optimization

1. For electrodes and spacing, use 1” diameter all-thread rebar spaced within the overlay panel at 19” on center on both sides of the panel with a 3” spacing on the center line of the test slab between inner electrodes.
2. Use a concrete vibrator to ensure full contact between the concrete and electrodes.

3. To reduce surface thermal cracking, use a curing blanket or plastic tarp to cover the entire slab during the early concrete curing stage. This covering will ensure limited or no shrinkage cracking.
4. Workability and finishability of electrically conductive concrete developed at the University of Arkansas is comparable to conventional concrete.

Anti-icing Experiments

1. Electric voltage and current within the electrically conductive concrete are at a level safe enough to touch the concrete overlay surface.
2. Batching of electrically conductive concrete should be done in a single mixer if possible to ensure concrete uniformity.
3. During anti-icing experiments, power supplied to the electrically conductive concrete ranged between 370 and 520 W.

Recommendations

1. The electrically conductive concrete mix design used at the University of Arkansas consisted of only two electrically conductive materials: graphite powder and steel fibers. For future work, other electrically conductive materials should be research. Some of these materials may include conductive cement, iron-rich or copper-rich aggregates, and graphite powders with smaller particles sizes.
2. Electrode material, geometry, and configuration affect the resistance within an electrically conductive concrete system. One inch diameter threaded steel rods were used to maximize the contact surface area with the concrete paste. Other geometries

such as plates and bars should be investigated. Electrode spacing should also be researched to develop optimal electrode spacing.

3. The University of Arkansas anti-icing system should be monitored for 5-10 years to provide data on long term serviceability and anti-icing results during the winter weather. A life-cycle cost analysis over a 5-10 year period should be created to compare the photovoltaic system cost to conventional deicing techniques and procedures.
4. A cost comparison should be conducted between different methods of deicing and anti-icing procedures.
5. Future research is needed in the possible usage of chemical admixtures to optimize the electrically conductive concrete mix design. Improvements in workability and finishability with high range water reducers and chemicals used to remove air voids will permit a higher electrically conductive material.

CHAPTER 8: REFERENCE MATERIAL

Conductive Concrete Mix Design Spreadsheets

The following pages contain spreadsheets used in conductive concrete trial batches.

Trial 1: Conductive Concrete Mix Design, Carbon Powder Only
A600, A625, A99 PDS Carbon Powder, 25%
Steel Fibers, 1.5%

Mix Proportion (SSD)

Material	Weight, lb	Volume, ft^3	
Steel Fiber	27	0.40	0.015
Cement	800.00	4.07	0.151
Fly Ash	200	1.46	0.054
Gr. Powder	940	6.73	0.249
Silica Fume	0	0.00	0.000
Coarse Agg	1300.00	7.18	0.266
Fine Agg	35.00	0.21	0.008
Water	400.00	6.41	0.237
Air	0.02	0.54	0.020
		27.00	1.000

Material Properties

	S.G.
Steel Fiber	1.08
Cement	3.15
Fly Ash	2.2
Silica Fume	2.2
Coarse Agg	2.9
Fine Agg	2.63
Gr. Powder	2.24

Mix Characteristics

W/C	0.400		
Unit Weight, lb	137.1		
Cementitious material (lb)	1000 lb		
Fly Ash replacement (%)	20	200 lb	
Gr. Powder replacement (%)	0	0 lb	Total
SF replacement (%)	0	0 lb	x 1.25

Moisture Content

Fine Agg pan	230		
rock pan	220.6		
Fine Agg +pan	2123.6		
rock + pan wt.	2021.7		
dry wt. Fine Ag	2000.7		
dry wt. rock	1989.9		
Fine Agg mc	6.940757892		
rock mc	1.797320974		
Fine Agg ssd	0.709	mc-ssd	0.062317579
rock ssd	0.861	mc-ssd	0.00936321

Batch Weights (yd^3)

Cement	800 lb
Fly Ash	200 lb
Gr. Powder	940 lb
Silica Fume	0 lb
Coarse Agg	1312 lb
Fine Agg	37 lb
Water	386 lb
HRWR	6 fl oz./cwt
HRWR	1774 ml

Batch Weights (ft^3)

Batch size	1.0 ft^3
Cement	29.6 lb
Fly Ash	7.4 lb
Gr. Powder	34.8 lb
Silica Fume	0.0 lb
Coarse Agg	48.6 lb
Fine Agg	1.4 lb
Water	14.3 lb
HRWR	65.7 ml
steel fibres	1.0 lb

Trial 2: Conductive Concrete Mix Design, Carbon Powder Only
4012 PDS Carbon Powder, 25%
Steel Fibers, 1.5%

Mix Proportion (SSD)

Material	Weight, lb	Volume, ft^3	
Steel Fiber	27	0.40	0.015
Cement	800.00	4.07	0.151
Fly Ash	200	1.46	0.054
Gr. Powder	940	6.73	0.249
Silica Fume	0	0.00	0.000
Coarse Agg	1300.00	7.18	0.266
Fine Agg	35.00	0.21	0.008
Water	400.00	6.41	0.237
Air	0.02	0.54	0.020
		27.00	1.000

Material Properties

	S.G.
Steel Fiber	1.08
Cement	3.15
Fly Ash	2.2
Silica Fume	2.2
Coarse Agg	2.9
Fine Agg	2.63
Gr. Powder	2.24

Mix Characteristics

W/C	0.400		
Unit Weight, lb	137.1		
Cementitious material (lb)	1000 lb		
Fly Ash replacement (%)	20	200 lb	
Gr. Powder replacement (%)	0	0 lb	Total
SF replacement (%)	0	0 lb	x 1.25

Moisture Content

Fine Agg pan	230		
rock pan	220.6		
Fine Agg +pan	2101.6		
rock + pan wt.	1999.5		
dry wt. Fine Ag	2000.7		
dry wt. rock	1989.9		
Fine Agg mc	5.698311402		
rock mc	0.542587464		
Fine Agg ssd	0.709	mc-ssd	0.049893114
rock ssd	0.861	mc-ssd	-0.003184125

Batch Weights (yd^3)

Cement	800 lb
Fly Ash	200 lb
Gr. Powder	940 lb
Silica Fume	0 lb
Coarse Agg	1296 lb
Fine Agg	37 lb
Water	402 lb
HRWR	6 fl oz./cwt
HRWR	1774 ml

Batch Weights (ft^3)

Batch size	1.0 ft^3
Cement	29.6 lb
Fly Ash	7.4 lb
Gr. Powder	34.8 lb
Silica Fume	0.0 lb
Coarse Agg	48.0 lb
Fine Agg	1.4 lb
Water	14.9 lb
HRWR	65.7 ml
steel fibres	1.0 lb

Trial 3: Conductive Concrete Mix Design, Carbon Powder Only
4015 PDS Carbon Powder, 25%
Steel Fibers, 1.5%

Mix Proportion (SSD)

Material	Weight, lb	Volume, ft^3	
Steel Fiber	27	0.40	0.015
Cement	800.00	4.07	0.151
Fly Ash	200	1.46	0.054
Gr. Powder	750	5.37	0.199
Silica Fume	0	0.00	0.000
Coarse Agg	1300.00	7.18	0.266
Fine Agg	258.08	1.57	0.058
Water	400.00	6.41	0.237
Air	0.02	0.54	0.020
		27.00	1.000

Material Properties

	S.G.
Steel Fiber	1.08
Cement	3.15
Fly Ash	2.2
Silica Fume	2.2
Coarse Agg	2.9
Fine Agg	2.63
Gr. Powder	2.24

Mix Characteristics

W/C	0.400		
Unit Weight, lb	138.3		
Cementitious material (lb)	1000 lb		
Fly Ash replacement (%)	20	200 lb	
Gr. Powder replacement (%)	0	0 lb	Total
SF replacement (%)	0	0 lb	x 1.25

Moisture Content

Fine Agg pan	230		
rock pan	220.6		
Fine Agg +pan	2101.6		
rock + pan wt.	1999.5		
dry wt. Fine Ag	2000.7		
dry wt. rock	1989.9		
Fine Agg mc	5.698311402		
rock mc	0.542587464		
Fine Agg ssd	0.709	mc-ssd	0.049893114
rock ssd	0.861	mc-ssd	-0.003184125

Batch Weights (yd^3)

Cement	800 lb
Fly Ash	200 lb
Gr. Powder	750 lb
Silica Fume	0 lb
Coarse Agg	1296 lb
Fine Agg	271 lb
Water	391 lb
HRWR	6 fl oz./cwt
HRWR	1774 ml

Batch Weights (ft^3)

Batch size	1.0 ft^3
Cement	29.6 lb
Fly Ash	7.4 lb
Gr. Powder	27.8 lb
Silica Fume	0.0 lb
Coarse Agg	48.0 lb
Fine Agg	10.0 lb
Water	14.5 lb
HRWR	65.7 ml
steel fibres	1.0 lb

Trial 4: Conductive Concrete Mix Design, Carbon Powder Only
4071 PDS Carbon Powder, 17%
Steel Fibers, 1.5%

Mix Proportion (SSD)

Material	Weight, lb	Volume, ft^3	
Steel Fiber	27	0.40	0.015
Cement	800.00	4.07	0.151
Fly Ash	200	1.46	0.054
Gr. Powder	750	5.37	0.199
Silica Fume	0	0.00	0.000
Coarse Agg	1300.00	7.18	0.266
Fine Agg	258.08	1.57	0.058
Water	400.00	6.41	0.237
Air	0.02	0.54	0.020
		27.00	1.000

Material Properties

	S.G.
Steel Fiber	1.08
Cement	3.15
Fly Ash	2.2
Silica Fume	2.2
Coarse Agg	2.9
Fine Agg	2.63
Gr. Powder	2.24

Mix Characteristics

W/C	0.400		
Unit Weight, lb	138.3		
Cementitious material (lb)	1000 lb		
Fly Ash replacement (%)	20	200 lb	
Gr. Powder replacement (%)	0	0 lb	Total
SF replacement (%)	0	0 lb	x 1.25

Moisture Content

Fine Agg pan	230		
rock pan	220.6		
Fine Agg +pan	2120.5		
rock + pan wt.	2015.9		
dry wt. Fine Ag	2000.7		
dry wt. rock	1989.9		
Fine Agg mc	6.765685887		
rock mc	1.469507715		
Fine Agg ssd	0.709	mc-ssd	0.060566859
rock ssd	0.861	mc-ssd	0.006085077

Batch Weights (yd^3)

Cement	800 lb
Fly Ash	200 lb
Gr. Powder	750 lb
Silica Fume	0 lb
Coarse Agg	1308 lb
Fine Agg	274 lb
Water	376 lb
HRWR	6 fl oz./cwt
HRWR	1774 ml

Batch Weights (ft^3)

Batch size	1.0 ft^3
Cement	29.6 lb
Fly Ash	7.4 lb
Gr. Powder	27.8 lb
Silica Fume	0.0 lb
Coarse Agg	48.4 lb
Fine Agg	10.1 lb
Water	13.9 lb
HRWR	65.7 ml
steel fibres	1.0 lb

Trial 5: Conductive Concrete Mix Design, Carbon Powder Only
4071 PDS Carbon Powder, 20%
Steel Fibers, 2.5%

Mix Proportion (SSD)

Material	Weight, lb	Volume, ft^3	
Steel Fiber	45	0.67	0.025
Cement	800.00	4.07	0.151
Fly Ash	200	1.46	0.054
Gr. Powder	750	5.37	0.199
Silica Fume	0	0.00	0.000
Coarse Agg	1300.00	7.18	0.266
Fine Agg	214.25	1.31	0.048
Water	400.00	6.41	0.237
Air	0.02	0.54	0.020
		27.00	1.000

Material Properties

	S.G.
Steel Fiber	1.08
Cement	3.15
Fly Ash	2.2
Silica Fume	2.2
Coarse Agg	2.9
Fine Agg	2.63
Gr. Powder	2.24

Mix Characteristics

W/C	0.400		
Unit Weight, lb	137.4		
Cementitious material (lb)	1000 lb		
Fly Ash replacement (%)	20	200 lb	
Gr. Powder replacement (%)	0	0 lb	Total
SF replacement (%)	0	0 lb	x 1.25

Moisture Content

Fine Agg pan	230		
rock pan	220.6		
Fine Agg +pan	2064.74		
rock + pan wt.	2006.9		
dry wt. Fine Ag	2000.7		
dry wt. rock	1989.9		
Fine Agg mc	3.616648783		
rock mc	0.960831967		
Fine Agg ssd	0.709	mc-ssd	0.029076488
rock ssd	0.861	mc-ssd	0.00099832

Batch Weights (yd^3)

Cement	800 lb
Fly Ash	200 lb
Gr. Powder	750 lb
Silica Fume	0 lb
Coarse Agg	1301 lb
Fine Agg	220 lb
Water	392 lb
HRWR	6 fl oz./cwt
HRWR	1774 ml

Batch Weights (ft^3)

Batch size	1.0 ft^3
Cement	29.6 lb
Fly Ash	7.4 lb
Gr. Powder	27.8 lb
Silica Fume	0.0 lb
Coarse Agg	48.2 lb
Fine Agg	8.2 lb
Water	14.5 lb
HRWR	65.7 ml
steel fibres	1.7 lb

Trial 6: Conductive Concrete Mix Design, Carbon Powder Only
4071 PDS Carbon Powder, 20%
Steel Fibers, 3.5%

Mix Proportion (SSD)

Material	Weight, lb	Volume, ft^3	
Steel Fiber	64	0.95	0.035
Cement	800.00	4.07	0.151
Fly Ash	200	1.46	0.054
Gr. Powder	750	5.37	0.199
Silica Fume	0	0.00	0.000
Coarse Agg	1300.00	7.18	0.266
Fine Agg	167.98	1.02	0.038
Water	400.00	6.41	0.237
Air	0.02	0.54	0.020
		27.00	1.000

Material Properties

	S.G.
Steel Fiber	1.08
Cement	3.15
Fly Ash	2.2
Silica Fume	2.2
Coarse Agg	2.9
Fine Agg	2.63
Gr. Powder	2.24

Mix Characteristics

W/C	0.400		
Unit Weight, lb	136.4		
Cementitious material (lb)	1000 lb		
Fly Ash replacement (%)	20	200 lb	
Gr. Powder replacement (%)	0	0 lb	Total
SF replacement (%)	0	0 lb	x 1.25

Moisture Content

Fine Agg pan	230		
rock pan	220.6		
Fine Agg +pan	2064.74		
rock + pan wt.	2006.9		
dry wt. Fine Ag	2000.7		
dry wt. rock	1989.9		
Fine Agg mc	3.616648783		
rock mc	0.960831967		
Fine Agg ssd	0.709 mc-ssd	0.029076488	
rock ssd	0.861 mc-ssd	0.00099832	

Batch Weights (yd^3)

Cement	800 lb
Fly Ash	200 lb
Gr. Powder	750 lb
Silica Fume	0 lb
Coarse Agg	1301 lb
Fine Agg	173 lb
Water	394 lb
HRWR	6 fl oz./cwt
HRWR	1774 ml

Batch Weights (ft^3)

Batch size	1.0 ft^3
Cement	29.6 lb
Fly Ash	7.4 lb
Gr. Powder	27.8 lb
Silica Fume	0.0 lb
Coarse Agg	48.2 lb
Fine Agg	6.4 lb
Water	14.6 lb
HRWR	65.7 ml
steel fibres	2.4 lb

Trial 7: Conductive Concrete Mix Design, Carbon Powder Only
4071 PDS Carbon Powder, 20%
Steel Fibers, 5%

Mix Proportion (SSD)

Material	Weight, lb	Volume, ft^3		
Steel Fiber	91	1.35	0.050	
Cement	800.00	4.07	0.151	
Fly Ash	200	1.46	0.054	
Gr. Powder	650	4.65	0.172	
Silica Fume	0	0.00	0.000	
Coarse Agg	1300.00	7.18	0.266	
Fine Agg	219.64	1.34	0.050	
Water	400.00	6.41	0.237	
Air	0.02	0.54	0.020	
		27.00	1.000	

Material Properties

	S.G.
Steel Fiber	1.08
Cement	3.15
Fly Ash	2.2
Silica Fume	2.2
Coarse Agg	2.9
Fine Agg	2.63
Gr. Powder	2.24

Mix Characteristics

W/C	0.400		
Unit Weight, lb	135.6		
Cementitious material (lb)	1000 lb		
Fly Ash replacement (%)	20	200 lb	
Gr. Powder replacement (%)	0	0 lb	Total
SF replacement (%)	0	0 lb	x 1.25

Moisture Content

Fine Agg pan	230		
rock pan	220.6		
Fine Agg +pan	2064.74		
rock + pan wt.	2006.9		
dry wt. Fine Ag	2000.7		
dry wt. rock	1989.9		
Fine Agg mc	3.616648783		
rock mc	0.960831967		
Fine Agg ssd	0.709	mc-ssd	0.029076488
rock ssd	0.861	mc-ssd	0.00099832

Batch Weights (yd^3)

Cement	800 lb
Fly Ash	200 lb
Gr. Powder	650 lb
Silica Fume	0 lb
Coarse Agg	1301 lb
Fine Agg	226 lb
Water	392 lb
HRWR	6 fl oz./cwt
HRWR	1774 ml

Batch Weights (ft^3)

Batch size	1.0 ft^3
Cement	29.6 lb
Fly Ash	7.4 lb
Gr. Powder	24.1 lb
Silica Fume	0.0 lb
Coarse Agg	48.2 lb
Fine Agg	8.4 lb
Water	14.5 lb
HRWR	65.7 ml
steel fibres	3.4 lb

Trial 8: Conductive Concrete Mix Design, Carbon Powder Only
4071 PDS Carbon Powder, 17%
Steel Fibers, 2.5%

Mix Proportion (SSD)

Material	Weight, lb	Volume, ft^3		
Steel Fiber	50	0.74	0.027	
Cement	800.00	4.07	0.151	
Fly Ash	200	1.46	0.054	
Gr. Powder	650	4.65	0.172	
Silica Fume	0	0.00	0.000	
Coarse Agg	1300.00	7.18	0.266	
Fine Agg	319.48	1.95	0.072	
Water	400.00	6.41	0.237	
Air	0.02	0.54	0.020	
		27.00	1.000	

Material Properties

	S.G.
Steel Fiber	1.08
Cement	3.15
Fly Ash	2.2
Silica Fume	2.2
Coarse Agg	2.9
Fine Agg	2.63
Gr. Powder	2.24

Mix Characteristics

W/C	0.400		
Unit Weight, lb	137.8		
Cementitious material (lb)	1000 lb		
Fly Ash replacement (%)	20	200 lb	
Gr. Powder replacement (%)	0	0 lb	Total
SF replacement (%)	0	0 lb	x 1.25

Moisture Content

Fine Agg pan	230		
rock pan	220.6		
Fine Agg +pan	2123.6		
rock + pan wt.	2021.7		
dry wt. Fine Ag	2000.7		
dry wt. rock	1989.9		
Fine Agg mc	6.940757892		
rock mc	1.797320974		
Fine Agg ssd	0.709	mc-ssd	0.062317579
rock ssd	0.861	mc-ssd	0.00936321

Batch Weights (yd^3)

Cement	800 lb
Fly Ash	200 lb
Gr. Powder	650 lb
Silica Fume	0 lb
Coarse Agg	1312 lb
Fine Agg	339 lb
Water	368 lb
HRWR	6 fl oz./cwt
HRWR	1774 ml

Batch Weights (ft^3)

Batch size	1.0 ft^3
Cement	29.6 lb
Fly Ash	7.4 lb
Gr. Powder	24.1 lb
Silica Fume	0.0 lb
Coarse Agg	48.6 lb
Fine Agg	12.6 lb
Water	13.6 lb
HRWR	65.7 ml
steel fibres	1.9 lb

Trial 9: Conductive Concrete Mix Design, BFS Aggregate
Blast Furnace Slag Aggregate (0.75" MSA)
4071 PDS, 70:30 - Cement:Carbon Powder, 5.5%
Steel Fibers, 2.5%

Mix Proportion (SSD)

Material	Weight, lb	Volume, ft^3	
Steel Fiber	50	0.74	0.027
Cement	630.00	3.21	0.119
Fly Ash	0	0.00	0.000
Gr. Powder	270	1.93	0.072
Silica Fume	0	0.00	0.000
Coarse Agg	1400.00	9.75	0.361
Fine Agg	948.32	5.78	0.214
Water	315.00	5.05	0.187
Air	0.02	0.54	0.020
		27.00	1.000

Material Properties

	S.G.
Steel Fiber	1.08
Cement	3.15
Fly Ash	2.2
Silica Fume	2.2
Coarse Agg.	2.3
Fine Agg	2.1
Gr. Powder	2.24

Mix Characteristics

W/C	0.350		
Unit Weight, lb	133.8		
Cementitious material (lb)	900	lb	
Fly Ash replacement (%)	0	0 lb	
Gr. Powder replacement (%	30	270 lb	Total
SF replacement (%)	0	0 lb	x 1.25

Moisture Content

sand pan	230		
rock pan	220.6		
sand +pan wt.	2123.6		
rock + pan wt	2021.7		
dry wt. sand	2000.7		
dry wt. rock	1989.9		
sand mc	0		
rock mc	0		
sand ssd	0.709	mc-ssd	-0.00709
rock ssd	0.861	mc-ssd	-0.00861

Batch Weights (yd^3)

Cement	630	lb
Fly Ash	0	lb
Gr. Powder	270	lb
Silica Fume	0	lb
Coarse Agg	1388	lb
Fine Agg	942	lb
Water	334	lb
HRWR	6	fl oz./cwt
HRWR	1597	ml

Batch Weights (ft^3)

Batch size	1.0	ft^3
Cement	23.3	lb
Fly Ash	0.0	lb
Gr. Powder	10.0	lb
Silica Fume	0.0	lb
Coarse Agg	51.4	lb
Fine Agg	34.9	lb
Water	12.4	lb
HRWR	59.1	ml
steel fibres	1.9	lb

Trial 10: Conductive Concrete Mix Design, Carbon Powder Only
Blast Furnace Slag Aggregate (0.75" MSA)
4071 PDS Carbon Powder, 17%
Steel Fibers, 2.5%

Mix Proportion (SSD)

Material	Weight, lb	Volume, ft^3		
Steel Fiber	50	0.74	0.027	
Cement	1000.00	5.09	0.188	
Fly Ash	0	0.00	0.000	
Gr. Powder	650	4.65	0.172	
Silica Fume	0	0.00	0.000	
Coarse Agg	1200.00	8.36	0.310	
Fine Agg	198.38	1.21	0.045	
Water	400.00	6.41	0.237	
Air	0.02	0.54	0.020	
		27.00	1.000	

Material Properties

	S.G.
Steel Fiber	1.08
Cement	3.15
Fly Ash	2.2
Silica Fume	2.2
Coarse Agg	2.3
Fine Agg	2.1
Gr. Powder	2.24

Mix Characteristics

W/C	0.400		
Unit Weight, lb	129.6		
Cementitious material (lb)	1000 lb		
Fly Ash replacement (%)	0	0 lb	
Gr. Powder replacement (%)	0	0 lb	Total
SF replacement (%)	0	0 lb	x 1.25

Moisture Content

Fine Agg pan	230		
rock pan	220.6		
Fine Agg +pan v	2123.6		
rock + pan wt.	2021.7		
dry wt. Fine Ag	2000.7		
dry wt. rock	1989.9		
Fine Agg mc	0		
rock mc	0		
Fine Agg ssd	0.709	mc-ssd	-0.00709
rock ssd	0.861	mc-ssd	-0.00861

Batch Weights (yd^3)

Cement	1000 lb
Fly Ash	0 lb
Gr. Powder	650 lb
Silica Fume	0 lb
Coarse Agg	1190 lb
Fine Agg	197 lb
Water	412 lb
HRWR	6 fl oz./cwt
HRWR	1774 ml

Batch Weights (ft^3)

Batch size	1.0 ft^3
Cement	37.0 lb
Fly Ash	0.0 lb
Gr. Powder	24.1 lb
Silica Fume	0.0 lb
Coarse Agg	44.1 lb
Fine Agg	7.3 lb
Water	15.2 lb
HRWR	65.7 ml
steel fibres	1.9 lb

Trial 11: Conductive Concrete Mix Design, Carbon Powder Only
4071 PDS Carbon Powder, 17%
Steel Fibers, 2.5%

Mix Proportion (SSD)

Material	Weight, lb	Volume, ft^3	
Steel Fiber	50	0.74	0.027
Cement	800.00	4.07	0.151
Fly Ash	200	1.46	0.054
Gr. Powder	650	4.65	0.172
Silica Fume	0	0.00	0.000
Coarse Agg	1300.00	7.18	0.266
Fine Agg	319.48	1.95	0.072
Water	400.00	6.41	0.237
Air	0.02	0.54	0.020
		27.00	1.000

Material Properties

	S.G.
Steel Fiber	1.08
Cement	3.15
Fly Ash	2.2
Silica Fume	2.2
Coarse Agg	2.9
Fine Agg	2.63
Gr. Powder	2.24

Mix Characteristics

W/C	0.400	
Unit Weight, lb	137.8	
Cementitious material (lb)	1000 lb	
Fly Ash replacement (%)	20	200 lb
Gr. Powder replacement (%)	0	0 lb
SF replacement (%)	0	0 lb

Moisture Content

Fine Agg pan	230		
rock pan	220.6		
Fine Agg +pan	2038.31		
rock + pan wt.	2009.3		
dry wt. Fine Ag	2000.7		
dry wt. rock	1989.9		
Fine Agg mc	2.12401875		
rock mc	1.096478833		
Fine Agg ssd	0.709	mc-ssd	0.014150187
rock ssd	0.861	mc-ssd	0.002354788

Batch Weights (yd^3)

Cement	800 lb
Fly Ash	200 lb
Gr. Powder	650 lb
Silica Fume	0 lb
Coarse Agg	1303 lb
Fine Agg	324 lb
Water	392 lb
HRWR	6 fl oz./cwt
HRWR	1774 ml

Batch Weights (ft^3)

Batch size	6.0 ft^3
Cement	177.8 lb
Fly Ash	44.4 lb
Gr. Powder	144.4 lb
Silica Fume	0.0 lb
Coarse Agg	289.6 lb
Fine Agg	72.0 lb
Water	87.2 lb
HRWR	394.3 ml
steel fibres	11.1 lb

Large Scale Heat Test Results

The following pages contain figures used in conductive concrete mat testing.

Initial Conditions and Surface Temperatures of Conductive and Control Testing Panels

July 28, 2011 @ 6:00 am
All temperature in °C

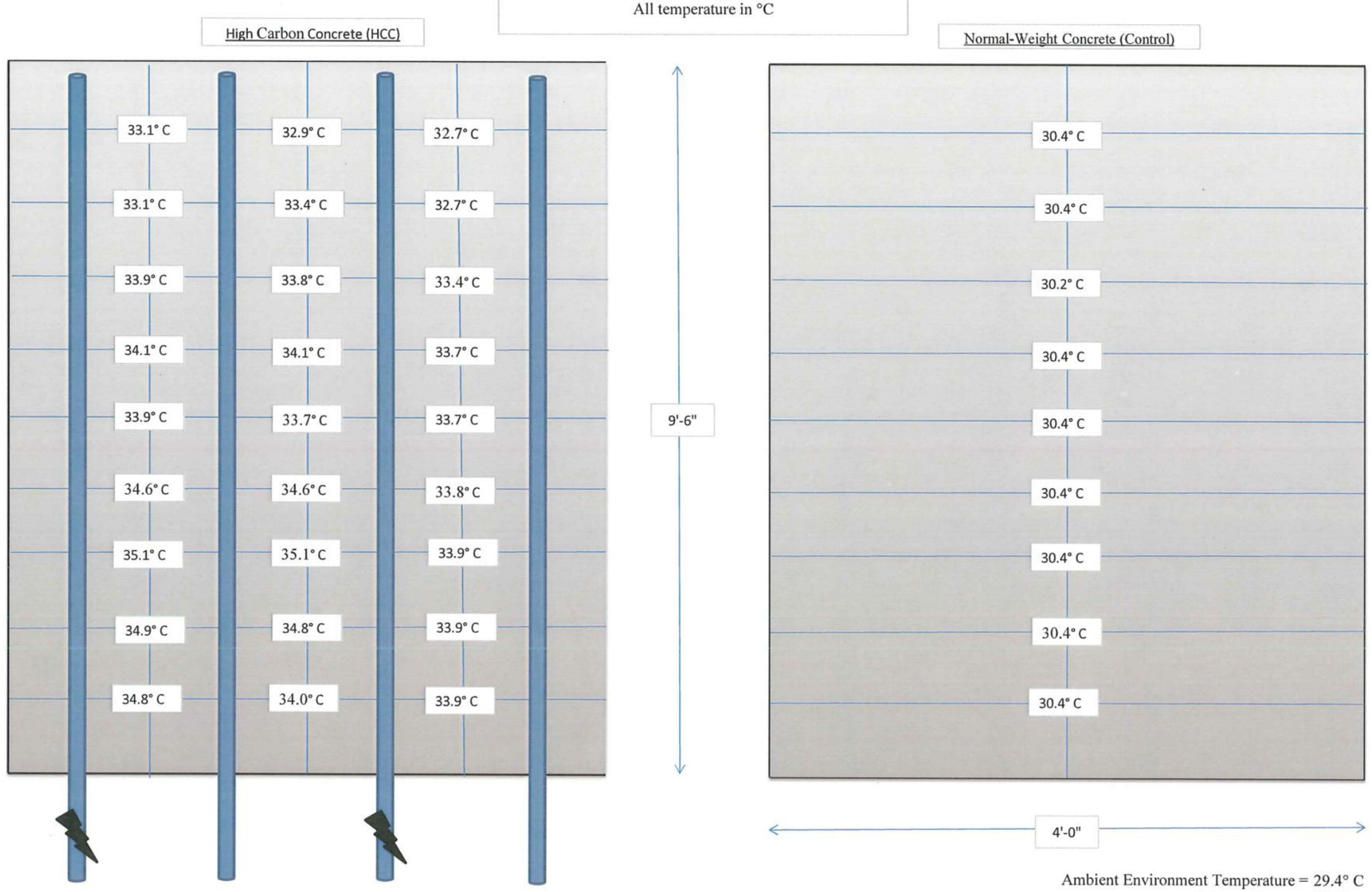

Panel is partitioned as a grid with 1'x1' sections.
Lightning signifies location of electrodes being used by current flow.

Ambient Environment Temperature = 29.4° C
Voltage Output = 48 V

Post Experiment Conditions and Surface Temperatures of Conductive and Control Testing Panels

July 28, 2011 @ 12:30 am
All temperature in °C

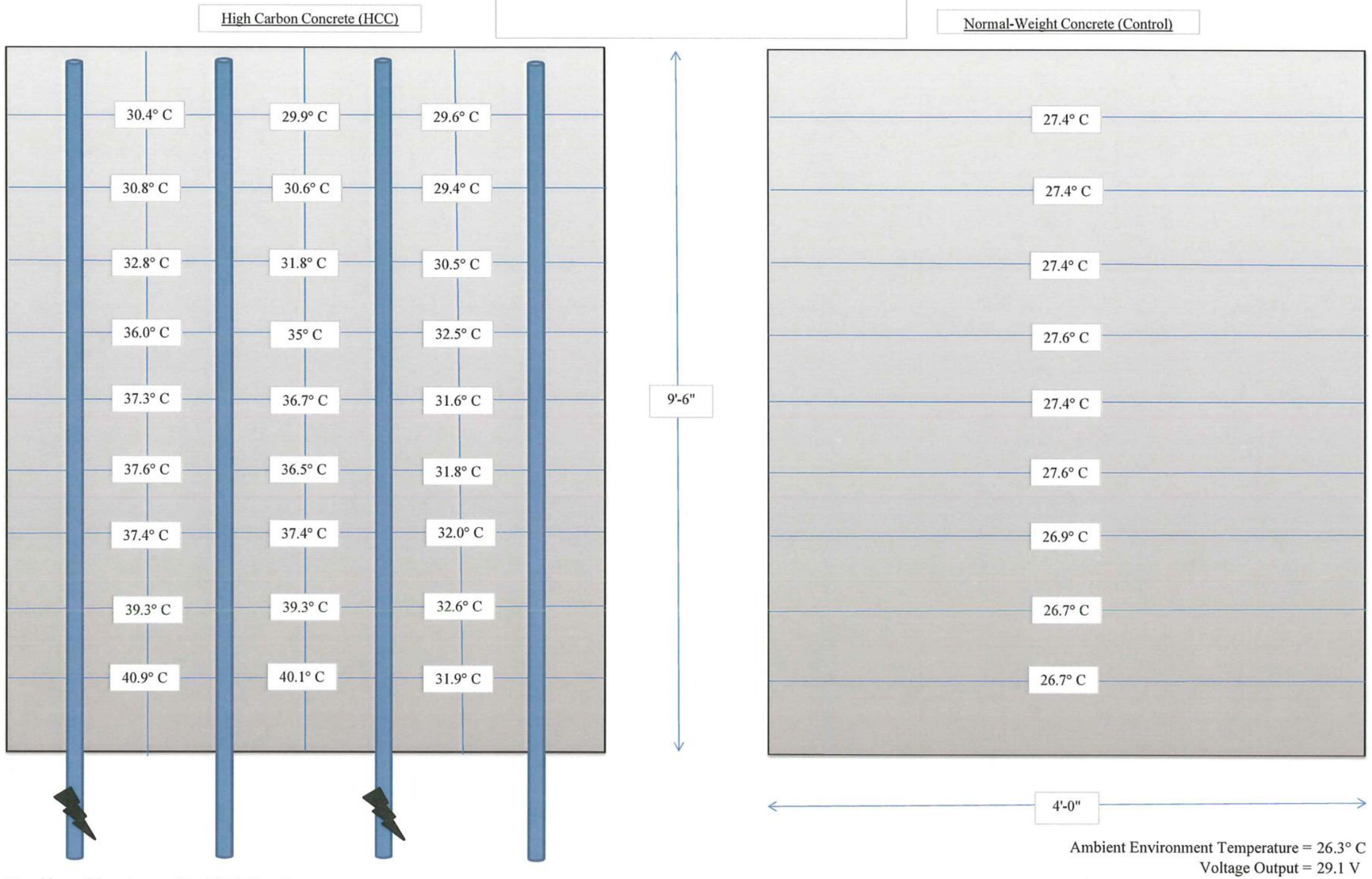

Panel is partitioned as a grid with 1'x1' sections.
Lightning signifies location of electrodes being used by current flow.

Ambient Environment Temperature = 26.3° C
Voltage Output = 29.1 V

Initial Conditions and Surface Temperatures of Conductive and Control Testing Panels

July 29, 2011 @ 12:30 am
All temperatures in °C

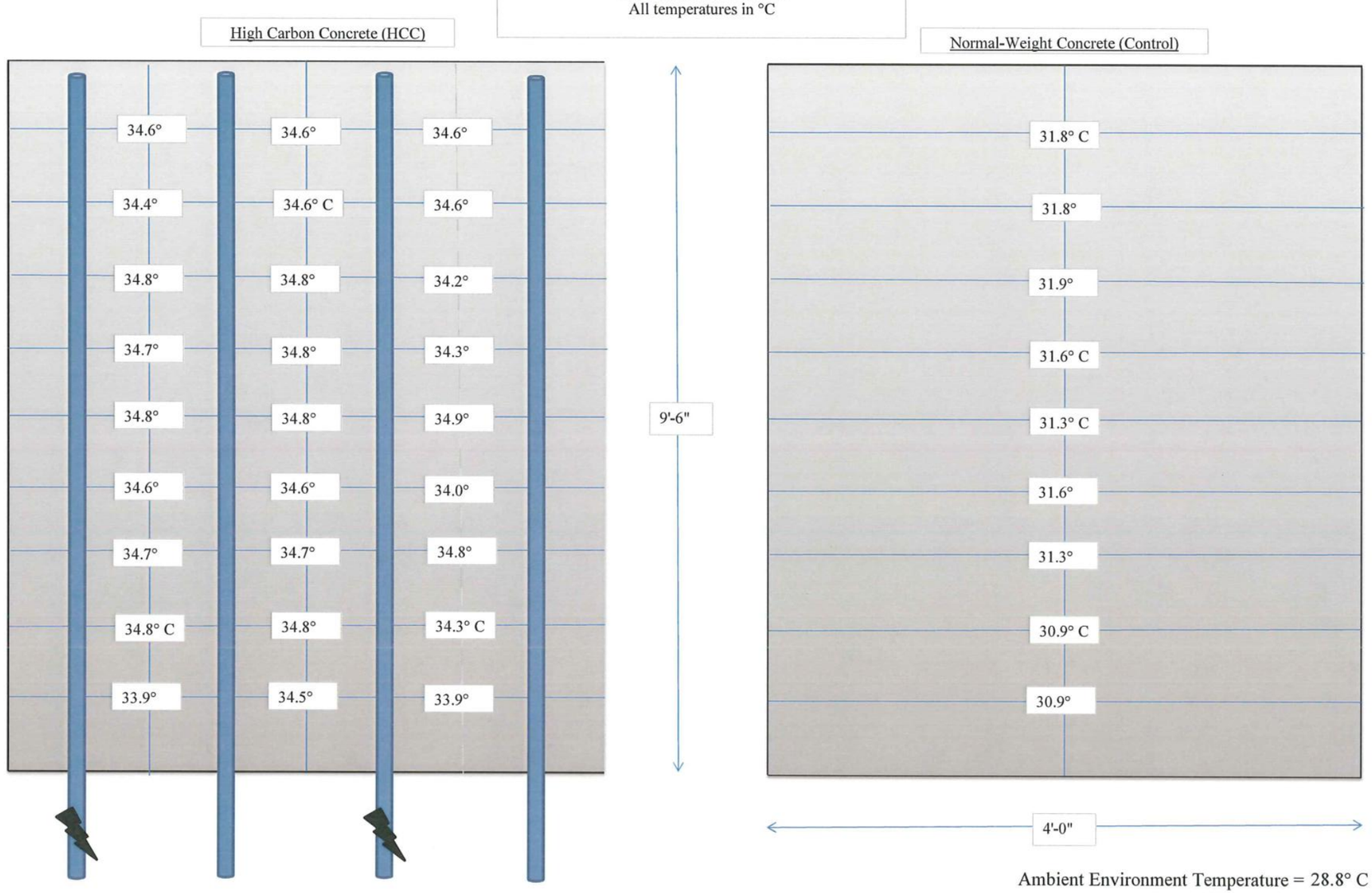

Panel is partitioned as a grid with 1'x1' sections.
Lightning signifies location of electrodes being used by current flow.

Ambient Environment Temperature = 28.8° C
Voltage Output = 50.2 V

Post Experiment Conditions and Surface Temperatures of Conductive and Control Testing Panels

July 29, 2011 @ 6:00 am
All temperatures in °C

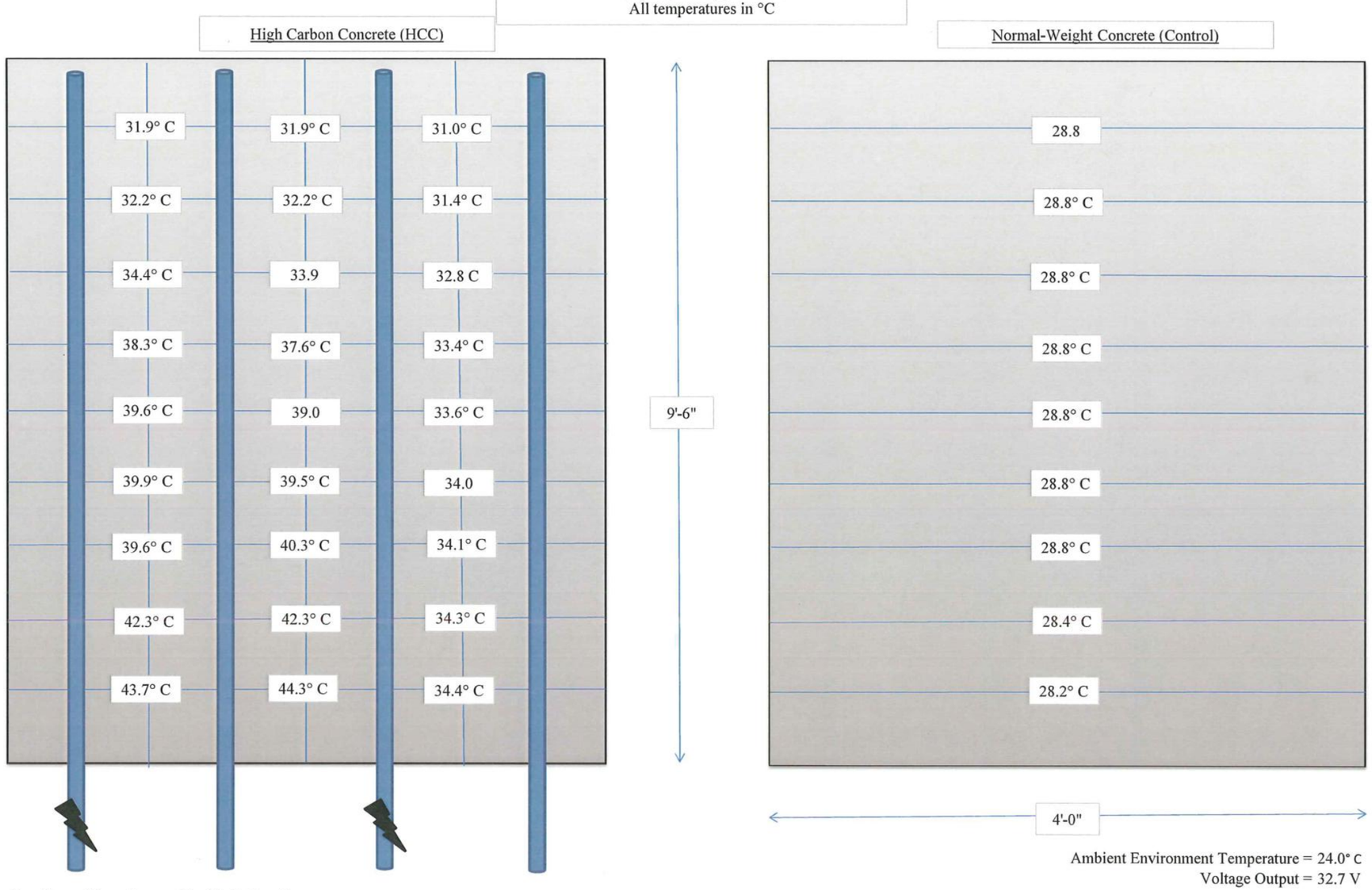

Ambient Environment Temperature = 24.0° C
Voltage Output = 32.7 V

Panel is partitioned as a grid with 1'x1' sections.
Lightning signifies location of electrodes being used by current flow.

Initial Conditions and Surface Temperatures of Conductive and Control Testing Panels

August 9, 2011 @ 12:30 am
All temperature in °C

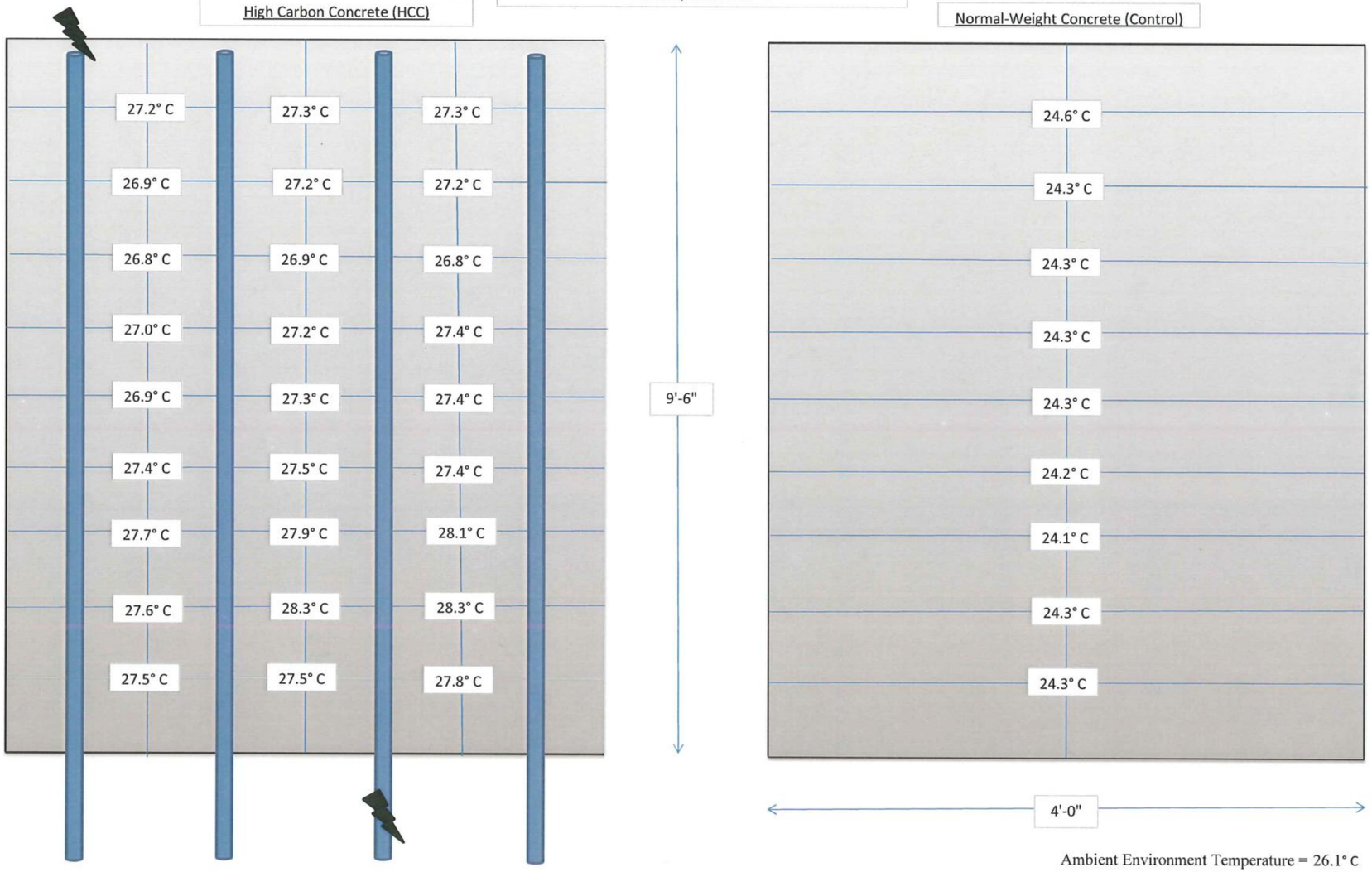

Ambient Environment Temperature = 26.1° C
Voltage Output = 50.2 V

Panel is partitioned as a grid with 1'x1' sections.
Lightning signifies location of electrodes being used by current flow.

Post Experiment Conditions and Surface Temperatures of Conductive and Control Testing Panels

August 9, 2011 @ 6:30 am
All temperature in °C

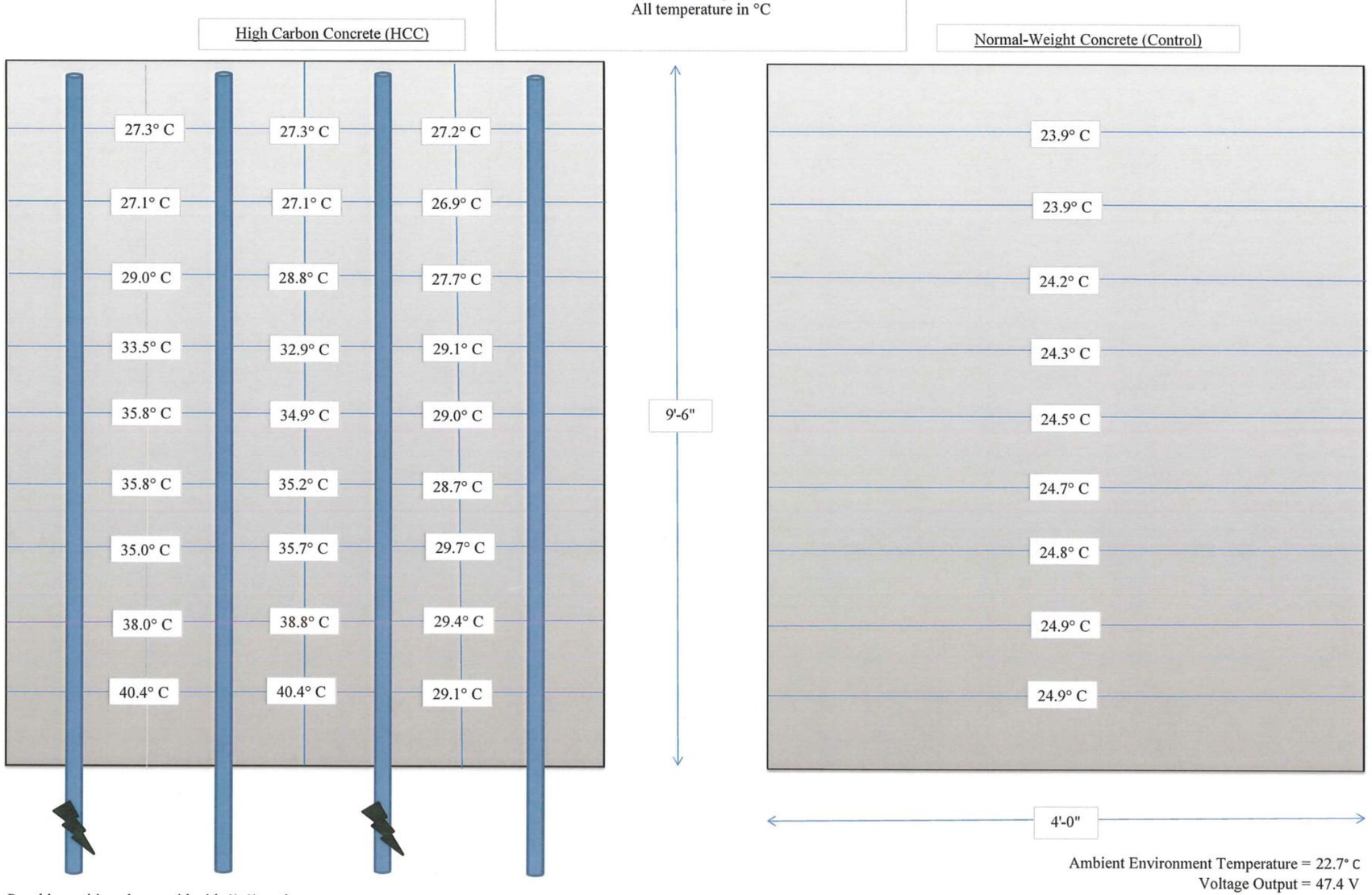

Panel is partitioned as a grid with 1'x1' sections.
Lightning signifies location of electrodes being used by current flow.

Ambient Environment Temperature = 22.7° C
Voltage Output = 47.4 V

Initial Conditions and Surface Temperatures of Conductive and Control Testing Panels

August 16, 2011 @ 12:30 am
All temperature in °C

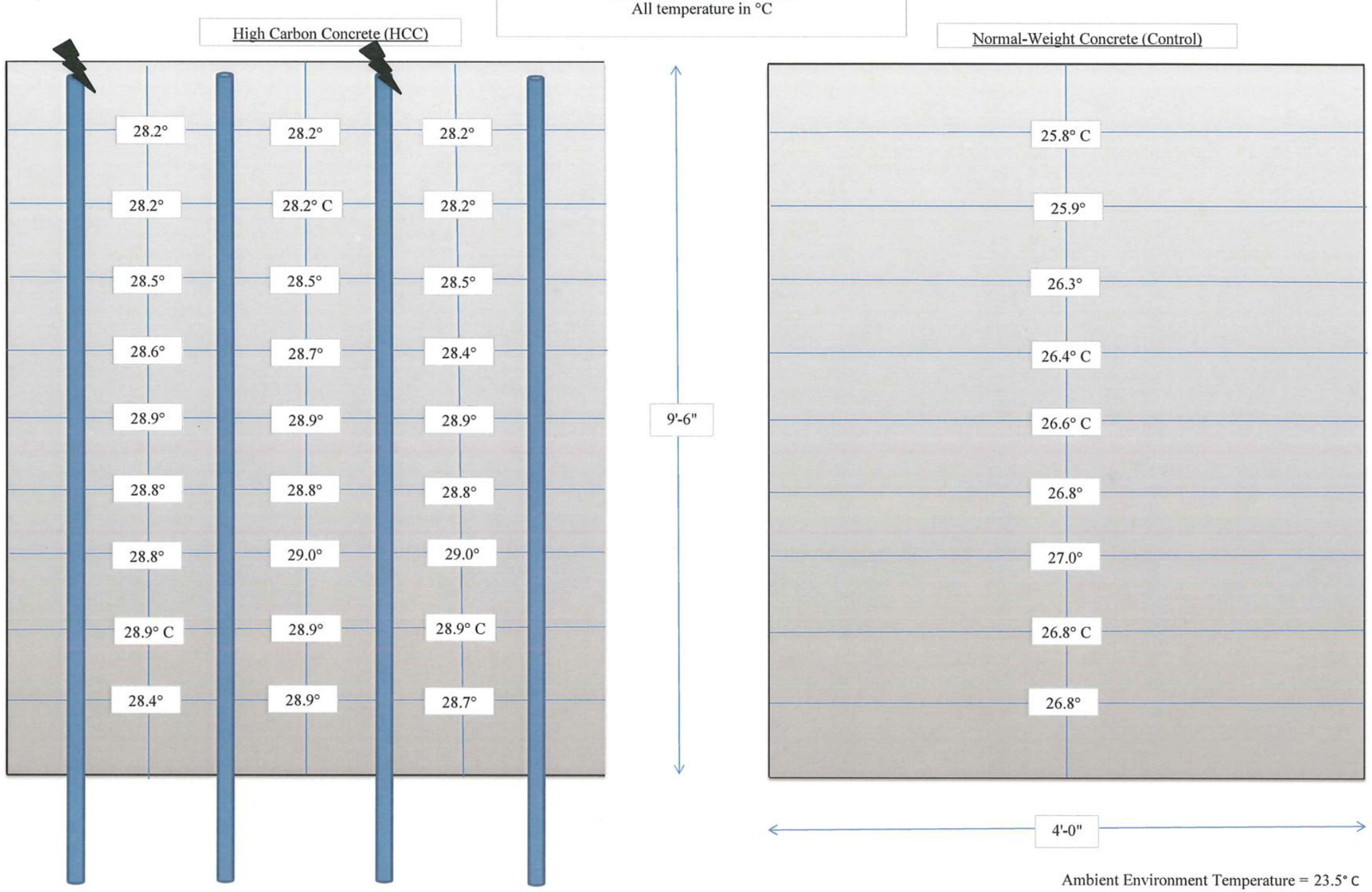

Ambient Environment Temperature = 23.5° C
Voltage Output = 51.5 V

Panel is partitioned as a grid with 1'x1' sections.
Lightning signifies location of electrodes being used by current flow.

Post Experiment Conditions and Surface Temperatures of Conductive and Control Testing Panels

August 16, 2011 @ 6:30 am
All temperature in °C

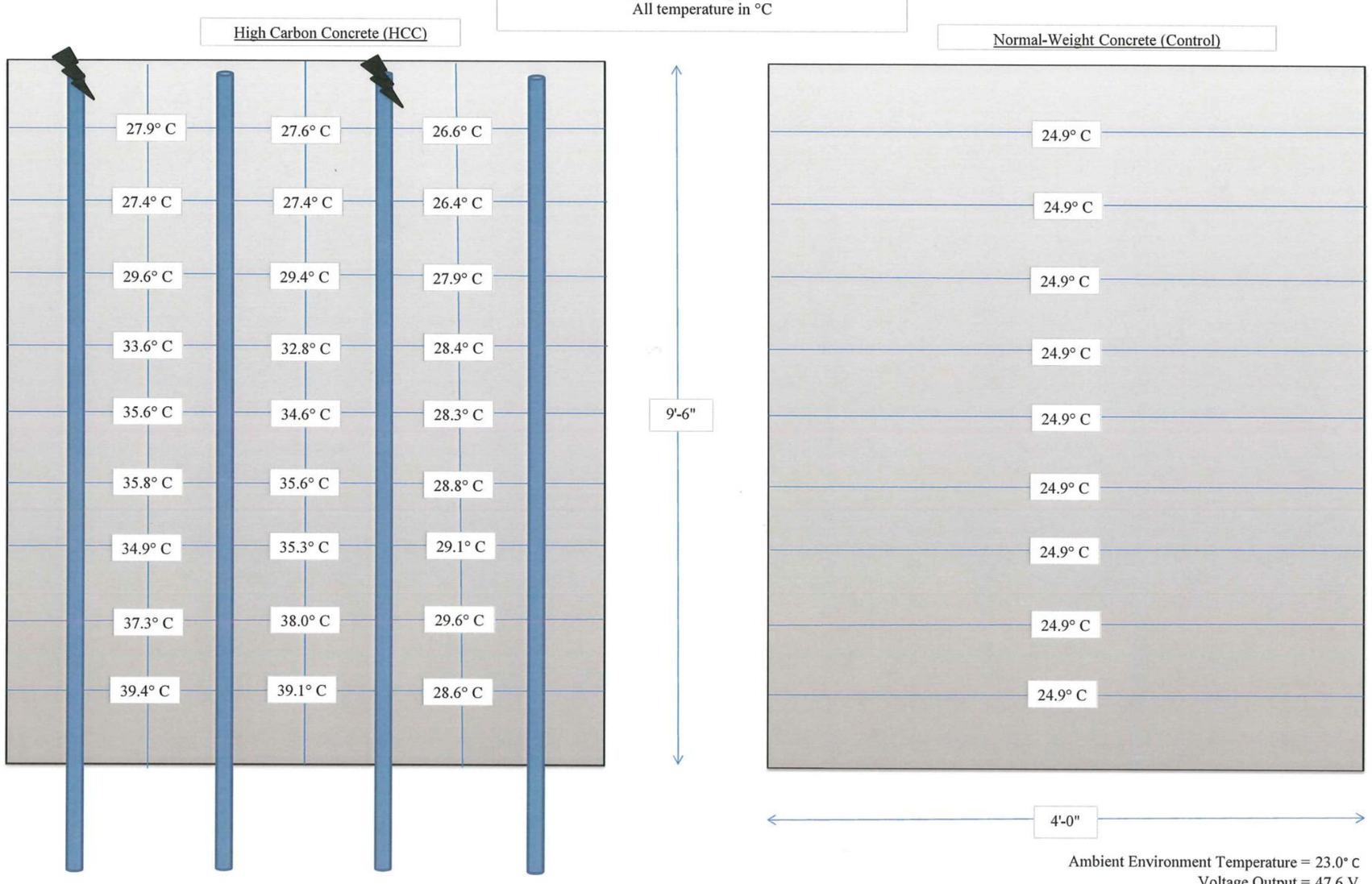

Panel is partitioned as a grid with 1'x1' sections.
Lightning signifies location of electrodes being used by current flow.

Ambient Environment Temperature = 23.0° C
Voltage Output = 47.6 V

Initial Conditions and Surface Temperatures of Conductive and Control Testing Panels

September 2, 2011 @ 12:30 am
All temperature in °C

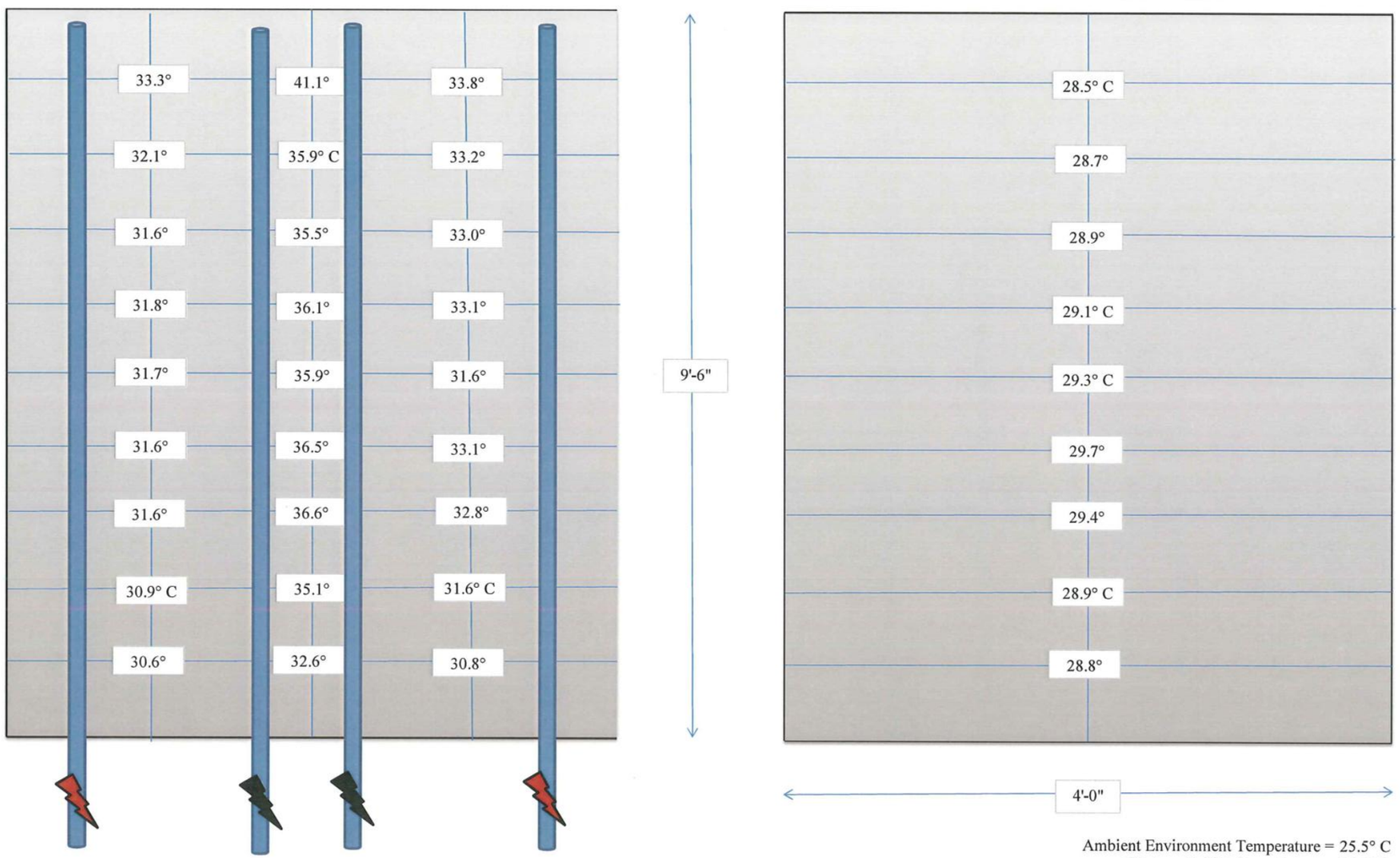

Panel is partitioned as a grid with 1'x1' sections.
Lightning signifies location of electrodes being used by current flow.

Ambient Environment Temperature = 25.5° C
Western Half Voltage Output = 24.2 V
Eastern Half Voltage Output = 25.8 V

Post Experiment Conditions and Surface Temperatures of Conductive and Control Testing Panels

September 2, 2011 @ 6:00 am
All temperature in °C

High Carbon Concrete (HCC)

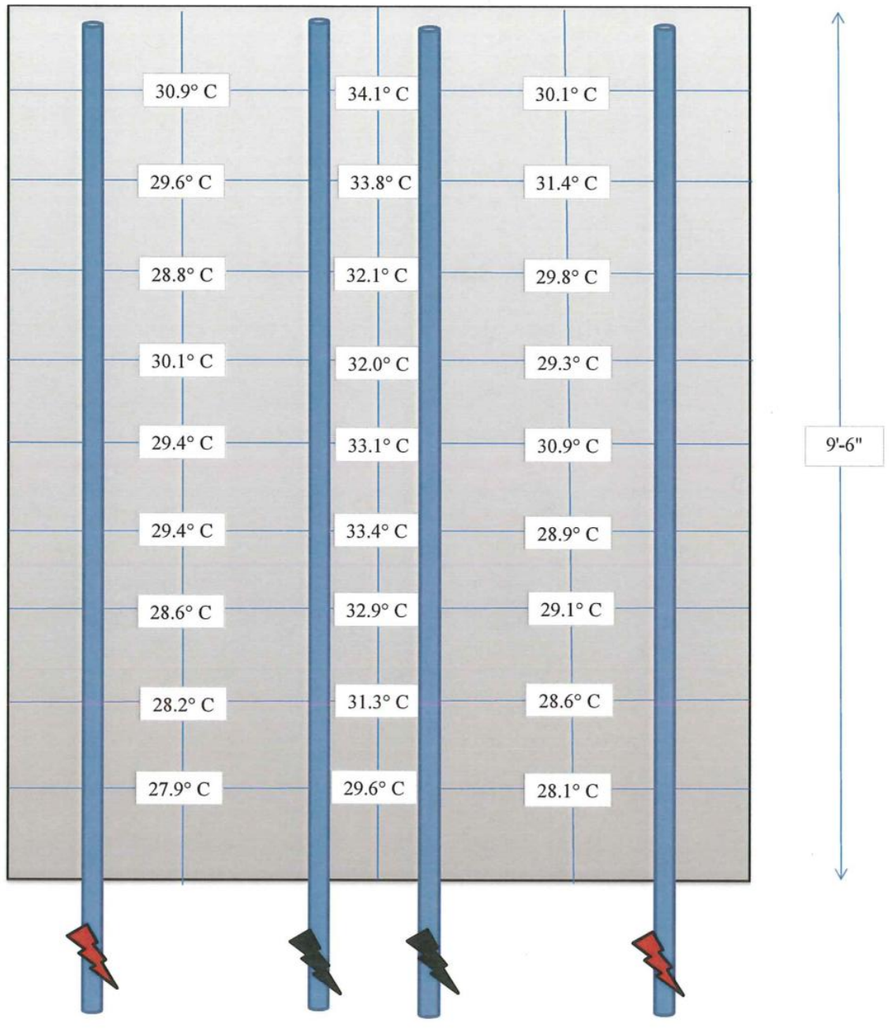

Normal-Weight Concrete (Control)

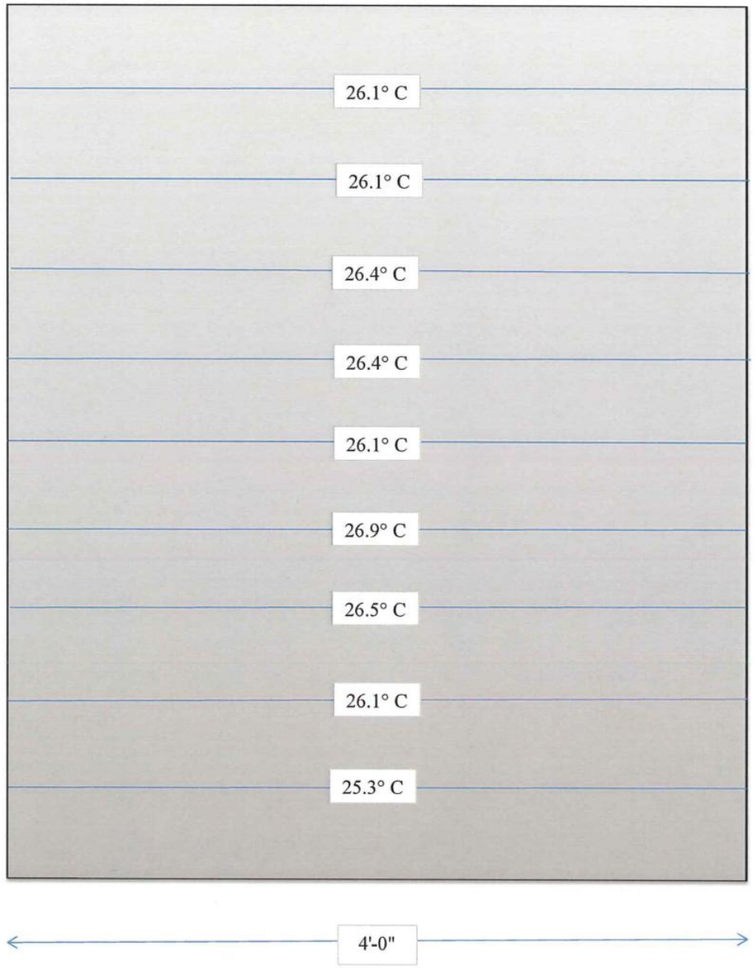

Panel is partitioned as a grid with 1'x1' sections.
Lightning signifies location of electrodes being used by current flow.

Ambient Environment Temperature = 24.8° C
Western Half Voltage Output = 24.0 V
Eastern Half Voltage Output = 25.6 V

Initial Conditions and Surface Temperatures of Conductive and Control Testing Panels

October 6, 2011 @ 11:30 am
All Temperature in °C

High Carbon Concrete (HCC)

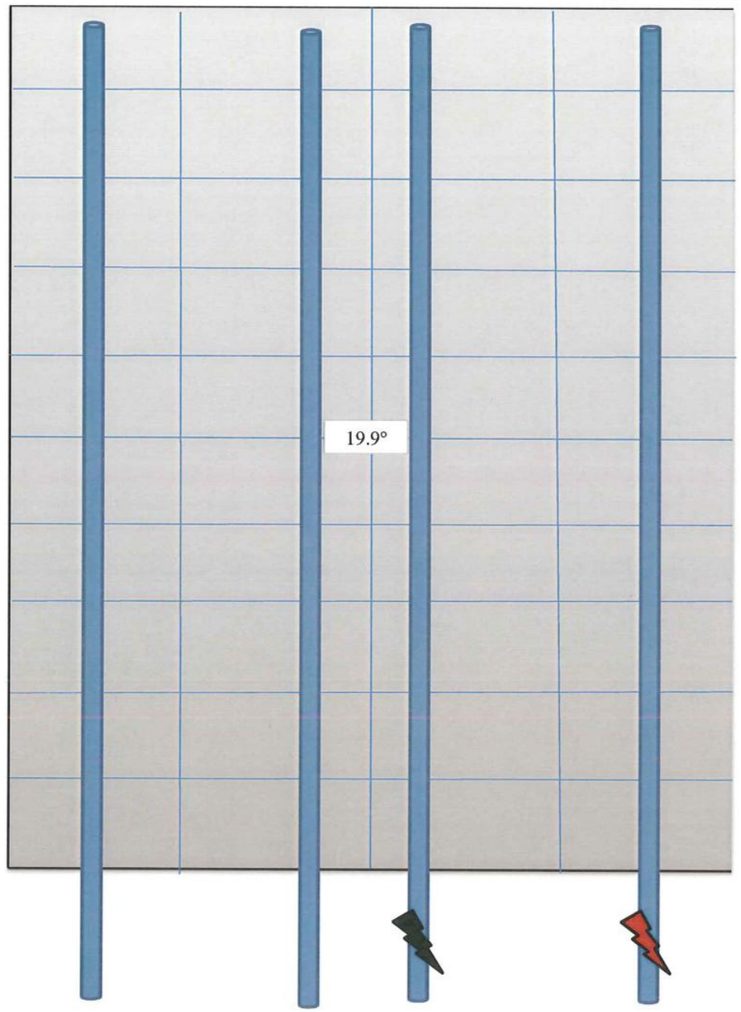

9'-6"

Normal-Weight Concrete (Control)

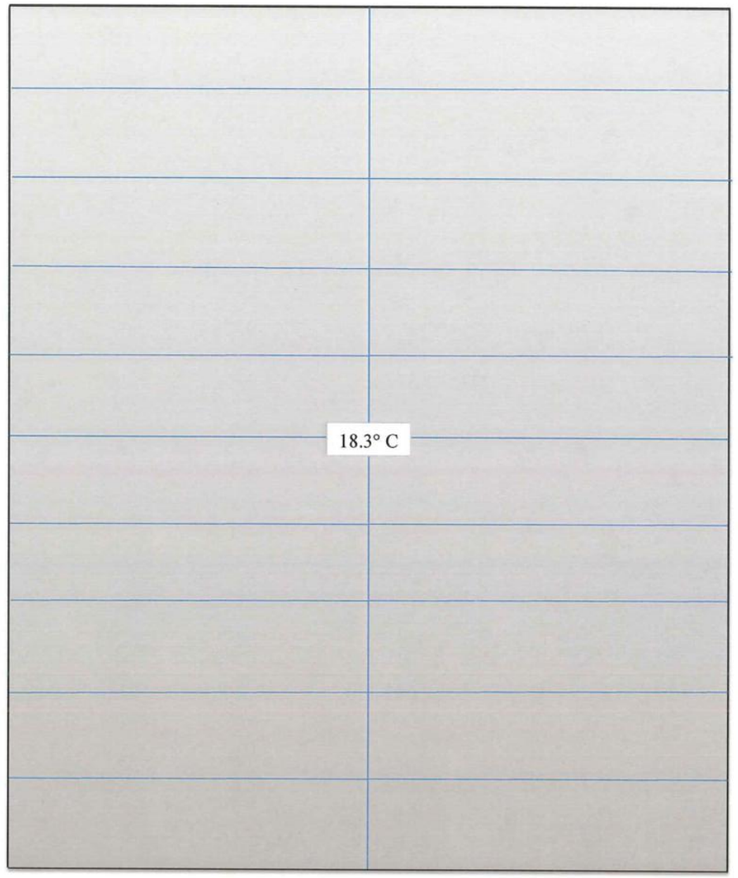

4'-0"

Panel is partitioned as a grid with 1'x1' sections.
Lightning signifies location of electrodes being used by current flow.

Ambient Environment Temperature = 17.7° C
Western Half Voltage Output = 49.8 V
Western Half Amperage Output = 27A

Post Experiment Conditions and Surface Temperatures of Conductive and Control Testing Panels

October 7, 2011 @ 6:30 am
All temperatures in °C

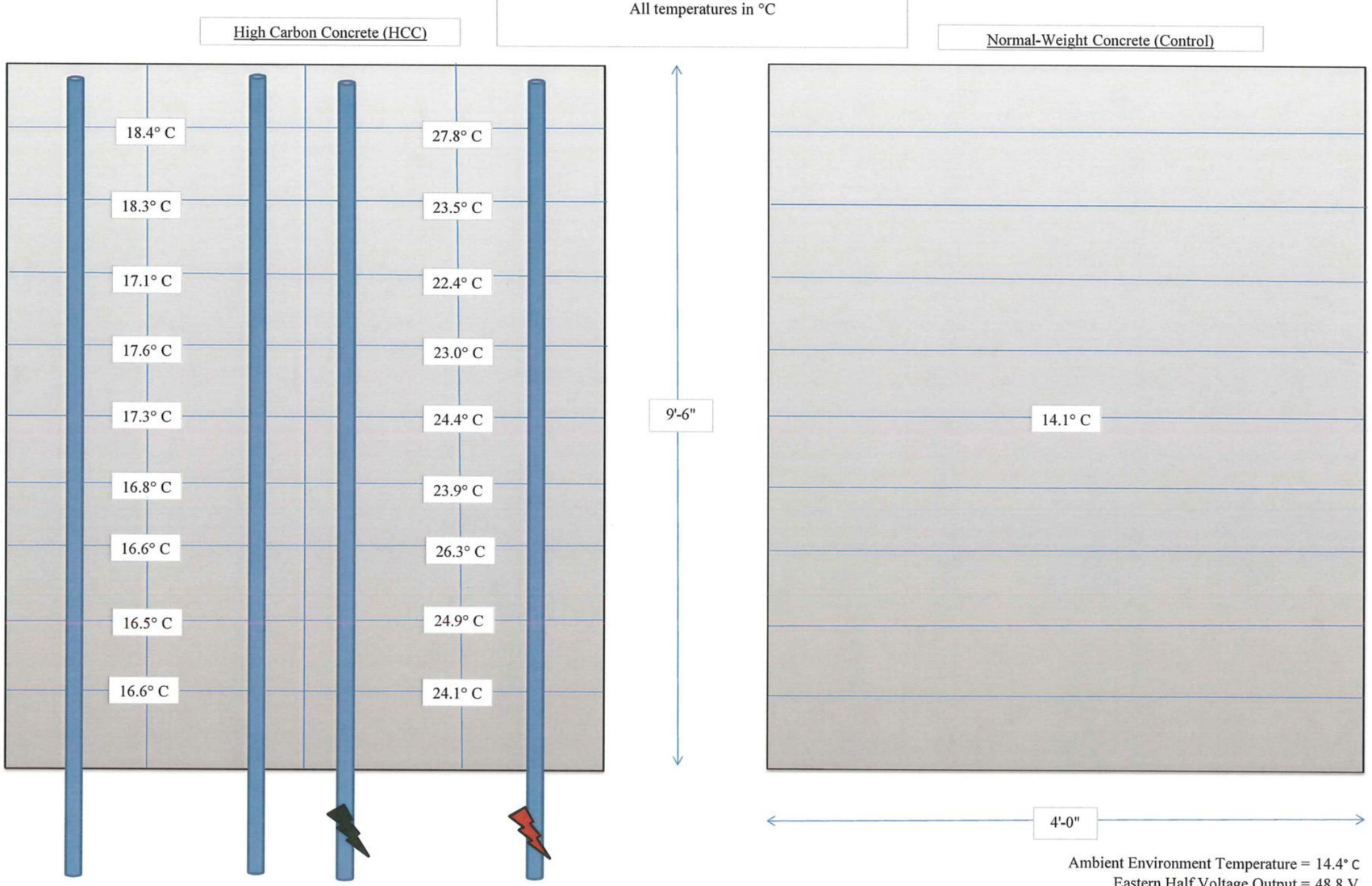

Panel is partitioned as a grid with 1'x1' sections.
Lightning signifies location of electrodes being used by current flow.

Ambient Environment Temperature = 14.4° C
Eastern Half Voltage Output = 48.8 V
Eastern Half Amperage Output = 9A

Initial Conditions and Surface Temperatures of Conductive and Control Testing Panels

October 20, 2011 @ 12:30 am
All temperature in °C

High Carbon Concrete (HCC)

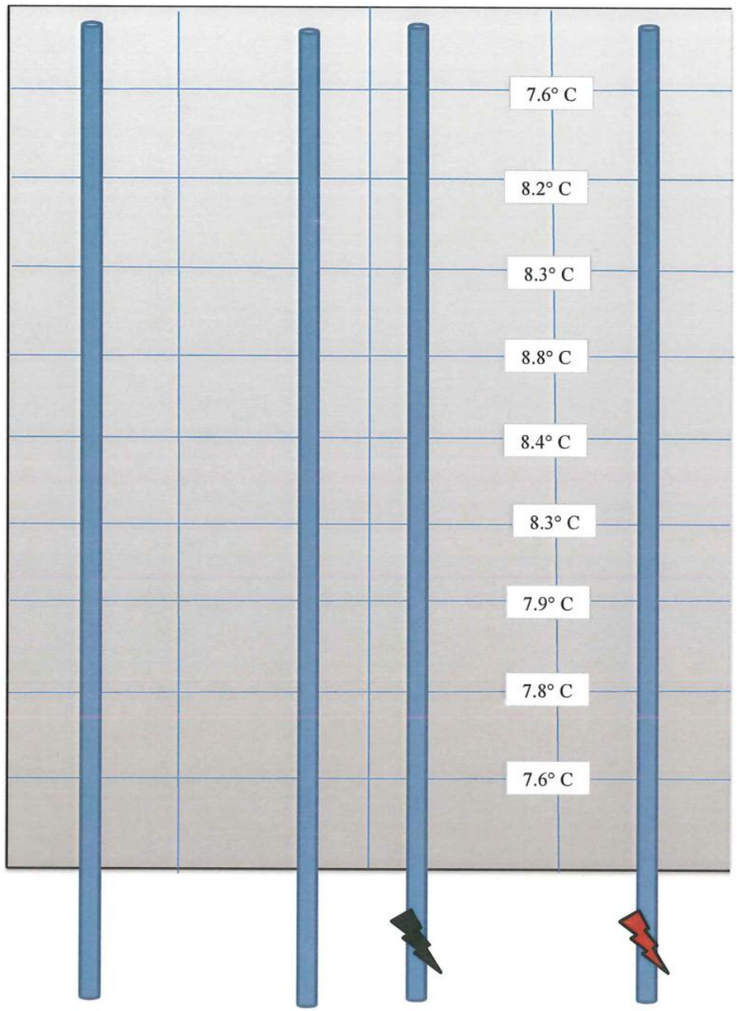

9'-6"

Normal-Weight Concrete (Control)

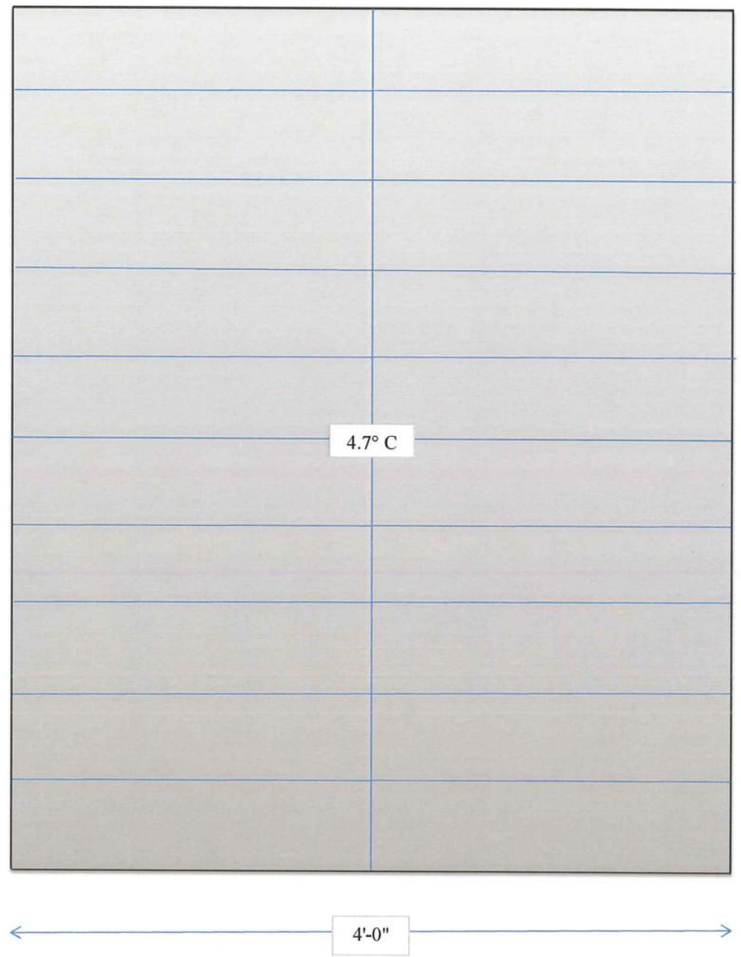

4'-0"

Panel is partitioned as a grid with 1'x1' sections.
Lightning signifies location of electrodes being used by current flow.

Ambient Environment Temperature = 0° C
Right Half Voltage Output = 53.9 V
Right Half Amperage Output = 9A

Post Experiment Conditions and Surface Temperatures of Conductive and Control Testing Panels

October 20, 2011 @ 6:30 am
All temperature in °C

High Carbon Concrete (HCC)

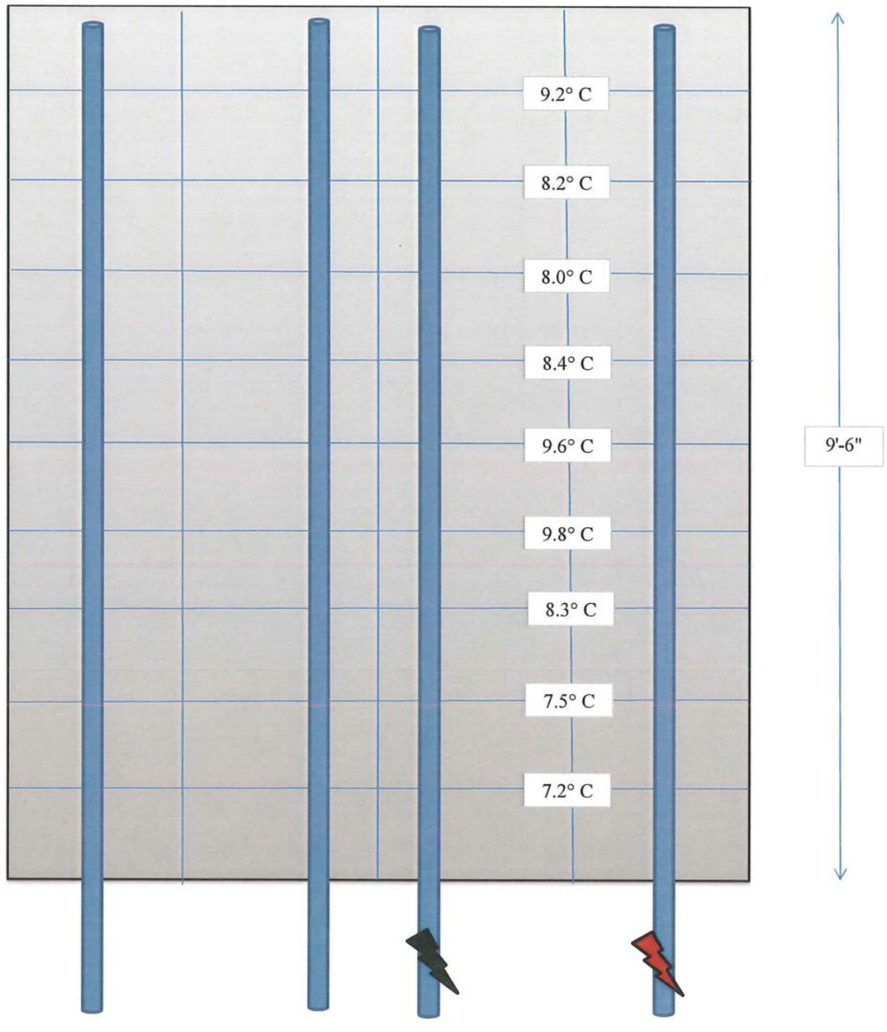

Panel is partitioned as a grid with 1'x1' sections.
Lightning signifies location of electrodes being used by current flow.

Normal-Weight Concrete (Control)

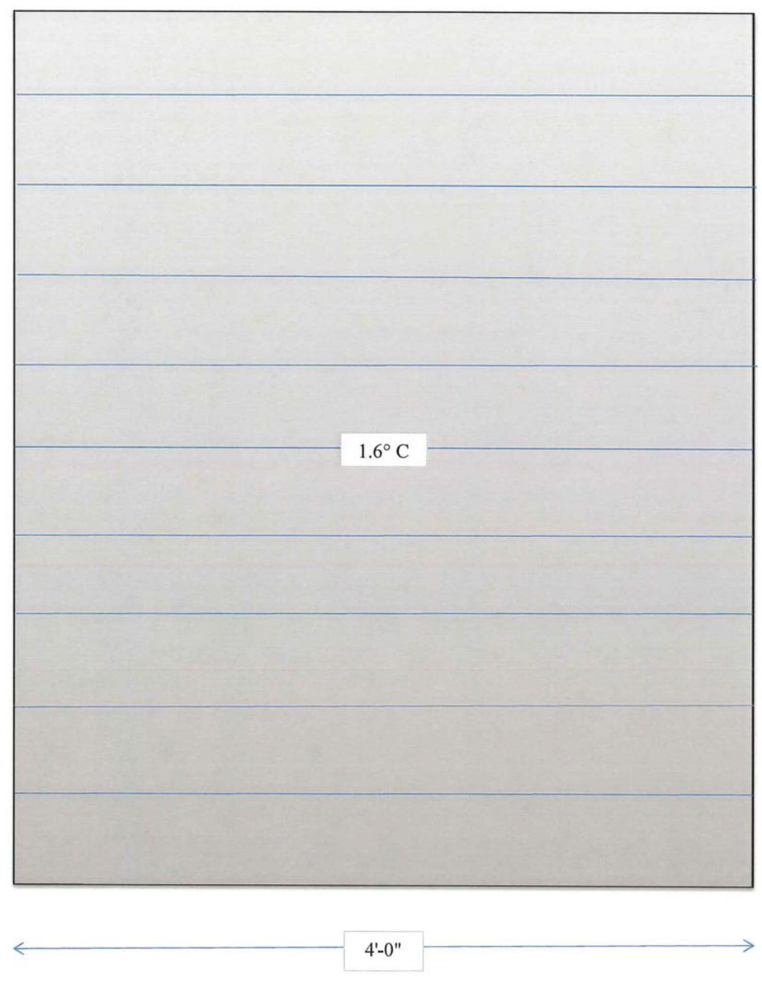

Ambient Environment Temperature = -2.2° C
Eastern Half Voltage Output = N/A
Eastern Half Amperage Output = N/A

Pre Experiment Conditions and Surface Temperatures of Conductive and Control Testing Panels

November 28, 2011 @ 12:30 am
All temperature in °C

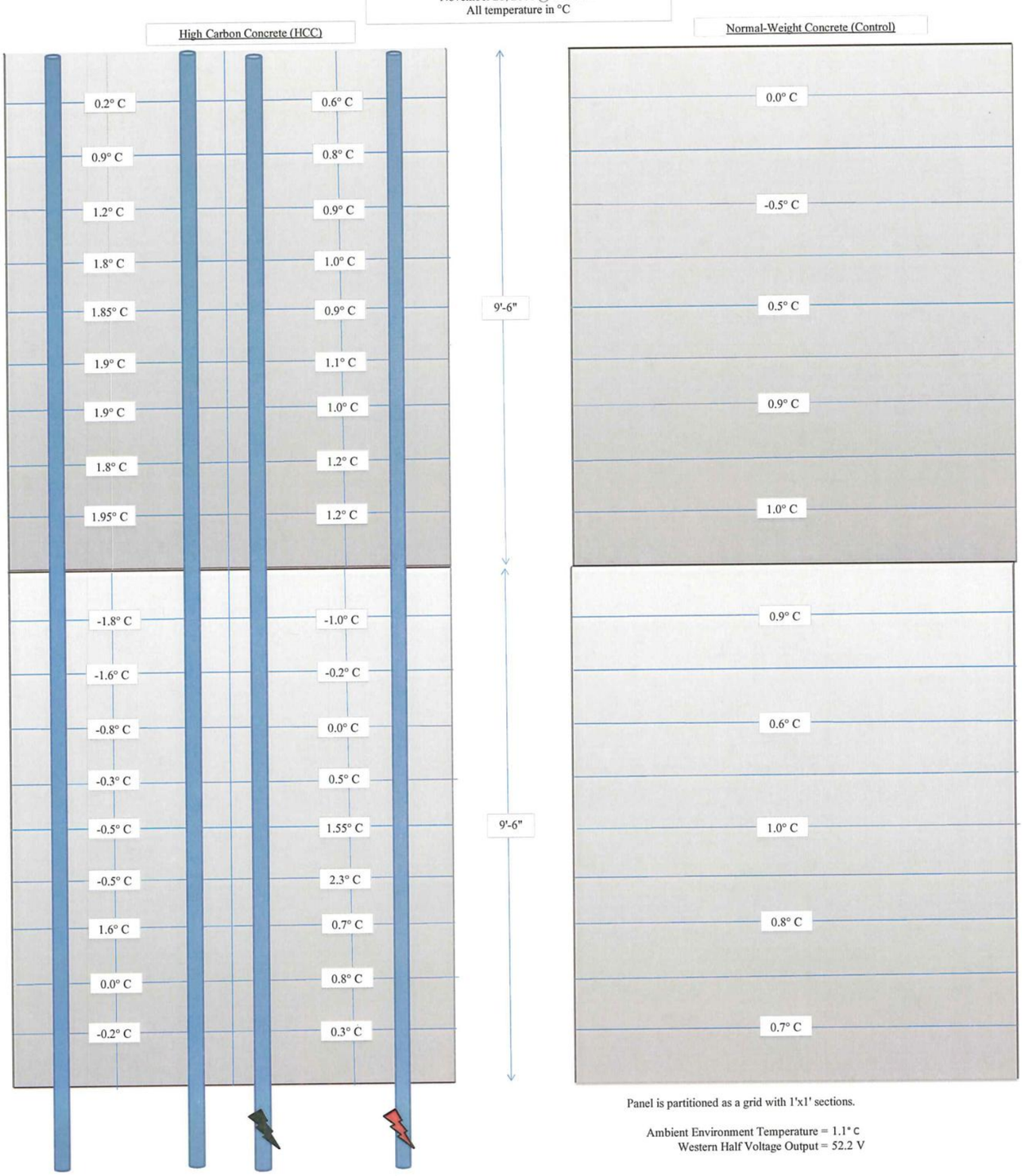

Panel is partitioned as a grid with 1'x1' sections.

Ambient Environment Temperature = 1.1° C
Western Half Voltage Output = 52.2 V

Post Experiment Conditions and Surface Temperatures of Conductive and Control Testing Panels

November 28, 2011 @ 6:30am
All temperature in °C

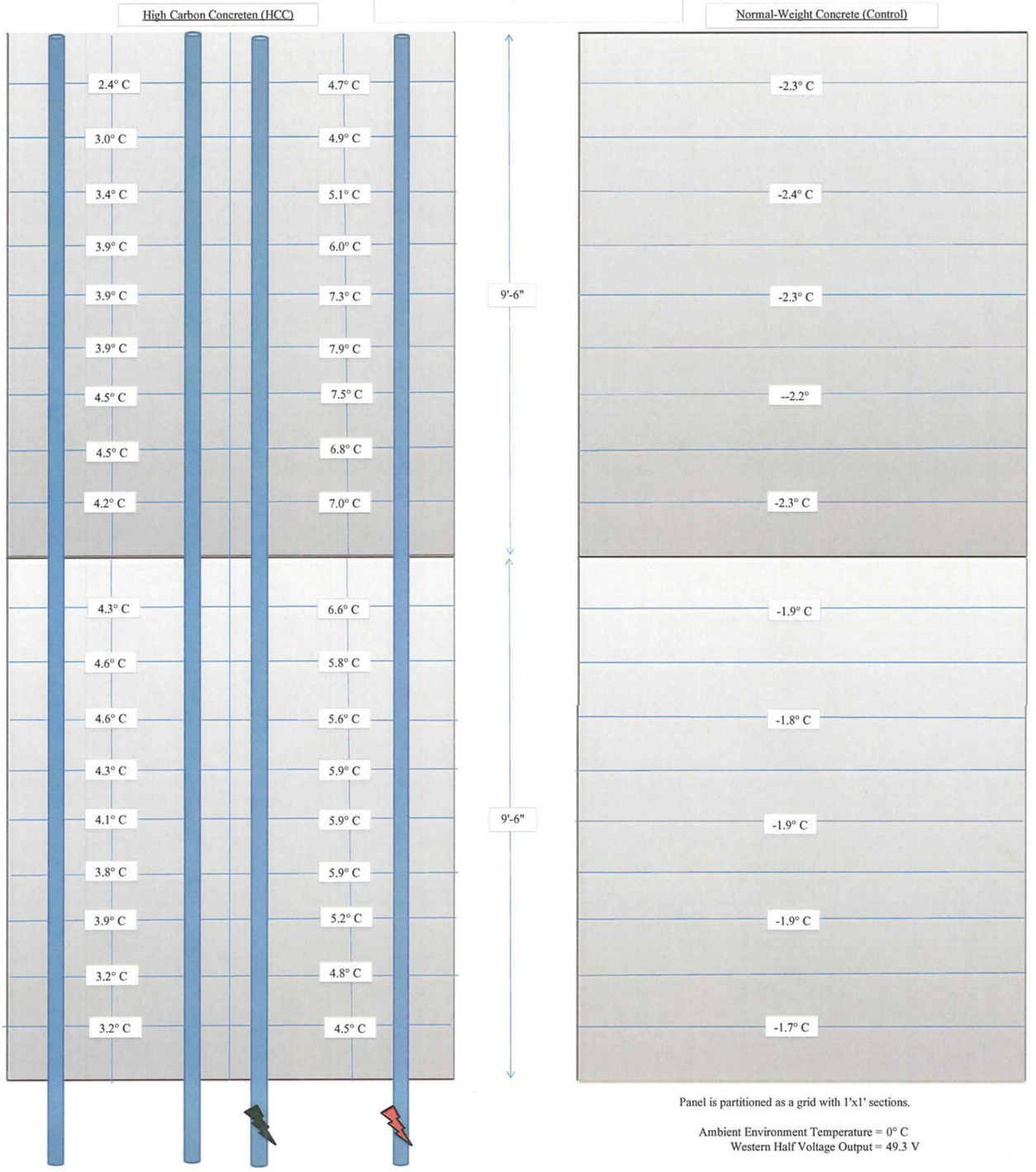

Panel is partitioned as a grid with 1'x1' sections.

Ambient Environment Temperature = 0° C
Western Half Voltage Output = 49.3 V

Post Experiment Conditions and Surface Temperatures of Conductive and Control Testing Panels

November 29, 2011 @ 12:30 am
All temperature in °C

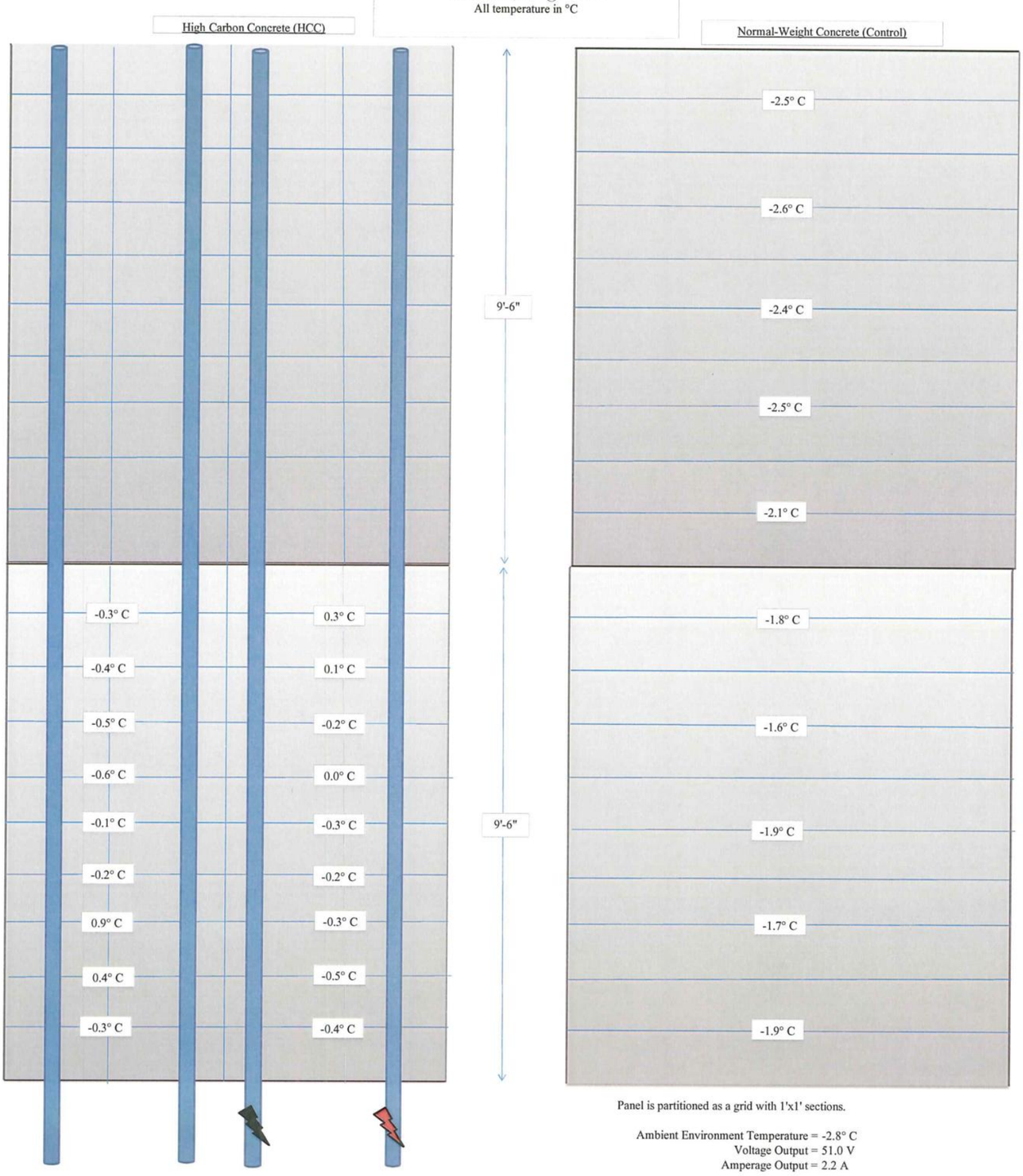

Panel is partitioned as a grid with 1'x1' sections.

Ambient Environment Temperature = -2.8° C
Voltage Output = 51.0 V
Amperage Output = 2.2 A

Post Experiment Conditions and Surface Temperatures of Conductive and Control Testing Panels

November 29, 2011 @ 6:30am
All temperature in °C

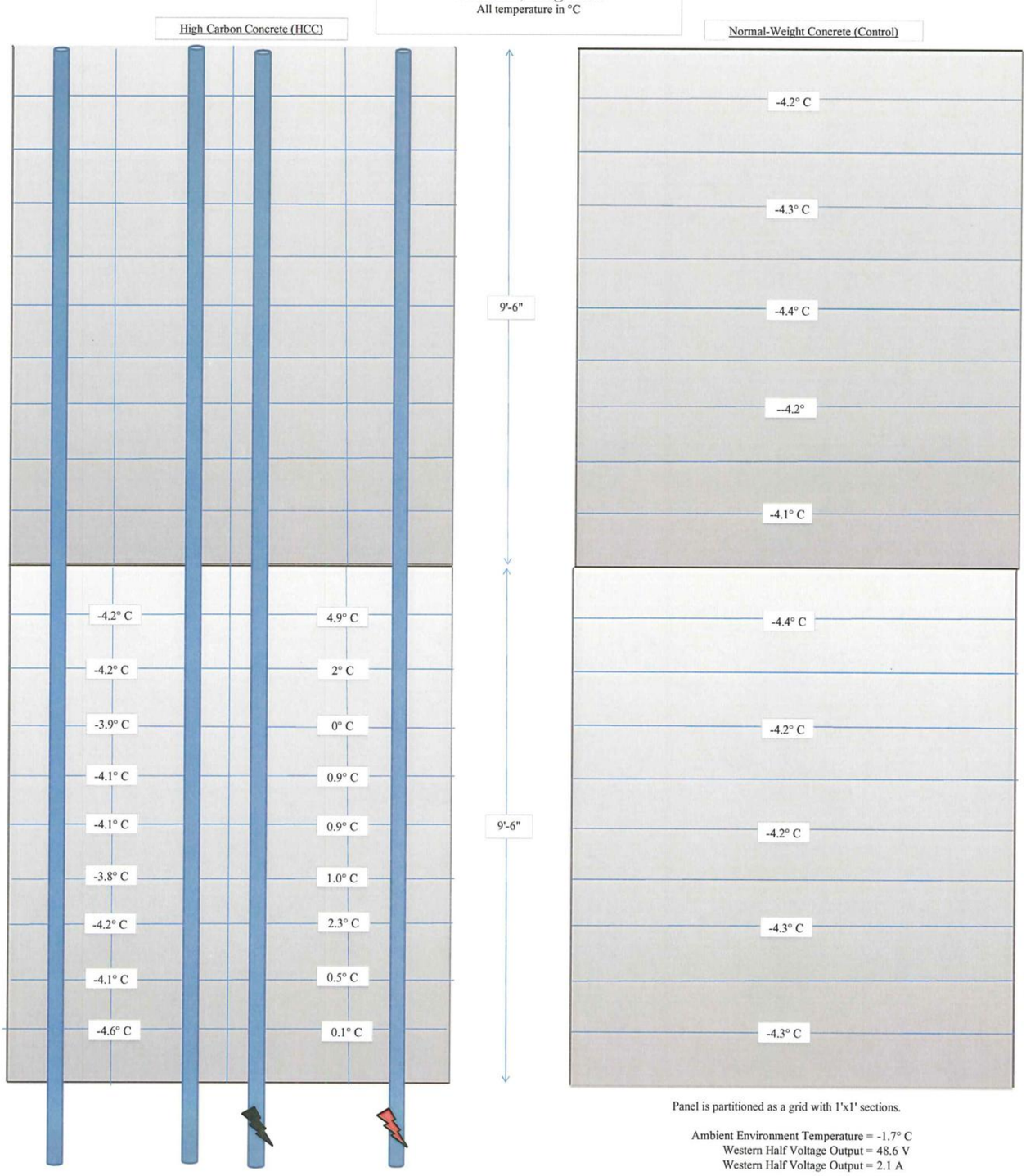

Panel is partitioned as a grid with 1'x1' sections.

Ambient Environment Temperature = -1.7° C
Western Half Voltage Output = 48.6 V
Western Half Voltage Output = 2.1 A

REFERENCES

American Concrete Institute, ACI Committee 306, "Cold Weather Concreting," ACI Materials Journal, 1992

American Concrete Institute, ACI Committee 544, "Guide for Specifying, Proportioning, Mixing, Placing, and Finishing Steel Fiber Reinforced Concrete," ACI Materials Journal, Vol. 90, No. 1, January-February, 1993, pp. 94-101.

Arioz, Omer, "Retained properties of concrete exposed to high temperatures: Size effect," Fire and Materials, John Wiley and Sons, Ltd., Hoboken, NJ, 2009, 33, pp 211-222.

Balaguru, P.N., and Ramakrishnan V., "Freeze-Thaw Durability of Fiber Reinforced Concrete," ACI Journal, May-June, 1986, pp. 374-382.

Balaguru, P.N., and Ramakrishnan V., "Properties of Fiber Reinforced Concrete: Workability, Behavior under Long-Term Loading, and Air-Void Characteristics" ACI Materials Journal, May-June, 1988, pp. 189-196.

Berwanger, C., and Sarkar, A.F., "Thermal Expansion of Concrete and Reinforced Concrete," ACI Journal, November 1976, pp. 618-621.

Binghamton University, Staff, "FAA to fund students' airport pavement project," Binghamton University Inside, September 2010

Bingöl, Ferhat A., and Gül, Rustem, "Effect of elevated temperatures and cooling regimes on normal strength concrete," Fire and Materials, John Wiley and Sons, Ltd., Hoboken, NJ, 33, 2009, pp. 79-88.

Browning, J., Darwin, D., Gong, L., Hughes, S.R., "Effects of Deicers on Concrete Deterioration," Structural Engineering and Materials Laboratory, SL Report 07-3, December, 2007, pp. 1-22.

Buell, Charles, "Spalling Concrete Due To Rusting Steel," Active Rain. December 2009. < http://activerain.com/blogsview/1391224/spalling-concrete-due-to-rusting-steel>

Carbons, Asbury, "Asbury Carbons, Graphite," February, 2011. <http://www.asbury.com/Graphite.html>

Concrete Ideas contributors. "De-Icing Effects on Concrete Surfaces." Concrete Ideas, September, 2011. <http://concreteideas.com/concrete/exterior-concrete/de-icing-effects-on-concrete-surfaces>

Corson, D.R. and Lorrain, P., "Introduction to Electromagnetic Fields and Waves," W.H. Freeman and Company, San Fransisco, 1962.

Freedman, Roger A., Young, Hugh D., "University Physics with Modern Physics," 12th Edition, 2007

Hale, Micah, "Concrete Materials, Class Lecture," University of Arkansas, Fayetteville, Arkansas, February, 2010, pp. 89-90.

Khoury, Gabriel Alexander, "Effect of fire on concrete and concrete structures," Progress in Structural Engineering and Materials, John Wiley and Sons, Ltd., Hoboken, NJ, 2000, 2, pp. 429-447.

Lee, H., Cody, R.D., Cody, A.M., Spry, P.G., "Effects of Various Deicing Chemicals on Pavement Concrete Deterioration," Mid-Continent Transportation Symposium 2000 Proceedings, pp. 151-155

Levy Group of Companies, The, "Intermediate Aggregate Blast Furnace Slag," < http://edwclevy.com/productpop.aspx?id=262>

Local Government and Municipal Knowledge Base contributors(LGAM). "Block Cracking," Local Government and Municipal Knowledge Base. January 2012 < http://lgam.wikidot.com/block-cracking>

Miller, Steven H., Ramme, Bruce W., "An Electric Freeway to the Future," Concrete International, May 2011, pp. 45-48

Mooney, J. M., "Just Add Sunshine: Solar Electricity Will Set You Free," 1997, pp. 1-105

National Ready Mixed Concrete Association, "Concrete In Practice: CIP 5-Plastic Shrinkage Cracking," <http://www.nrmca.org/aboutconcrete/cips/05p.pdf>, 1998

Osweiler, A. Implementing Conductive Concrete with Photovoltaic Energy to Develop Anti-Icing Airport Runways," University of Arkansas Master's Thesis, December, 2012

Petersen, L., Lohaus, L., Polak, M.A., "Influence of Freezing-and-Thawing Damage on Behavior of Reinforced Concrete Elements," ACI Materials Journal, Vol. 104, No. 4, July-August, 2007, pp. 369-378.

Power, T.C., "Freezing Effects in Concrete," American Concrete Institute, Publication SP-47-1, 1975, pp. 1-11

Slag Association, National, "Blast Furnace Slag: The Aggregate of choice for Portland Cement Concrete," March

Tuan, C.Y., "Conductive Concrete for Bridge Deck Deicing and Anti-Icing," Nebraska Department of Roads, Project No. SPR-PL-1(037) P512, July, 2004, pp. 167

Tuan, C.Y., "Implementation of Conductive Concrete for Deicing (Roca Bridge)," Nebraska Department of Roads, Project No. SPR-P1 (037) P565, July, 2008, pp. 154

Wei, H. and Hongjun, Y., "Recovery Energy from the Separated and Gravity Type of Heat Pipe Exchanger in China," Journal of Petroleum and Gas Engineering Vol. 2 (1), pp. 1-6, January 2011

City of Omaha contributors, "Pavement Repair," City of Omaha Website, August, 2012. < http://www.cityofomaha.org/pw/whodoicontact/streets.html>

Willam, K., Rhee, I., and Xi, Y., "Thermal Degradation of Heterogeneous Concrete Materials," Journal of Materials in Civil Engineering, ASCE, Reston, VA., V. 17, No. 3, June 2005, pp. 276-285.

Xie, P., Gu, P., and Beaudoin, J.J., "Conductive Concrete Cement-Based Compositions," U.S. Patent 5,447,564, 1995, 10 pp.

Xie, P., and Beaudoin, J.J., "Electrical Percolation Phenomena in Cement Composites Containing Conductive Fibres," Journal of Materials Science 31, 1996, pp. 4093-4097

Xie, P., and Beaudoin, J.J., "Electrically Conductive Concrete and Its Application in Deicing," Advances in Concrete Technology, Proceedings of the Second SANMET/ACI International Symposium, Las Vegas, Nevada, 1995, pp. 399-417.

Xuan, D. X., Shui, Z. H., "Temperature dependence of thermal induced mesocracks around limestone aggregate in normal concrete," Fire and Materials, John Wiley and Sons, Ltd., Hoboken, NJ, 2009, Interscience.com.

Yehia, S.A., and Tuan, C.Y., "Conductive Concrete Overlay for Bridge Deck Deicing," ACI Materials Journal, Vol. 96, No. 3, May-June, 1999, pp. 382-390.

Yehia, S.A., and Tuan, C.Y., Ferdon, D., and Chen, B., "Conductive Concrete Overlay for Bridge Deck Deicing: Mix Design, Optimization, and Properties," ACI Materials Journal, Vol. 97, No. 2, March-April, 2000, pp. 172-181.

Yehia, S.A., and Tuan, C.Y., "Evaluation of Electrically Conductive Concrete Containing Carbon Products for Deicing," ACI Materials Journal, Vol. 101, No. 4, July-August, 2004, pp. 287-293